Approaches to identify groundwater discharge towards and within lowland surface water bodies on different scales

Dissertation zur Erlangung des akademischen Grades

Doktor rerum natuarlium

(Dr. rer. nat.)

im Fach Geographie

eingereicht an der

Mathematisch – Naturwissenschaftlichen Fakultät

Der Humboldt Universität zu Berlin

von

Dipl.-Geogr. Franziska Pöschke

Präsident der Humboldt-Universität zu Berlin

Prof. Dr. Jan-Hendrik Olbertz

Dekan der Mathematisch-Naturwissenschaftlichen Fakultät

Prof. Dr. Elmar Kulke

Gutachter 1: Prof. Dr. Gunnar Nützmann

Gutachter 2: Prof. Dr. Tobias Krüger

Gutachter 3: Prof. Dr. Stefan Krause

Tag der mündlichen Prüfung: 19. September 2016

Declaration of independent work

I declare that I have completed the thesis independently using only the aids and tools specified. I have not applied for a doctor's degree in the doctoral subject elsewhere and do not hold ta corresponding doctor's degree. I have taken due note of the Faculty of Mathematics and Natural Sciences PhD regulations, published in the Official Gazette of Humboldt-Universität zu Berlin no 126/2014 on 18/11/2014.

Acknowledgement

Most of all I would to thanks my supervisors Dr. Jörg Lewandowski and Prof. Dr. Gunnar Nützmann, who gave me the freedom of following my personal research interests. Thanks also to Prof. Dr. Peter Engesgaard for the support in groundwater modeling and the opportunity for working in his group in Copenhagen.

Many thanks also to Dr. Georigy Kirillin and Dr. Christof Engelhardt, who stirred up my enthusiasm for lake physics and gave me another perspective on groundwater – surface water interaction.

I also want to thank Uwe Kaboth, who had an invaluable knowledge about the local and regional hydrogeology of the federal state of Brandenburg.

Special thanks also to all the people who supported me during my field work: Christine Sturm, Jörg Friedrich, Grit Siegert, Hauke Dämpfling, Adrian Brox, Sandra Bölck, Hendrik Schlichting, Bibiana Menosi, Hans-Jürgen Exner, Elke Zwirnmann, Gabriele Mohr and Michael Sachtleben.

I need to thank the whole team of the AQUALINK graduate school. They enabled me an insight into different scientific fields and were a great support during my whole PhD time. Especially, I like to say thanks to Christian Lehr for his support in statistics and the great cooperation.

Furthermore, I need to thank all of my colleagues and friends for the support and fruitful discussions during the last years, namely Karin Meinikmann, Stefanie Burkert, Sebastian Rudnick and Andrea Sacher.

Last but not least I thank my family and friends, who always believed in me and helped me to find my way.

Abstract

Although the point sources of nutrient input into surface water were significantly reduced in the past decades, there is still an ongoing eutrophication in the lakes and rivers in the North-Eastern German Lowlands. This is mainly related to the diffuse entering pathways. One relevant pathway might be the groundwater. However, the characterization of subsurface flow and its interaction with the surface water in lowlands is difficult. The main reasons for that are the heterogeneously deposited unconsolidated rocks, in which complex and nested aquifer systems (local, intermediate, and regional) establish. Hence, groundwater discharge occurs on different scales, whereas each scale is dominated by different drivers.

The aim of the presented thesis is to apply different methods to determine the parts of lowland aquifer systems which contribute mass, substances and energy into specific surface waters. Therefore, two approaches were used (1) a hydrogeological and (II) a limnological/hydrological one.

The focus of the *hydrogeological approach* was set on the characterization of groundwater flow systems on different spatial scales. On a small scale (10^2 m) a principle component analysis was conducted on time series of water level measurements in a river and in the adjacent groundwater of the floodplain. According to different responses of the groundwater on surface water induced pressure waves, areas with different hydraulic connectivity were identified. For the same aquifer, the small scale nutrient ($\leq 10^1$ m) distribution in the near-surface groundwater was also investigated. A close linkage between the nutrient distribution and the small-scale topography within the floodplain was detected. Both studies illustrate that comparatively “easy–to-measure” data in a high spatial and temporal resolution are sufficient for the detection of subsurface preferential flow paths as well as spots of potential nutrient sources. On a larger scale (10^3 m) a study was conducted which investigated the impact of groundwater leakage on the characteristics of a local flow system. Therefore, a simple 2D numerical groundwater model (steady state) was set up for the subsurface catchment of a lake. The model could illustrate that leakage lead to a decrease of the amount of groundwater, which enters the lake and, an increase of the length of the groundwater flow paths. Hence, groundwater leakage needs to be considered for the determination of local groundwater flow systems.

The *limnological approach* based on the hypothesis that physical and chemical differences between groundwater and lake water can be used to identify areas, where groundwater is exfiltrating. The presented studies tested if it is possible to use temperature measurements at the lake surface (thermal infrared imaging and *in situ* measurements) in spring, when the warmer groundwater is floating on the colder lake water. However, the comparison of the temperature measurements with hydrogeological and lake data, indicate that in the present case the observed temperature pattern are the result of lake internal processes. However, the aerial detection of groundwater spots should be possible at least for lakes with small volumes and intense groundwater discharge.

Zusammenfassung

Der Eutrophierungsprozess schreitet in vielen Oberflächengewässern im Norddeutschen Tiefland weiter voran, obwohl die punktuellen Quellen des externen Nährstoffeintrags in die Gewässer zum Großteil beseitigt wurden. Der Grund dafür ist der Eintrag aus diffusen Quellen, wie zum Beispiel dem Grundwasser. Die unterirdischen Fließsysteme und deren Interaktion mit den Vorflutern sind jedoch sehr schwer zu quantifizieren. Dies liegt vor allem an der räumlichen Heterogenität der abgelagerten Lockergesteine, in denen sich hydraulisch komplexe Aquifersysteme ausbilden. Der Grundwasserabfluss findet somit auf verschiedenen Skalen statt, wobei auf jeder Skala andere Steuerungsgrößen wirken.

Ziel der vorliegenden Arbeit ist es mittels verschiedener Ansätze die Bereiche in einem Tieflandsaquifer zu ermitteln, die zum Massen-, Stoff- und Energieeintrag in Oberflächengewässer beitragen. Dazu wurden zwei Herangehensweisen gewählt: (I) die hydrogeologische und (II) die limnologische/ hydrologische.

Der Schwerpunkt der Ersteren liegt auf der Charakterisierung der unterirdischen Fließsysteme auf verschiedenen räumlichen Ebenen. Auf kleinskaliger Ebene ($<10^3$ m) wurde mittels einer Hauptkomponentenanalyse von Zeitreihen von Grundwasser- und Oberflächenwasserständen diejenigen Bereiche eines Auenaquifers ermittelt, die eine besonders hohe hydraulische Konnektivität zum Vorfluter haben. Im selben Aquifer wurde auch das kleinskalige Vorkommen ($\leq 10^1$ m) der Nährstoffe im oberflächennahen Grundwasser untersucht. Hier wurde ein enger Zusammenhang zwischen kleinskaliger Topographie und der Nährstoffverteilung nachgewiesen. Beide Arbeiten zeigen, dass mit Hilfe vergleichsweiser einfacher Datengrundlagen präferentielle unterirdische Fließwege sowie die Lage potentieller Nährstoffquellen abgeschätzt werden können. Grundlage dafür ist eine hohe räumliche und zeitliche Auflösung der Daten. Auf großskaliger Ebene ($>10^3$ m) wurde eine Studie durchgeführt, die die Interaktion zwischen lokalem und regionalem Grundwasserfluss und deren Einfluss auf die Hydrologie eines tiefen, nährstoffarmen Sees untersucht. Dies erfolgte mittels eines nummerischen 2D Grundwassermodells (steady state) für das Grundwassereinzugsgebiet des Sees. Das Modell zeigt folgende Effekte der Tiefenversickerung auf das Grundwasserfließgeschehen im lokalen Fließsystem: Die Menge an Grundwasser, welche in den See entwässert verringert sich. Außerdem erzeugt der in die Tiefe gerichtete Gradient eine Verlängerung der unterirdischen Fließpfade. Somit konnte die Studie zeigen, dass bei Ermittlung des Grundwassereintrags in einen Vorfluter Tiefenversickerung berücksichtigt werden sollte.

Die limnologische Herangehensweise baut auf der Hypothese auf, dass physikalische und chemische Unterschiede zwischen Grund- und Oberflächenwasser genutzt werden können, um die Bereiche, in denen Grundwasserexfiltration in einem See stattfindet, zu identifizieren. In der vorliegenden Arbeit wurde getestet, ob dies an Hand von Temperaturmessungen an der Seeoberflächen (thermische Infrarotaufnahmen und *in situ* Messungen) möglich ist. Dafür wurden Messungen im Frühjahr nach der Vollzirkulation in zwei aufeinander folgenden Jahren durchgeführt. Der Vergleich der Oberflächenwassertemperaturen mit hydrogeologischen Daten und zusätzlichen Informationen zu seeinternen Prozessen zeigte jedoch für die zwei untersuchten Seen, dass bei seeinternen Prozesse die Temperaturverteilung an der Seeoberfläche dominieren. Es ist allerdings nicht auszuschließen, dass diese Methode zur Detektion von Grundwasserzustrom an Seen mit anderen Randbedingungen (kleineres Seevolumen, größerer Grundwasserzustrom) funktioniert.

Contents

Figures

Tables

1. Introduction

1.1 Groundwater discharge towards and within surface water bodies

In the past decades the ongoing eutrophication of surface water bodies in the North German Lowlands became an issue in public and science (e.g. LUGV, 2009; Hupfer and Nixdorf, 2011). After the reduction of point sources the diffusive entry pathway got the major role in nutrient import into lakes and rivers (e.g. Schindler, 2006). Beside diffuse imports via re-suspension from the sediment or atmospheric deposition (Schwoerbel and Brenelberger, 2005), groundwater can act as major source for dissolved substances like nutrients (e.g. Meinikmann, 2015). This fact points to a high connectivity between both water bodies. In lowland areas the connection is given by high permeable sediments forming large and thick aquifers where the surface waters are embedded. However, the physical, chemical and biological properties of groundwater and surface water differ a lot (Table 1.1-1), which is the main reason for investigating both water bodies separately in the past and the little knowledge about the consequences of the tide connection between both water bodies.

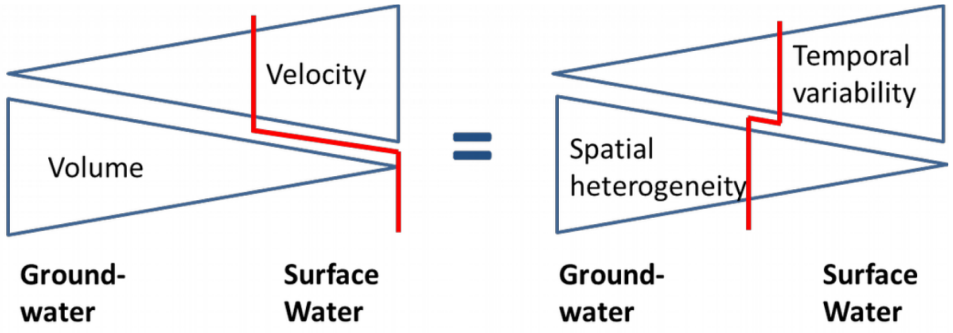

Figure 1.1-1: Concept of volume and velocity properties of groundwater and surface water and its relation to the spatial and temporal dimension. The red line represents the properties of the interface.

To understand the processes occurring in both systems requires knowledge about their spatial and temporal scales (Figure 1.1-1). The spatial extension of the groundwater is much larger in comparison to the surface waters. Beside the overall hydraulic gradient, the groundwater flow is determined by the sediment. Since this is not evenly distributed there is a large spatial heterogeneity of groundwater flow within an aquifer. For instance, Skøien and Blöschl (2003) analyzed the groundwater level fluctuations of 3539 wells for Austria and found that the relationship is limited to 7 km. Furthermore, the sediments cause a slowdown of the groundwater flow velocity. This also implies that the reaction on

short term temporal fluctuations is small and dampened in comparison to the meteorological input. The surface waters behave in the opposite way. The spatial heterogeneity is smaller and also easier to determine as for aquifer systems whereas the short-term temporal variability is increased due to the direct reaction of meteorological forces like precipitation, snow melt or wind.

Table 1.1-1: Examples for characteristic physical, chemical and biological properties of groundwater and surface water bodies in temperate regions

	Groundwater	**Surface water**	
		river	lake
Physical properties			
general flow characteristics	laminar	turbulent	turbulent
flow velocity scale [m s^{-1}]	≤ 10^{-3}	1 - 10^{1}	10^{-1}
average residence times	large	small	medium
temperature	constant	seasonal variability	Epilimnion: seasonal variability Hypolimnion: constant
Chemical properties			
redox conditions	Decreasing oxygen with depths	oxygenated	Oxygenated during mixis, decreasing oxygen with depth during stratification
Biological properties			
dominant trophy	heterotrophic	autotrophic & heterotrophic	autotrophic & heterotrophic
metabolism	decreased due to low temperature, no light and less organic matter	high, depending on the water temperature	high, depending on the water temperature and oxygen saturation

Since both systems are different in characteristics and behavior they share an interface, which is characterized by sharp biogeochemical and physical gradients. So even if this interface is comparably small (Figure 1.1-1), the flow and processes such as microbial turnover, storage and release of substances are faster than in the adjacent groundwater. This lead to an increased interest in science during the past decades (e.g. Winter, 1995; Woessner, 2000; Fleckenstein et al., 2010; Wondzell, 2015). The results can be summarized as follows:

(1) The exchange between groundwater and surfaces water does not occur over the whole interface and is further concentrated in specific areas (*spatial heterogeneity*) (McBride and Pfannkuch, 1975; Krause et al., 2014).

(2) Even if a specific area is known, there are *temporal variations* according to the season and the general weather situation (Winter, 2005).

(3) The significance of the impact also depends on the *size and the volume* of the surface water and the adjacent groundwater body (Rosenberry et al., 2015).

(4) The *anthropogenic manipulation* of surface waters superimposes the complex natural conditions (Winter et al., 1999; Gessner et al., 2014).

As all four dimensions are highly dynamic, recent research focused on smaller spatial and temporal scales to understand the detailed processes occurring at the interface (Fleckenstein et al., 2010). Hence, there is basic knowledge about small to medium scale flow pattern within the interface but there are fewer answers on the following questions:

1. Where does the groundwater entering the interface come from? So it needs to be clarified in which way different source areas contribute to the groundwater exfiltration into surface waters.

2. When the water has passed the interface, where does it go and what kind of effects does it have on the surface water?

Answers to these questions would improve management measures or definition of protection areas.

The question concerning the source of the groundwater is of special interest for lowland areas, as bigger a catchment results in a larger possibility of entering pathways. Tóth (1963) illustrated that there is a layered system within unconfined aquifers. He described a nested gravity driven groundwater flow system, which is controlled by the topography of the water table and the sediment. He also identified three main flow systems: local, intermediate and regional. Winter (1983) could further illustrate that these flow systems are not constant in time and space. Their spatial extension

mainly depend on the recharge conditions and, therefore, on climatic factors. These findings imply that water recharging the groundwater within a specific catchment does not necessarily discharge into the closest surface water. Assuming that there is a decreasing anthropogenic impact from local to regional flow systems, the water supply from deeper flow systems would be able to buffer the import of substances by dilution (Falkenmark and Allard, 1991). However, the determination of the origin of the exfiltrating groundwater is still a challenge. Nowadays it is possible to distinguish clearly between infiltrated surface water and “real” groundwater close to the shoreline e.g. by measuring the stable isotopes relation of δO^{18} and deuterium (Dincer, 1968; Krabbenhoft et al., 1994; Hofmann et al. 2008). This allows the clear identification of exfiltration areas of groundwater into the surface water and the infiltration areas of surface water into the aquifer. However, using natural tracers like stable isotopes always requires a significant difference between the observed compartments to distinguish the flow path (Käss, 2004), which is difficult to determine in a single hydrological compartment by simple field investigation. In most cases, flow systems were determined by multi-factorial analysis (e.g. Menció et al. 2012) and by numerical groundwater modeling mostly in combination with chemical transport modeling (e.g. Blair et al., 1991; Frapporti et al, 1995; Hunt et al., 2001; Frind et al., 2002). The second approach allows the evaluation of different driving and controlling variables of the system, like the hydraulic conductivity, anisotropy and groundwater recharge. Nevertheless, there are still large uncertainties according to choice of the right variable or variable combination to explain a measured parameter (Frapporti et al., 1995). Furthermore, also models are related to a specific spatial scale and temporal resolution depending on the available input data and the computational effort (Blöschl, 2011).

Beside the determination of the size of the local system and the loadings in this part of the aquifer, knowledge about the groundwater *flow paths* is required. These are mainly determined by the sediments within an aquifer (e.g. Freeze and Cherry, 1979; Hölting and Coldewey, 2009). Already small variations in the grain size composition lead to significant differences in groundwater flow, due to higher and lower hydraulic resistances. This is especially a challenge for areas connected to surface waters, like riverine floodplains. Since these parts of the aquifer were formed by the river activity itself it is characterized by its patchiness (e.g. Bridge, 2003). Hence, the characterization of the sediment distributions in these areas is still a challenge. Classical methods like drill logging deliver high resolved information at the point scale, but are coarse at the spatial scale. Geophysical approaches cover larger areas, but on the other hand they are cost-intensive, sometimes difficult to interpret and difficult to handle in hardly accessible areas.

The second question is dealing with the detection of groundwater within the surface water and the groundwater impact on it. From marine settings it is known, that exfiltration areas can be detected by temperature and conductivity measurements. This is based on the fact that the density of the marine

waters is higher due to the salinity and the groundwater is floating on the top of the surface water (e.g. Danielescu et al. 2009, Peterson et al., 2009, Garcia-Solsona et al., 2010). For freshwater systems it is assumed that the detection depends on the type of surface water. Due to the highly turbulent character of streams and rivers, the entering groundwater is mixed immediately with the surface water. However, a heat signal of the groundwater is still detectable if the stream is small and the groundwater discharge is large enough (Torgersen et al., 2001; Schuetz and Weiler, 2011). This is different for lakes. Depending on the thermal cycle of the lake, inflowing water will float in a specific layer (Peeters and Kipfer, 2009), e.g. for groundwater this can be shown by measuring radon concentrations along a vertical depth profile (Kluge et al., 2007). Radon concentration is a natural tracer for groundwater. Its half-life is about 3.8 days and in the surface water there is little production of radon. Additionally, as soon radon-rich water gets in contact with air it outgases into the atmosphere. Therefore, surface waters contain only small radon concentration in comparison to groundwater. The study of Kluge et al. (2007) could show that there was an enrichment of radon concentration in the thermocline, which was related to discharging groundwater. So if it is possible to detect the areas of groundwater exfiltration within a surface water body it would also narrow the source areas of the entering groundwater (Lewandowski et al. 2013, study IV).

1.2 Research objectives and hypothesis

The overall aim of the present thesis is to contribute to the general understanding of the dynamics of groundwater – surface water interactions in temperate low land areas. The focus was set on the determination of subsurface areas exfiltrating into specific surface water and the detection of the areas, where groundwater exfiltration occurs in the surface water. Therefore, two different approaches were used: (I) The hydrogeological and (II) The limnological/ hydrological approach.

The hydrogeological approach aimed in (1) the identification of subsurface flow paths towards rivers and lakes and, (2) the determination of the extension of groundwater flow systems contributing to surface water. Therefore, it is necessary to consider the scale dependent control parameters of groundwater flow. On small scale ($\leq 10^3$ m) controlling parameters are sediment, topography, vegetation and water stage fluctuations of the river. For instance, in floodplains the parameters are spatially heterogeneous distributed due to fluvio-geomorphodynamics. As a result of the patchiness, floodplains are highly effective concerning nutrient retention, turnover and transport. However, it is still a challenge to identify the parameter distribution in a sufficient good resolution, e.g. to detect areas with higher or poorer hydraulic connection to surface water.

Hypothesis (1) assumes a linkage between small-scale parameters impacting groundwater flow and nutrient distribution within lowland floodplains. If this is the case, it would be sufficient to capture one parameter to get a rough idea of subsurface flow paths and potential sources for nutrients.

With increasing scale ($>> 10^3$ m) the position of the surface water within a landscape decides about the size of the subsurface catchment (Tóth, 1963, Winter et al., 2003); the topographically lower a surface water is situated, the more complex is the groundwater flow towards those water bodies. Hence, lakes and rivers in head areas - where groundwater recharge occur - receive water only from local groundwater catchment, which extension can be determined easily. However, groundwater leakage into deeper aquifers is present in head waters, which should affect the extension of the local flow system.

Hypothesis (2) says that groundwater leakage into deeper aquifers needs to be considered for the determination of local groundwater flow systems of a lake in lowland head waters.

The limnological/ hydrological objective aims in determining areas where groundwater exfiltrates into surface water. Therefore, it is assumed, that there are different physical and chemical properties of groundwater and surface water which can be used as tracer. In the present thesis temperature was used.

Hypothesis (3) assumed that groundwater of a constant temperature of 10 °C will float on the surface of a lake, when: (a) The lake starts to stratify after spring overturn and has surface temperatures of >4 °C and < 10 °C. (b) There is no wind and (c) The heat flux is from the atmosphere to the surface water body (air temperature > lake temperature). Airborne methods such as thermal infrared imaging can be used for detection.

2. Material and Methods

2.1 North Eastern German Lowlands

The North Eastern Lowlands of Germany were formed during the past ice ages; the Saalian ice age (~130.000 years before present) dominates the southern and the western part, whereas the Weichselian ice age (~10.000 years before present) formed the northern and the eastern part (Figure 2.1-1). The glacial deposits consist mainly of glacial till and (glaci)-fluvial sand layers of several tens to hundreds meter thickness (Lischeid et al., 2010) with decreasing thickness from north to the south (Jordan and Weder, 1988). Since the unconsolidated sediments are well permeable, the portion of surface water runoff (5%) is much smaller than the subsurface runoff (95%) (Merz and Pekdeger, 2011). This implies a large system of confined and unconfined aquifers with different flow directions and residence times (Lischeid et al., 2010).

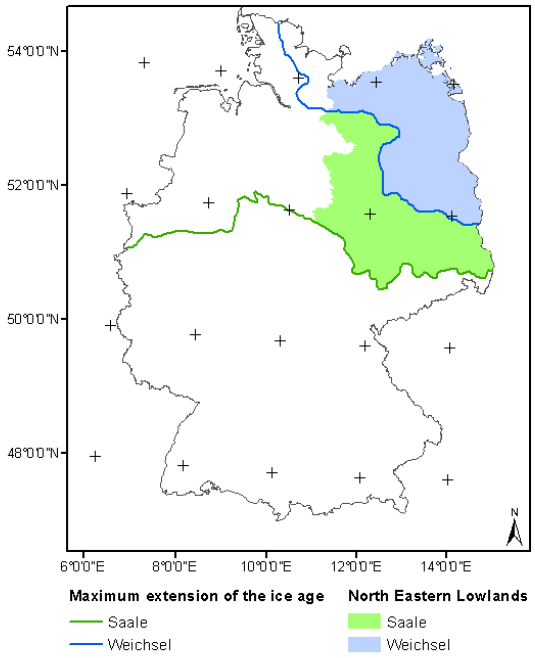

Figure 2.1-1: Location of the North-Eastern German Lowlands and subdivision into the different kind of landscapes and hydrological regimes of the Saalian and Weichselian ice ages.

The main difference between the northern and the southern part of the North Eastern Lowlands can be addressed to the geomorphology and the related surface water network. The Saalian area is characterized a fairly flat, only slightly undulating topography. This is the result of the erosion of former glacial formation and wind induced sedimentation during the Weichselian ice age, when this area was situated in the periglacial. The predominant surface water network consists of large perennial

rivers with extensive floodplains and smaller streams, which can be periodic or episodic. The main discharge area is the Northern Sea. In contrast, the Weichselian part is dominated by comparably young glacial formations (e.g. end moraines, outwash plains). Hence, a surface water network is underdeveloped and the discharge areas are predominated by closed basins, like lakes and wetlands. Rivers are mainly situated in former melt water channels. The discharge is entering into the Northern as well as the Baltic Sea.

As a consequence of the highly permeable sediment and the flat topography, the hydraulic gradient is low (in average 0.1‰ for surface runoff) (Lischeid and Natkhin, 2011) resulting in also low flow velocities and a high water retention capacity. This also indicates a slow substance transport, e.g. nutrients or contaminants. Therefore, they have a long reaction and retention time, which is a big advantage as long as the filter capacities of the sediment are not exhausted (Meinikmann et al., 2015).

The climatic conditions of this landscape are comparably dry. The average precipitation is about 600 mm per year and the evapotranspiration is about 500 mm per year. Hence, the average recharge is only about 100 mm (Lischeid and Natkhin, 2011). Viewed in the context of climate change, calculations indicate an increasing evaporation. Meaning the recharge will get even worse.

The land use in this area is dominated by agriculture (~ 55 %) and forest (~ 30 %) (DESTATIS, 2014). The latter is mainly dominated by pines (Pinus silvestris) (Lischeid and Natkhin, 2011) which have the potential to reduce the groundwater recharge to 10 % (Schindler et al., 2008). Furthermore, there is a decrease of groundwater and surface water levels in the past decades induced by drainage measures: closed basin lakes were connected by channels, rivers were straightened and wetlands drained.

In the presented thesis three different study sides situated in different parts of the lowlands were investigated (Figure 2.1-2). All sides belong to the warm and temperate climate region (Köppen, 1936) (Table 2.1-1). For detailed description see the different studies.

Table 2.1-1: Long-term average of precipitation and temperature from 1981-2010 for weather stations close to the study sites (data source: Deutscher Wetterdienst, 2014)

Station	**N**	**E**	**P**	**T**
			[mm a^{-1}]	**[°C]**
Lindenberg	52°12’30.568’’	14°07’04.703’’	576	9.2
Neuruppin	54°54’13.334’’	12°48’25.938	562	9.2
Seehausen	52° 53' 28.09"	11° 43' 46.909"	353	9.2

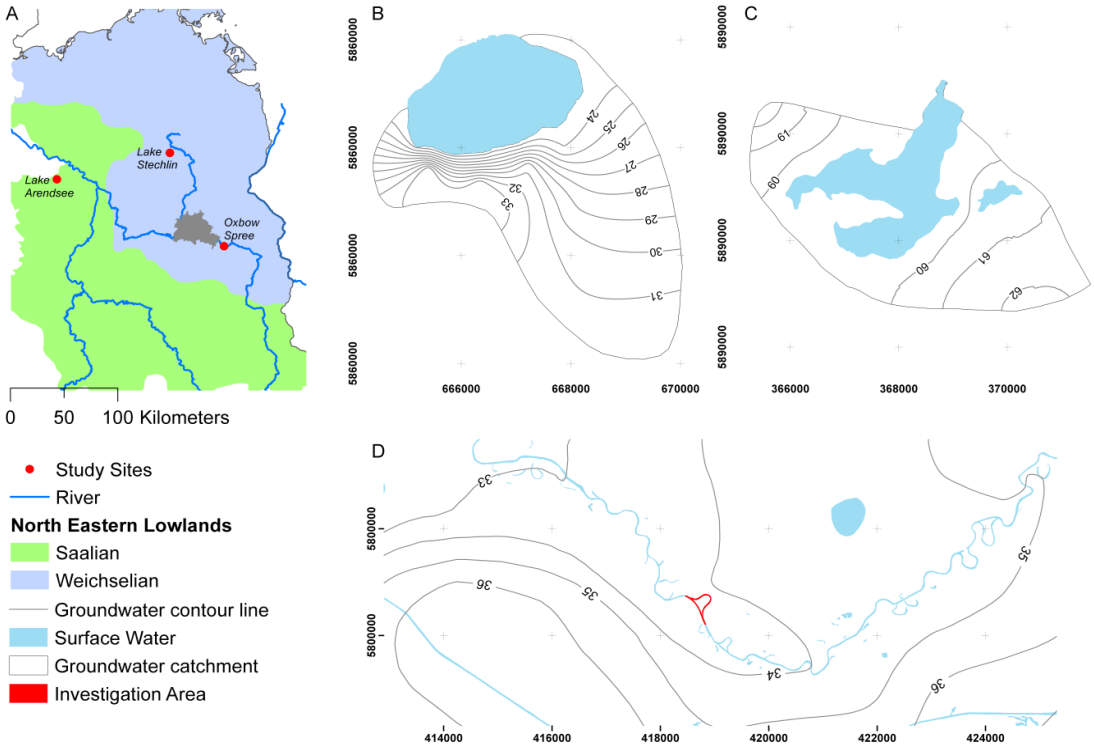

Figure 2.1-2: Position of the three study sites within in the North-Eastern German Lowlands (A). Subsurface catchment of the upper aquifer and the interpolated contour lines for groundwater heads for Lake Arendsee (B), Lake Stechlin (C) and the investigated oxbow of the river Spree (D). The groundwater data from Lake Arendsee ground on Meinikmann et al. (2013). The determination of the groundwater catchment and contour lines for Lake Stechlin are based on available data from the Landesamt für Umwelt, Gesundheit und Verbraucherschutz (LUGV) Brandenburg (2012). The groundwater contour lines for the River Spree were made available from the LUGV (2012). The data from Lake Arendsee are projected in WGS 84 UTM 32N and in WGS 84 UTM 33N for Lake Stechlin and the oxbow of the river Spree.

2.1.1 Lake Arendsee

Lake Arendsee (N52°53’28.3’’ E11°28’31.1’’) is an eutrophic lake in the Saalian moraine area. It was formed by a collapse of a salt dome about 11.000 BC (Leineweber et al., 2009). Hence, it is the only lake in this area. It is mainly characterized by an almost circular shape; steep in-lake slopes to the shorelines and a flat bottom.

The groundwater catchment is about 15 km² big and is dominated by fine sands and interstratified clay layers (Meinikmann et al., 2013). The Holocene sediments are in direct contact to a Miocene layer, which appears to the surface at the western part of the catchment. Due to the shallow topography, the

unsaturated zone is small (< 10 m), with an exception in the southern part of the catchment, which is covered by a dune belt.

The catchment is covered mainly by forest (35%), cropland (35%), grassland (15%) and urban area (15%) (Meinikmann et al., 2013). The agricultural used areas are drained by drainage ditches, which enter the lake at four different points. However, their impact on the lake water balance is comparably small (8 – 14 %), but leads to a drastic decrease in groundwater recharge (~ 30 %) for the drained areas (Meinikmann et al., 2013).

2.1.2 Lake Stechlin

Lake Stechlin (N53° 9' 6.343" E13° 1' 38.644") is one of the last oligotrophic lakes at the Mecklenburg Lake District in the North Eastern Lowlands. The lake is situated in two former glacial melt water channels, where dead ice remained after withdrawal of the inland ice sheet (Feierabend and Koschel, 2011). Due to the channels, the lake is very narrow and steep. The catchment was formed by this channels and the surrounding glacial outwash plain, which results in an unconfined aquifer with a thickness of up to 40 m. The aquifer sediments are comparably homogeneous and have a high permeability (Ginzel and Kaboth, 1999). However, there is a large variability of the thickness of the unsaturated zone: It is about 0.3 m close to the lake and about 30 m at the outwash plain. Nevertheless, the hydrogeological situation in this area is quite complicated. Holzbecher (2001) could illustrate that the groundwater catchment contracts or extents in dependency on the overall meteorological conditions (Figure 2.1-3) and measures an average of 11 km². Hence, there are only two areas which constantly deliver groundwater towards the lake: the north-western and south-eastern outwash plains.

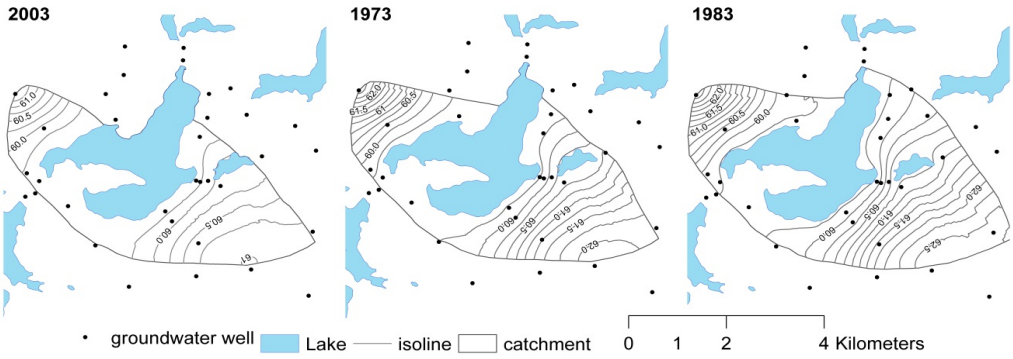

Figure 2.1-3: Interpolation of the average annual catchment according to the findings of Holzbecher (2001) for three years with different precipitation condition: dry (2003); average (1973) and wet (1983).

2.1.3 Oxbow site at the River Spree

At the study site the River Spree (N52°22’06’’ E13°48’25’’) follows the former course of the glacial valley. During the ice age, coarse sandy sediments were accumulated, which were superimposed by fluvial sediments during the Pleistocene (Driescher, 1999). Together, this forms an unconfined aquifer of about 20 m thickness. Since the study site is directly located within the floodplain of the river, the unsaturated zone is very shallow and reaches from 0 of 1.5 m (Lewandowski et al. 2009).

The site can be described as artificial island, which was formed around 1960, when the river was straightened and the meander was cut off. This was done according to melioration measures and resulted in an increase of the surface water discharge and a decrease of the overall groundwater level in the whole area. Since the discharge of the river is also regulated via a weir, the natural discharge is more homogeneous within a year as it would be under natural conditions. The floodplain is used as agricultural meadow.

2.2 Identification of subsurface flow paths & flow systems

2.2.1 Water level fluctuations

Water level measurements are the basis for understanding surface water and groundwater systems. Even if surface water hydrology and hydrogeology are separate scientific fields, these data were and are always available when answering hydrological questions. The main reason is that water levels are easily measureable parameter providing a lot of information, e.g. about the flow conditions or allowing the determination of subsurface catchments (Hölting and Coldeway, 2009).

Following the law of Pascal for hydrostatic pressure $p = \rho g h$, with the density of the water, the acceleration of the earth and the water level above a given datum h, it can be seen that water level and hydrostatic pressure directly depend on each other. This implies that processes inducing a change in pressure will also cause a water level change (Todd, 1980). In groundwater the most common process inducing a water level change is groundwater recharge; however there are a lot of other possibilities such as changing atmospheric pressure, tides, earthquakes, irrigation and streamflow (Todd, 1980) with the latter being important for the groundwater–surface water interaction. Some studies show that there is a strong correlation between surface water levels and the water levels in the adjacent groundwater (e.g. Van Geer, 1987, Seibert et al. 2003; Lewandowski et al., 2009). Lewandowski et al. (2009) illustrate that this strong correlation is not the result of water transport towards or from the aquifer. Rather the surface water table fluctuations induce pressure waves which are traveling through the aquifer. However, the spread of the pressure wave depends on the period and the amplitude of the

water level fluctuation as well as on the transmissivity and the storage coefficient of the aquifer (Ferris, 1951). With increasing distance to the surface water the pressure wave dampens.

Hence, analyzing of surface water and groundwater levels in an area where both are closely connected should allow conclusions on the sediment properties an aquifer. This was done by a principle component analysis for a lowland river floodplain equipped with 15 groundwater observation wells including level loggers and 2 river stages recorders (Lehr et al., 2015, study I).

2.2.2 Nutrients and hydromorphological characteristics

The use of tracers in hydro(geo-)logy to determine flow direction and flow velocity is an accepted and often used scientific method (Davis et al., 1980). There is a wide range of possibilities to do so. Either by adding artificial tracers (e.g. chloride, dye or fluorescein) or using natural tracers (e.g. stable isotopes, nitrate). The main advantages for natural tracers are that they are measurable over a larger range of scales and deliver insights into the spatial and temporal variability of the hydrological system, but beside this they do not disturb the natural conditions of the groundwater flow (Moser, 2004). However, the application of these kind of tracers requires natural differences in concentrations, e.g. of surface water, soil water, groundwater (Käss, 2004). Therefore, the difference has to be investigated first, before these tracers can be used. Natural tracers are distinguished between: reactive and non-reactive. The first are useful to determine the flow path and the last are more applicable for estimating residence times (Lischeid, 2008).

Nutrient concentrations in the groundwater (e.g. dissolved phosphate, ammonium, and nitrate) depend on: (1) the source (e.g. the amount of degradable organic material, fertilizer), (2) the binding capacity of the sediment (3) the redox conditions, (4) the demand of the vegetation, (5) the temperature and (6) the flow velocity or reaction time, respectively. The concentrations of nutrients in the groundwater can vary a lot and do not fulfill the requirements of a perfect tracer (compare Davis et al., 1980; Käss, 2004). Nevertheless, the spatial distribution of nutrients allow insights into turnover and transport processes, assuming that the temporal variations in shallow aquifers are small in comparison to the spatial variations (compare Bjerg and Christensen, 1992, Lewandowski and Nützmann, 2010, Schot and Pieber, 2012).Accordingly, the flow direction can be estimated.

In study II (Pöschke et al., 2015 b) the distribution of the phosphate and nitrogen concentrations in a shallow floodplain aquifer were related to small scale topography and sediment structure. This was done by multi-level sampling (Graham, 2009) in a vertical spatial resolution of 10^{-1} m over a depth range of 2.4 m. The samplers were installed at 6 locations within the floodplain with an average distance of 50 m in between. Additionally, temporary piezometers with a horizontal distance of 3 m

were installed in the upper meter of the groundwater along a transect. The results were related to a digital elevation model with a spatial resolution of one meter and ground penetrating radar images.

2.2.3 Groundwater modeling

An adequate tool for determining the pattern of groundwater flow from a catchment towards surface water is numerical groundwater modeling. It delivers basic insights on the general distributions of e.g. flow paths and flow timescales. Moreover, it is helpful for the identification of hydrogeological characteristic areas within the catchment as well as the estimation of the reaction of the hydrological system on different impacts, like climate change or anthropogenic water extraction.

Besides the improved computational opportunities for numerical simulations in the past years, the data basis which can be used for modeling has also increased. Now, long term observations of groundwater and surface water levels allow better identification of system drivers and therefore improve the calibration process (Hill and Tiedeman, 2007). Additionally, the advanced data basis can be used to identify the drivers for changes in subsurface and surface flow processes.

In study III a simple 2D groundwater modeling approach was used to determine the impact of the groundwater leakage into deeper aquifers on groundwater discharge towards Lake Stechlin in NE Germany. At first, a conceptual model was developed to determine the factors driving the groundwater flow towards the lake. Therefore, time series of monthly water levels for lake and groundwater were available from 1957 – 2012. Furthermore, information of topography and geology and meteorological data (precipitation, groundwater recharge) was used. The conceptual model assumes that there is a subsurface flow towards deeper aquifers, due to abrupt changes in the hydraulic gradient in the catchment and measured high hydraulic gradient towards the depth. The implemented numerical model considered different hydraulic conductivities and different leakage areas and leakage amounts into deeper aquifers. At the end the model results were compared to measured groundwater exfiltration. Furthermore, the realistic model results were analysed for groundwater flow path and changes in the catchment extension.

2.3 Impact of groundwater on surface water

2.3.1 Temperature as tracer

A measured temperature of a gas, fluid or solid matter is a result of the (1) initial temperature, (2) the physical properties of the compartment and (3) the amount of external energy/heat input. There are two important external heat sources for natural water bodies: the natural heat of the earth and the solar

radiation of the sun. The first is characterized by an almost linear increase of temperature with increasing depth in the subsurface (1°C/ 20 – 40m) (Anderson, 2005). The importance of the geothermal heat source for water bodies depends on the geologic area (geologic active regions vs. inactive region), the depth of the water body and the thermal properties (e.g. Magri et al. 2015). In contrast, the intensity and temporal variability of the solar radiation depends on the longitude, the continentality and the elevation (Malberg, 1997). In the case of aquatic systems, the physical properties affecting the heat distribution are the heat capacity and conductivity of the water and the surrounding sediment, the velocity and the volume of the water.

Hence, a measured temperature is always a mixed signal of the physical properties and the variability of the heat input source. Still, it is hard to identify the driving parameters which result in the measured value. Therefore, temperature measurements can be addressed as integrative. This provides a usage for different spatial and temporal scales and therefore, it is a useful tool to identify flow pattern in groundwater (e.g. Stonestrom and Constantz, 2003; Miyakoshi et al. 2003). In the past decades, heat was also used as a tracer to detect groundwater – surface water interactions based on the assumption that groundwater temperatures are more or less constant throughout the year and the surface water underlies an annual temperature cycle (e.g. Schmidt et al. 2006, Anderson, 2005).

Another important characteristic of temperatures is the continuous distribution in time and space. It is always questionable if a point measurement is an adequate representation, especially for flowing systems. Hence, an extensive detection of thermal structures would allow conclusions, if a point measurement were representative for the whole aquatic system at a given scale. One possibility is aerial thermal infrared imagery (TIR) (Beck, 2006). This technique is able to detect thermal patterns at a high resolved spatial scale by temporal snapshots. However, as mentioned before, temperatures are mixed signals and have to be interpreted carefully.

In the present study temperature was used to detect surface temperature pattern within lakes and relate this to a specific process. The first study hypothesized that groundwater discharge areas are detectable by TIR when the groundwater is less dense than the surface water and is floating on the surface and there are windless conditions (Lewandowski et al. 2013; study IV). The second study investigates the effect of the wind on the skin surface temperature distribution. Therefore, two lakes were investigated by TIR, lake surface temperature and temperature depth measurements (Pöschke et al., 2015 a; study V).

3. Studies

3.1 Survey of studies and authors contribution

Lehr, C., Pöschke, F., Lewandowski, J., Lischeid, G. 2015. A novel method to evaluate the effect of a stream restoration on the spatial pattern of hydraulic connection of stream and groundwater. Journal of Hydrology. 527. 394 – 401.

The first study (I) addresses a larger spatial scale of the same floodplain (100 m). Measured water level of groundwater and surface waters were analyzed by a principle component analysis (PCA) to describe the spatial variability of the hydraulic connectivity between groundwater and surface water (hypothesis 1).

Contribution: I interpreted the results (30%) and wrote the paper (30%).

Pöschke, F., Lewandowski, J., Nützmann, G. 2015. Impact of alluvial structures on small-scale nutrient heterogeneities in near-surface groundwater. Ecohydrology. 8. 682-694

The study (II) is dealing with near surface groundwater in a floodplain aquifer. The small - scale distribution (10 cm to 1 m) of redox sensitive parameters and sediments was used to characterize flow and redox process in a restricted area of a local flow system (hypothesis 1)

Contribution: I conceptualized and designed the study (60%), performed the field work and analytics (70%), interpreted the results (70%) and wrote the paper (80%).

Pöschke, F., Nützmann, G., Engesgaard, P., Lewandowski, J. The hole in the aquifer - effects of groundwater leakage on the local groundwater flow system of a lake (Draft)

The manuscript (study III) present the results of a numerical groundwater modeling approach to estimate the effects of groundwater leaking on the groundwater discharge towards a lake. The results indicate, that leaking might influence the local flow system by reducing the amount of groundwater entering the lake and increases the traveling time of the groundwater. (hypothesis 2).

Contribution: I conceptualized and designed the study (50%), performed the field work and the modeling (80%), interpreted the results (70%) and wrote the paper (90%).

Lewandowksi, J., Meinikmann, K., Ruhtz, T., Pöschke, F., Kirillin, G. 2013. Localization of lacustrine groundwater discharge (LGD) by airborne measurement of thermal infrared radiation. Remote Sensing of Environment. 138. 119 – 125. DOI: 10.1016/j.rse.2013.07.005

The study (IV) presents a study conducted at a lake with the aim to identify the groundwater exfiltration areas on the lake surface by thermal infrared imaging at the beginning of lake stratification period (hypothesis 3).

Contribution: I performed the field work (50 %), interpreted the results (20 %) and wrote the paper (10 %).

Pöschke, F., Lewandowski, J., Engelhardt, C., Preuß, K., Oczipka, M., Ruhtz, T., Kirillin, G. 2015. Upwelling of deep water during thermal stratification onset - A major mechanism of vertical transport in small temperate lakes in spring? Water Resources Research. 51. 9612 – 9627.

The study (V) presents also the usage of thermal infrared imaging. In contrast to Paper III it end up with the result, that wind driven processes predominate the lake surface temperature pattern within two lakes (hypothesis 3).

Contribution: I conceptualized and designed the study (50%), performed the field work (80%), interpreted the results (70%) and wrote most of the paper (65%).

3.2 A novel method to evaluate the effect of a stream restoration on the spatial pattern of hydraulic connection of stream and groundwater

Christian Lehr[1,2], Franziska Pöschke[3,4], Jörg Lewandowski[3,4], Gunnar Lischeid[1,2]

[1] Leibniz Centre for Agricultural and Landscape Research (ZALF) Institute of Landscape Hydrology

[2] University of Potsdam, Institute of Earth and Environmental Science

[3] Institute of Freshwater Ecology and Inland Fisheries, Ecohydrology Department

[4] Humbodt University Berlin, Geography Department,

Published in: Journal of Hydrology

Lehr, C., Pöschke, F., Lewandowski, J., Lischeid, G. 2015. A novel method to evaluate the effect of a stream restoration on the spatial pattern of hydraulic connection of stream and groundwater. Journal of Hydrology. 527. 394 – 401.

http://dx.doi.org/10.1016/j.jhydrol.2015.04.075

© 2015 The Authors. Published by Elsevier B.V.

This is an open access article under the CC BY license (http://creativecommons.org/licenses/by/4.0/)

Abstract

Stream restoration aims at an enhancement of ecological habitats, an increase of water retention within a landscape and sometimes even at an improvement of biogeochemical functions of lotic ecosystems. For the latter, good exchange between groundwater and stream water is often considered to be of major importance. In this study hydraulic connectivity between river and aquifer was investigated for a four years period, covering the restoration of an old oxbow after the second year. The oxbow became reconnected to the stream and the clogging layer in the oxbow was excavated. We expected increasing hydraulic connectivity between oxbow and aquifer after restoration of the stream, and decreasing hydraulic connectivity for the former shortcut due to increased clogging. To test that hypothesis, the spatial and temporal characteristics of the coupled groundwater-stream water system before and after the restoration were analyzed by principal component analyses of time series of groundwater heads and stream water levels. The first component depicted between 53% and 70% of the total variance in the dataset for the different years. It captured the propagation of the pressure signal induced by stream water level fluctuations throughout the adjacent aquifer. Thus it could be used as a measure of hydraulic connectivity between stream and aquifer. During the first year, the impact of stream water level fluctuations decreased with distance from the regulated river (shortcut), whereas the hydraulic connection of the oxbow to the adjacent aquifer was very low. After restoration of the stream we observed a slight but not significant increase of hydraulic connectivity in the oxbow in the second year after restoration, but no change for the former shortcut. There is some evidence that the pattern of hydraulic connectivity at the study site is by far more determined by the natural heterogeneity of hydraulic conductivities of the floodplain sediments and the initial construction of the shortcut rather than by the clogging layer in the oxbow.

3.2.1 Introduction

In the past decades there has been an increasing effort on research and practice according to the restoration of rivers and their floodplains. The main reasons for that are the valuation of river ecosystems as place for species conservation and habitat diversity, recreational and aesthetic purposes, flood protection, enhancing the potential of contaminant deposition and nutrient degradation (Bernhardt et al., 2007; Kondolf et al., 2007; Hester and Gooseff, 2010; Pander and Geist, 2013; Schirmer et al., 2013). This is also reflected in a growing body of legislative directives (Pander and Geist, 2013; Schirmer et al., 2013), e.g. the EU Water Framework Directive demands a good chemical and ecological status of groundwater and surface water (European Commission, 2000). The chemical and ecological status of surface waters is impacted by the adjacent connected aquifer and vice versa. Hence both waters have to be considered when assessing water qualities of either of them. Nevertheless, in river restoration practice the measures most often focus solely on surface waters, whereas the connection of the river and the groundwater below the river bed and the adjacent floodplain is often neglected (Boulton, 2007; Boulton et al., 2010; Hester and Gooseff, 2010). Previous studies identified the transition zone between stream water and groundwater, the hyporheic zone, as highly relevant for mass exchange, residence time of water and substances in the stream or in the sediment, the chemical and metabolic turnover and in general as crucial for water quality (Brunke and Gonser, 1997; Sophocleous, 2002; Boulton, 2007). The spatial extent of the hyporheic zone is mainly determined by two drivers, the hydraulic gradient between the river and the groundwater and the sediment structure (Kasahara et al., 2009), especially the permeability of the stream bed and aquifer sediments (Woessner, 2000; Kalbus et al., 2009). Therefore, clogging of the stream bed, i.e. the sealing of the stream bed with sediments of very low hydraulic conductivity, has been identified as major problem for exchange of surface water and groundwater and the related ecological functions of the hyporheic zone (Sophocleous et al., 1995; Brunke and Gonser, 1997; Sophocleous, 2002).

Fluxes are spatially and temporally heterogeneous due to the spatial heterogeneity of hydraulic conductivity of the sedimentsand spatial and temporal variability of hydraulic gradients (Woessner, 2000; Malard et al., 2002; Krause et al., 2011; Binley et al., 2013). Different methods are available to estimate fluxes across the interface in a river-groundwater system (Kalbus et al., 2006). Selective approaches, such as vertical temperature profiles (e.g. Schmidt et al., 2006; Anibas et al., 2009), heat pulse sensors (e.g. Lewandowski et al., 2011), hydraulic gradients (e.g. Krause et al., 2012) or seepage meters (e.g. Rosenberry and LaBaugh, 2008) are able to monitor the flux over time for a specific point, but it is not possible to draw conclusions for a whole river section.

A method to capture larger areas is distributed temperature sensing (DTS) (e.g. Selker et al., 2006a,b; Krause and Blume, 2013), which is able to detect spots with intense groundwater ex- and infiltration. Another option is to use natural or artificial tracers to determine the degree of interactions (e.g. Négrel

et al., 2003; Cox et al., 2007). Beside the different measuring techniques, numerical modelling was often used to examine groundwater-surface water interactions (e.g. Nützmann et al., 2013). One advantage of the latter method is that it does not have to be restricted on the hyporheic zone itself and can include the adjacent floodplain. All methods have in common the large temporal and monetary effort and in most case the restriction to certain areas or certain seasons. Furthermore, most approaches rely on information about hydraulic conductivity or related parameters, which are hard to estimate and result in uncertainties.

Another method which directly estimates the spatial distribution of the hydraulic properties of the sediments is hydraulic tomography (e.g. Yeh and Liu, 2000; Zhu and Yeh, 2005). In a network of spatially distributed wells the response to an artificial pressure signal induced by a pump at one well is recorded at all other wells. The procedure is repeated by sequentially circulating the pump through the other wells. With packers each well can be segregated in different depth intervals and by circulating the pump through the depth intervals at all wells the depth integrated estimation of hydraulic properties can be enhanced to a 3D-tomography (Yeh and Liu, 2000; Cardiff and Barrash, 2011). With an inverse model the spatial distribution of the hydraulic properties of the aquifer is estimated from the interplay of all the observed hydraulic head series. Up to now most of the non-numerical hydraulic tomography studies aimed to map the small scale variability of the hydraulic properties of the sediments on the lab to plot scale and used artificial pressure pulses (Yeh et al., 2009; Cardiff and Barrash, 2011). Recently there were attempts to extend hydraulic tomography to the groundwater basin scale and to use natural pressure signals, e.g. river stage fluctuations as signal (Yeh et al., 2009).

Similarly we use in the present study river stage fluctuations as natural pressure signals and study their propagation in the aquifer before and after a stream restoration measure to study groundwater-stream water interactions. Time series of hydraulic head reflect effects of different causes, like river stage fluctuations, groundwater recharge, precipitation, evapotranspiration, measurement errors, etc. (Yeh et al., 2009). In contrast to the aforementioned approaches we decomposed the hydraulic head series into independent components using a principal component analysis in order to disentangling the different effects.

The study was conducted at a section of the river Spree and its floodplain in the east of Berlin. Here an island is formed by an artificial stream channel (shortcut) and an oxbow. As restoration measure the shortcut was detached from the river at its upstream end, the former oxbow was reconnected to the stream and its clogging layer was excavated. The site was equipped with 15 groundwater observation wells, 2 river stages and 2 hyporheic wells, where data loggers measured every hour two years before and after the restoration. Please note that in our study we do not focus on the small scale heterogeneity of the hydraulic properties of the sediments as it would be important e.g. for estimations of the flow paths of contaminants or the study of biogeochemical processes in the hyporheic zone. Instead we

investigated the effect of the removal of the clogging layer and the change of the river course on the hydraulic connection of stream and groundwater.

Our analysis is based only on hydraulic head data and does not require any additional information. Please note that therefore our analysis is restricted to the transmission of pressure waves. We use the term ‘‘hydraulic connectivity’’ in contrast to the broader concept of ‘‘hydrologic connectivity’’ which is defined by Pringle (2001) as ‘‘water-mediated transfer of matter, energy, and/or organisms within or between elements of the hydrologic cycle’’ to account for that. The presented approach does not allow direct conclusions on related mass fluxes, flowpaths and water exchange rates (Lewandowski et al., 2009; Page et al., 2012). Instead the permeability for pressure signals is a necessary prerequisite for the exchange of mass fluxes. Thus, the hydraulic connectivity between the observation wells can be used as proxy for the relative differences in effective hydraulic conductivity of the floodplain sediments between the observation wells. With this integrative measure the problem of measuring the small scale variability of hydraulic conductivity in the floodplain is avoided.

To that end, we followed the approach presented by Lewandowski et al. (2009) for a time period where the river section was not restored and applied a principal component analysis on time series of groundwater heads and stream water levels. Based on the findings of Lewandowski et al. (2009) we hypothesized that (1) due to the restoration the hydraulic connectivity between the oxbow and the nearby groundwater will increase and that (2) in the shortcut the river bed will be clogged due to the reduced stream velocity, resulting in decreasing hydraulic connectivity between the shortcut and the adjacent groundwater.

3.2.2 Material and Methods

Study Site

The Freienbrink site is situated in the floodplain of the lowland river Spree about 30 km east of the center of Berlin (N52° 22’ 06’’, E13°48’25’’). The discharge of the river Spree is regulated by the Weir Grosse Tränke located 10 km upstream and varies usually between 5 and 20 $m^3 s^{-1}$ (Nützmann et al., 2013). At the site, a straight, artificial channel (shortcut) and an old meander (oxbow) form an artificial island. The shortcut was constructed in the 1960s to increase the flow velocity within the river and lower the surrounding groundwater table for agricultural purposes. In the first two years of the monitoring period, the shortcut served as the main stream channel and the oxbow was nearly completely blocked at its upstream end with a dam (Figure 3.2-1). Some pipes inside the dam that connected the oxbow to the main stream were blocked with fine sediments. Therefore, the flow velocity in the oxbow was almost zero and as a consequence an organic silt layer had developed in the oxbow with thicknesses varying spatially between zero and more than 1 m (Nützmann and

Lewandowski, 2009). The organic silt layer had a hydraulic conductivity k_f between 10^{-6} and 10^{-5} m s^{-1} and an effective porosity n_e of 0.5. Compared to the surrounding aquifer with k_f of 10^{-4} to 5 * 10^{-5} and n_e of 0.15 - 0.2 (Nützmann et al., 2013), the organic layer can be attributed as a clogging layer.

At the end of the second year of measurements, in October/November 2008, the clogging mud in the oxbow was excavated with a suction dredger. The oxbow was reconnected as main stream channel on the 27th November 2008. After the reconnection of the oxbow, a dam was built at the upstream end of the shortcut and closed on the 9th December 2008. Hence, there was a switch in the river course from the shortcut to the oxbow (Figure 3.2-1). In the subsequent two years of the monitoring period the former shortcut was blocked with the dam at the upstream end and the former oxbow was reactivated. Only at high water levels the dam was overflown.

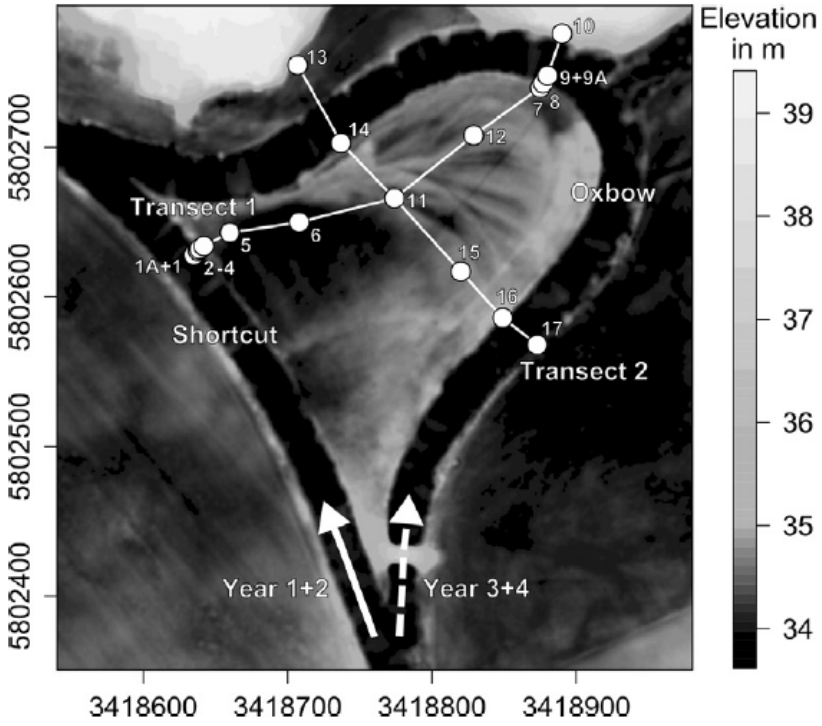

Figure 3.2-1: Elevation map based on a LIDAR-Scan from 3rd December 2009 with 1 m grid size and 0.3 m resolution for altitude in projection ETRS89 UTM Zone 33. First transect of groundwater observation wells in west-northeast direction and second transect in northwest-southeast direction. At both ends of the first transect there was a water level gauge situated in the stream (1A + 9A). The filled arrow marks the main stream flow in the first two years of the study, the dashed arrow the main stream flow in the third and fourth year. The flow through the other reach was blocked in both situations.

The river intersects an unconfined aquifer of about 20 m thickness. The floodplain consists mainly of medium to fine grained sandy sediments of glacial and fluvio-glacial origin (Lewandowski et al., 2009). In the northern part the floodplain adjoins a steep hillslope to a 5 m higher plateau (Lewandowski et al., 2009). The topography of the floodplain is the result of morphological work of the river (Figure 3.2-1). The western part of the floodplain is characterized by a depression with fine grained sand and silt, where the groundwater level repeatedly exceeded the surface. Starting from the middle of the floodplain, a ridges-swales structure with about 0.4 m difference in elevation established due to the meandering oxbow. Here, coarser sediments with intermediate organic layers are present (Pöschke et al., 2015 b).

Most of the time groundwater is exfiltrating into the stream. A mean groundwater exfiltration rate of 233 L m^{-2} d^{-1} with a groundwater flow velocity between 10^{-7} and 10^{-6} m s^{-1} was estimated by Nützmann et al. (2013). Maximum lateral infiltration of river water into the aquifer is less than 4 m (Lewandowski et al., 2009). Velocity of pressure wave propagation (celerity) from the stream into the aquifer was found to be about 1550 m d^{-1}, thereby three to four orders of magnitude higher than the velocity of groundwater mass flux (Lewandowski et al., 2009). For a general elaboration on velocity of pressure waves (celerity) vs. velocity of water particles (mass fluxes) in hydrology, see McDonnell and Beven (2014).

Water level measurements

Groundwater heads at 15 groundwater observation wells, hydraulic head at 2 hyporheic wells and stream water levels at 2 river stages were measured at hourly intervals with data loggers (Aquatronic, Kirchheim/Teck, Germany, ±1 mm) along two transects. Most of the groundwater wells had filter screens of 2 m length and the upper end of the filter screen at approximately 25–70 cm below the ground, with the exception of observation well No. 11 with 9 m filter length. The first transect consisted of 10 shallow groundwater wells crossing the island in southwest-northeast direction from the shortcut to the oxbow (Figure 3.2-1). Measurements were conducted from 1st October 2006 to 1st October of 2010. Additionally, at both ends of the first transect surface water level was measured in the oxbow and in the shortcut (gauges no. 1A and 9A). Adjacent to the stream water gauges two hyporheic wells no. 1 and 9 were installed that screened at 0.5 to 1.5 m below the riverbed at gauge no. 1A and between 1.5 and 2.5 m at gauge no. 9A (Lewandowski et al., 2009). The second transect consisted of five additional groundwater observation wells that crossed the island in northwest-southeast direction and the first transect at observation well no. 11 (Figure 3.2-1) and measured groundwater level from 12th November 2007 to 1st October of 2010.

Pre-processing of data

Short data gaps of up to seven hours, which resulted from the biweekly water quality sampling and maintenance of the pressure transducers and loggers, were interpolated using natural splines (less than 0.5% of the readings per year at all wells). Apparent offsets between subsequent periods that could have been due to inexact reinstallation of the devices were adjusted with the offset of the linear extrapolation before and after the corruption. Lengthening of the cable of the devices in the wells were identified by comparison with biweekly manual readings of water levels and groundwater heads and corrected with simple linear regression.

Longer gaps in the data or periods with distorted data were interpolated with the best multiple linear regression model (package 'leaps' in R (R Core Team, 2014). Two abrupt shifts in the water level of the oxbow compared to the water level in the shortcut and the nearby groundwater wells at 27th November 2008 12:00 and 9th December 2008 15:00 were attributed to the reconnection of the oxbow and the later decoupling of the shortcut with the new dam and hence were not corrected. At maximum, correction comprised 3026 consecutive readings, that is, 34.5% of the readings of the fourth year at groundwater well no. 5. Second most affected was well no. 11 with 538 consecutive readings (6.1%) in the third and 421 consecutive readings (4.8%) in the second year. At another ten events correction was up to 250 consecutive readings or 2.9 % of the readings per year.

Principle component analysis

Time series of groundwater and river water level show a very close linear correlation ($r = 0.98$), which indicates a good hydraulic connectivity between both water bodies. Nevertheless, there is no perfect correlation. Aside from measurement noise and possible artefacts, these differences presumably have to be ascribed to different factors that affect different sites to different degrees. Among these, pressure signals induced by river water level fluctuations as well as groundwater recharge, depending on vegetation and the soil properties of the overlying vadose zone, are considered to play a major role (Lewandowski et al., 2009). Thus every water level series can be regarded to be the result of different superimposing effects. Our analysis aimed at extracting the effect of river water level fluctuations from these mixed signals by following the approach presented by Lewandowski et al. (2009).

Firstly, the deviation from the mean of groundwater heads and river water level was calculated for each time step. Afterwards, each of these residual time series was normalized to zero mean and unit variance to ensure equal weighting. Then, a principal component analysis (PCA) was applied to the prepared data. PCA performs an eigenvalue decomposition of a data matrix, yielding a series of

independent components. We considered these components as depicting different drivers of hydraulic head fluctuations.

In order to analyze for long-term shifts PCA was performed for single hydrologic years separately (October throughout September yielding 8760 readings at each observation well and 8784 readings in the second year, respectively). For the first transect four years of water level measurements were available since 2006, whereas measurements at the second transect started one year later. To enable comparison between the two transects, a joint analysis with data from both transects was performed for the second, the third and the fourth year. Since the data acquisition at the second transect started at the 24. November 2007 (7476 readings at each observation well), the second year does not cover the full hydrological year 2007/2008. The documentation of the changes in the system in annual resolution is a compromise between comparability with the preceding study of Lewandowski et al. (2009), precision of the effect of the restoration we wanted to measure and comparability of the different PCAs among each other. Furthermore, the PCA was performed for each quartile of the hydrologic year to account for inter-annual variability.

Loadings on a component are the expression of a component at the different sites. They were calculated as Pearson correlation coefficients of the z-normalized residuals of the water level series and the values (scores) of the component (compare Lewandowski et al., 2009). The stability of the loadings in each observation year was estimated with the mean of the loadings of the 4 quartiles of the hydrologic year and their corresponding confidence intervals. The areal expression of the first component was estimated as thin plate splines – a kriging variant implemented in the package ‘fields’ in R (R Core Team, 2014) – based on the mean of loadings of the 4 quartiles of the third observation year, as it was the year with the lowest inter-annual variability.

All the statistics and calculations were done with the free software package R, version 3.0.1 (R Core Team, 2014).

3.2.3 Results

Characteristics of water level dynamics and floods

The mean amplitude of groundwater level fluctuations was approximately 0.9 m for the first three years of the monitoring and approximately 1.3 m in the last year of the study. The groundwater observation wells, except the two hyporheic wells, have a mean distance of groundwater level to the surface of approximately 60 cm with a standard deviation of approximately 20 to 25 cm. The mean difference in water level from one hour to the next hour was between two to three mm. The mean difference in water level among the groundwater observation wells on the island was in the magnitude of a few cm. The mean groundwater level increased from the first year to the second year by approximately 15 cm and from the third year to the fourth year by approximately 13 cm. The increase in mean groundwater level and amplitude in the last year is due to several flood events: one week of flooding in December 2009, three weeks in January 2010 and 1 month of flooding from the mid of August to the mid of September 2010. For more details including graphs of the water level series characteristics please see Lewandowski et al.'s (2009) examination of the first year of the observation period.

Principle component analysis

For the data set of the first transect the first principal component depicted 70% of the total variance in the first year and 70%, 65% and 63% in the subsequent years (Figure 3.2-2). Please note, that the range of loadings on the first component describes the *relative* differences in the correlations of the first component with the original water level series at the observation wells because the PCA was applied on the z-normalized residuals of the water level series. Hence, we refer to loadings close to one as high loadings and loadings close to minus one as low loadings.

At the stream water gauges no. 1A in the shortcut and no. 9A in the oxbow loadings were very high on the first component throughout the observation period with the exception of lower loadings for no. 9A in the third year (Figure 3.2-3). At the groundwater observation wells next to the shortcut (no. 2, 3, 4) loadings were very high on the first component and exhibited approximately the same loadings compared to the gauges in the stream (Figure 3.2-3). The hyporheic well no. 1 below the stream bed depicted substantial lower loadings than observation wells no. 2 to 4 in the second year, and slightly lower loadings in the first and fourth year (Figure 3.2-3). Only in the third year loadings at observation well no. 2 were slightly lower than loadings at hyporheic well no. 1.

Groundwater wells next to the oxbow showed very low loadings with slightly increasing loadings on the last meter to the oxbow from observation well no. 7 to 9 (Figure 3.2-3). Only in the fourth year

loadings were substantially higher at observation wells no. 8 and 9 than in the years before. Observation well no. 12 was on the same level as the gauges next to the oxbow. Observation wells no. 5, 6 and 11 in the middle part of the island showed decreasing loadings along the first transect from the shortcut to the oxbow. The loadings in this middle part showed the highest variability between the years and also within their quartiles. From the first to the second year all loadings in the middle part increased and decreased thereafter until the fourth year.

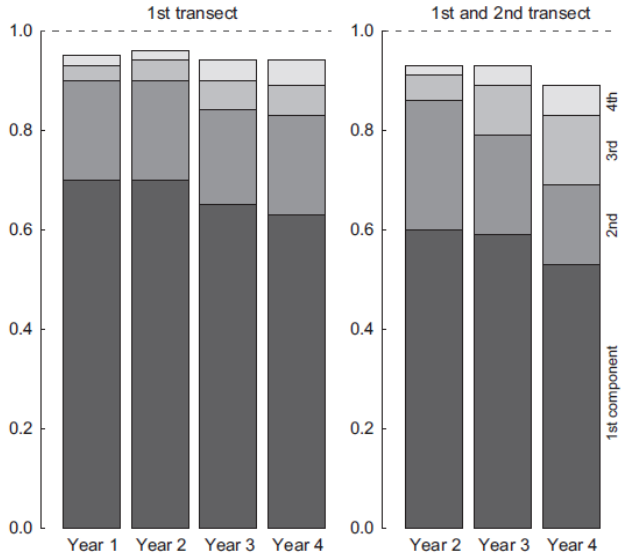

Figure 3.2-2: Ratio of overall variance explained by the first four principle components of the PCA of the data set of the first transect (left) and of the PCA of the joint data set from both transects (right).

For the joint data set (water level data from both transects) the first principal component depicted 60% in the second year and 59% and 53% in the third and fourth year (Figure 3.2-2). The main pattern in the first transect with high loadings next to the shortcut, and decreasing loadings to the east was similar to that of the separate analysis based on the first transect. The loadings of the two variants were correlating in the three common years with an r^2 of at least 0.97.

In the northern part of the second transect groundwater well no. 13 was loading constantly low and groundwater well no. 14 constantly loading high on the first principal component over the entire observation period (Figure 3.2-4). In the southern part of the second transect groundwater wells no. 11, 15, 16 and 17 were jointly shifting from slightly positive loadings in the second year towards negative loadings in the third year and stayed on this level in the fourth year (Figure 3.2-4). Inter-annual variability was prominent in the second year for wells no. 11, 15, 16 and 17 and in the last year for wells no. 13, 16 and 17 (Figure 3.2-4). There was no regular seasonal pattern along both transects. The overall spatial pattern remained relative stable throughout the observation period (Figure 3.2-3 - Figure 3.2-5).

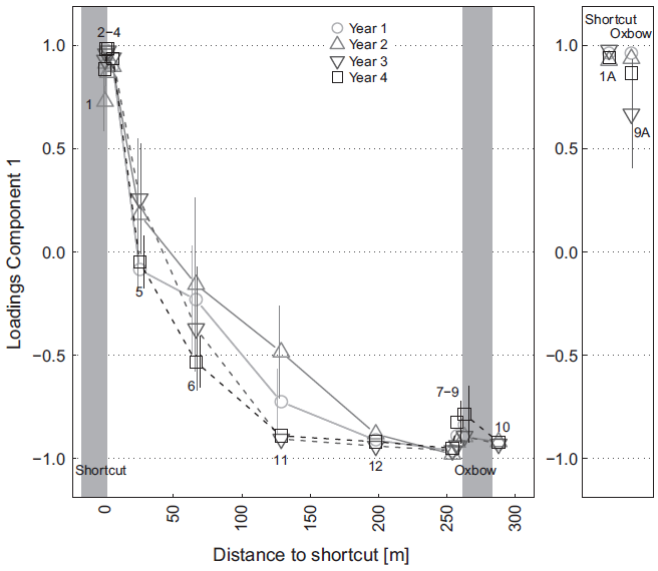

Figure 3.2-3: Loadings of groundwater observation wells of the first transect on the first principle component vs. distance to shortcut (left) and of the stream water gauges (right). Mean of loadings of the 4 quartiles of the hydrologic year (Oct.-Sept.) and their corresponding confidence intervals. Only confidence intervals > 0.2 are shown. On the left panel the grey bars indicate the position of the stream.

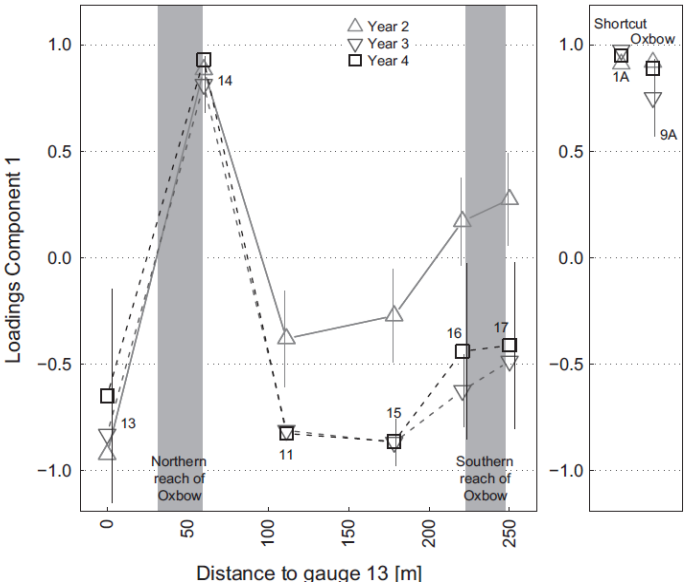

Figure 3.2-4: Loadings of the groundwater observation wells of the first principle component of the second transect vs. distance to the northern end of the transect two at observation well 13 (left) and of the stream water gauges (right). Mean of loadings of the 4 quartiles of the hydrologic year (Oct. – Sept.) and their corresponding confidence intervals. Only confidence intervals > 0.2 are shown. On the left panel the grey bars indicate the position of the river.

3.2.4 Discussion

Interpretation of the first component

In a more detailed analysis of the first year of the dataset, Lewandowski et al. (2009) identified the first component as dampening and delay of the fluctuations of the water level in the river. We follow their interpretation as loadings of the stream water level gauges exhibit loadings close to one in all of our analyses (Figure 3.2-3 and Figure 3.2-4). Thus the first component explains almost 100% of the deviation of the stream gauges from the mean behavior of all observation wells. This implies that processes that impact the groundwater head in the wells could hardly have any additional effect on the stream water level gauges. Thus, the loadings on the first component can be used as a quantitative measure for the hydraulic connectivity between river and groundwater.

High positive loadings on the first component imply that the respective time series of the groundwater head deviates from the spatial mean in the same way as the stream water level gauges. That allows the conclusion that groundwater head at the respective site is strongly affected by the stream water level fluctuations. In contrast, high negative loadings point to a weak impact relative to the other observation wells, and zero loadings to intermediate effects.

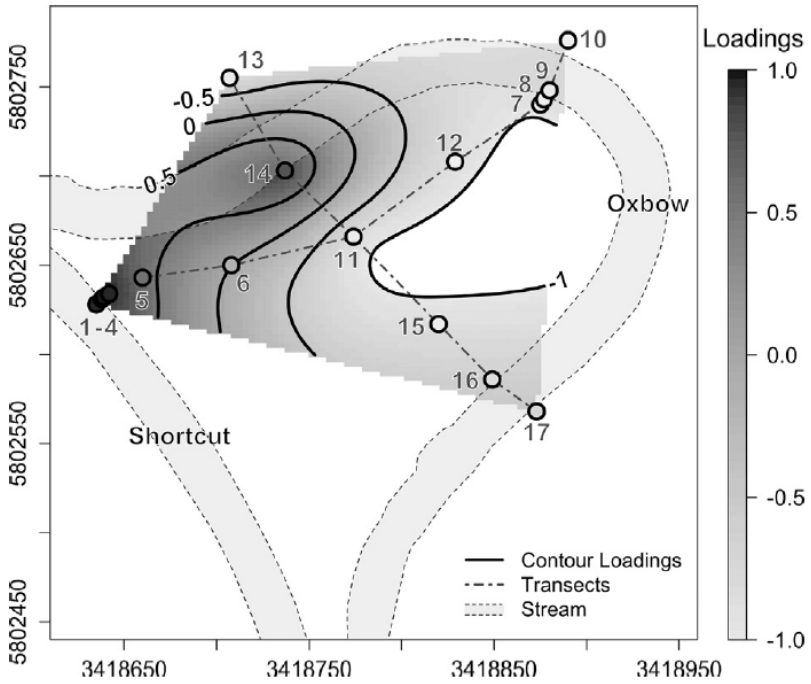

Figure 3.2-5: Spatial interpolation of loadings of the first component based on the mean of the loadings of the 4 quartiles of the third observation year (Oct. – Sept.). Projection is in ETRS89 UTM Zone 33. Values < -1 are artefacts and excluded.

Our prior assumption was that the observed water level dynamics at the single sites are a mixture of different superimposing effects. In fact the first component explains only 53–70% of the spatial variance, indicating that other factors have substantial effects on the observed groundwater heads as well. To investigate in particular the hydraulic connection of the river and the groundwater by analyzing the original time series, e.g. using cross-correlation, would therefore not have been satisfactory.

Spatial pattern of hydraulic connectivity

The oxbow and the shortcut have been connected at their downstream end throughout the entire study period and exhibited the same water level. The slightly lower loadings at hyporheic well no. 1 compared to observation wells no. 2 to 4 on the western end of the first transect are interpreted as slightly lower hydraulic conductivity of the river bed compared to the river bank. Along the first transect (Figure 3.2-1) the impact of river level fluctuations decreased with distance from the stream up to well no. 11 and remained approximately stable for the eastern half of the transect (Figure 3.2-3). As the loadings of the groundwater wells in the eastern part of the island are substantial lower than the loadings of the stream wells and the loadings of the groundwater wells in the western part of the island, we conclude that groundwater wells in the eastern part of the first transect are hydraulically disconnected from the oxbow relative to their hydraulic connection to the shortcut (Figure 3.2-5). Only groundwater wells no. 8 and 9 adjacent or even underneath the oxbow are slightly more influenced by the water level fluctuations in the oxbow (Figure 3.2-3). The same pattern was already found by Lewandowski et al. (2009) who suggested that the slight increase is either due to the heterogeneity of the aquifer or due to a very low - but not zero - hydraulic connectivity of the clogging layer.

Results from the second transect show high connectivity with the oxbow only for well no. 14 in its northern reach, which is also not affected by the stream channel restoration, since the pattern stays stable over the four years (Figure 3.2-4). This specifies the hypothesis of areas of relatively better hydraulic connection in the north-western part of the island (Figure 3.2-5). Observation wells no. 16 and 17 close to the southern reach of the oxbow show higher hydraulic connectivity with the stream than the observation wells no. 11 and 15 in the middle of the island and also than the observation wells in the north-eastern part of the first transect. This specifies the area of lowest hydraulic connectivity in the north-eastern part of the island, which is the area where the inner bank of the meander is and was located. Since the flow velocity is lowest at this position during the formation of the meander, material of finer grain sizes has been accumulated in that area. This explanation is also supported by investigations of Pöschke et al. (2015 b), who conducted a ground penetrating radar survey to characterize the sediment composition. They could show that the north-eastern part of the island is

characterized by finer grain sizes close to the meander (well no. 7) in comparison to the western part, where the sediment adjacent to the channel bed is much coarser.

The low hydraulic connectivity of the observation wells no. 10 and 13 in the hillslope of the adjoining plateau is not due to the hydraulic gradient induced by the topographic gradient, because the first component captures the pressure-wave signals of the river.

Temporal variation of hydraulic connectivity

The analysis was performed for single years separately in order to capture changes of connectivity. Loadings of the stream gauges were constantly close to one as it is mandatory for the interpretation of the first component as influence of river level fluctuations on groundwater levels. The lower loading at stream gauge no. 9A in the third year (Figure 3.2-3) could be ascribed to the reconnection of the oxbow and the construction of the new dam in the shortcut.

Loadings of observation wells close to the Spree river at the western end of the first transect, and of groundwater well no. 14 close to the oxbow in its northern reach were close to one in all years of our study, pointing to a constant high connectivity between river and aquifer. Clogging of the stream bed in the shortcut due to the reduced stream velocity was not detected during the two years after the restoration. We assume that the first clogging sediments that settled throughout the first year have been removed due to the intense floods in the fourth year. Nonetheless we expect clogging of the shortcut in successive years.

In the central and south-easterly part of the island wells no. 5, 6, 11, 15, 16 and 17 exhibit substantial shifts between single years, although the general spatial pattern remains approximately the same (Figure 3.2-3 and Figure 3.2-4). There the loadings are highest for the second year and smallest in the fourth year, whereas those of the third year are similar to those of the fourth year. We did not find an unequivocal explanation for that temporal shift. Such systematic shift can hardly be explained by artefacts of the measurements. In addition, a corresponding change of the properties of the aquifer can be excluded. All of these wells are located close to the same former river bed, although this had not been intended. The associated interbedding of different substrates such as gravel, silt, former clogging layers and peat might still affect groundwater flow paths and lead to a closely coupled behavior (Nützmann and Lewandowski, 2009).

Wells no. 8 and 9 close to the north-easterly reach of the oxbow exhibit almost no shift in time. Loadings are close to minus one for the first three years, indicating low hydraulic contact with the oxbow. This suggests that the clogging layer is not the only reason for the lower hydraulic connectivity of the hyporheic well no. 9 below the oxbow compared to the hyporheic well no. 1 below the shortcut.

Instead we suggest that the effective hydraulic conductivity of the sediments around the shortcut in the north western part of the island is higher than of the sediments around the oxbow (Figure 3.2-5). This can be attributed to the construction of the shortcut. The shortcut itself and the surroundings are situated in sandy sediments, which were dislocated artificially. In contrast, the sediments around the oxbow are characterized by inclined layers of sand and organic material of the recent and former point bars. On the other hand the loadings at well no. 14 are close to one for the whole observation period of the second transect, suggesting a strong impact of natural spatial heterogeneity of effective hydraulic conductivity of the floodplain sediments (Figure 3.2-4).

Only in the fourth year loadings at wells no. 8 and 9 are slightly higher (but not significantly higher), pointing to increased, although still fairly low connectivity (Figure 3.2-3). Likewise a minor increase of loadings between the third and fourth year is observed at wells no. 13, 16 and 17 close to the oxbow (Figure 3.2-4). This is consistent with our prior assumptions of increasing connectivity due to stream channel restoration. However, this is more a little piece of evidence rather than a proof and the development has to be checked in the following years. Anyhow, the effect is much weaker than assumed.

3.2.5 Conclusion

The data driven PCA approach used in this study is easy to apply and requires only time series of hydraulic heads in the aquifer and in the stream. It splits up the water table dynamics into independent components which represent different drivers of the hydraulic head dynamics in the system and the spatial expression of those drivers can be analysed. In the present study, the first component captures the propagation of river stage fluctuations into the aquifer and can therefore be used to describe the hydraulic connectivity of groundwater and stream water. Areas of relative low and high hydraulic connectivity could be identified, although it is not possible to quantify mass fluxes and water exchange rates. Despite the small differences in water table of a few cm along the groundwater possible to derive throughout the observation period spatial and temporal consistent patterns of one distinct hydraulic process, namely the propagation of the river water table fluctuations, on the hectare-scale (Figure 3.2-3 to Figure 3.2-5). One benefit of the presented approach is that hydraulic head devices are long established and often already permanent part of hydrologic monitoring networks.

Once installed the operating effort is very low. The hydraulic head data are usually measured with relative high temporal resolution of minutes to hours and stored with data loggers. The presented approach can be used to optimize the monitoring network and monitor further developments of the groundwater-stream water system (Page et al., 2012), as in our example after a stream channel restoration. It can also provide a framework for further modelling of groundwater-stream water

interactions (Lewandowski et al., 2009), help to identify the hydrological active functional properties on the landscape scale (Lischeid et al., 2010), regionalize the different hydrological contributions to the aquifer dynamics (Longuevergne et al., 2007), or be used as explorative data analysis tool to develop hypothesis such as the spatial patterns of areas of relative low and high effective hydraulic conductivity of floodplain sediment as done in the present study.

Our results demonstrate that even two years after the restoration hydraulic connectivity of stream water and the groundwater next to the new main stream channel (oxbow) had not reached the level of connectivity next to the old artificial stream channel (shortcut). We identified three factors to explain this finding. That is (1) that the change in stream velocity and sedimentation rate in the oxbow and in the shortcut due to the switch of the main stream channel might need more time to effectively change the stream bed permeability in such a scale that it alters the spatial pattern of hydraulic connectivity in the floodplain. The two other options are that hydraulic connectivity around the shortcut is in the long run higher than around the oxbow due to the spatial heterogeneity of the sediments in the floodplain, whether the heterogeneity is (2) natural or (3) induced by the digging of the artificial shortcut directly into the sandy floodplain sediments. To distinguish between this three factors and their relative contribution to the observed spatial pattern of hydraulic connectivity further analysis of the spatial distribution of the sediments around the stream channels and their hydraulic conductivities, as well as the further monitoring of the development of hydraulic connectivity after the restoration is necessary.

With this study the importance of comprehensive monitoring of restoration measures even several years after the restoration and the explicit identification of specific properties of the system to be restored is underpinned (Kondolf, 1995). Option one of our suggested set of influencing factors exemplifies that restoration of connectivity of groundwater and surface water is a process that might last for several years after the initial restoration of the surface water, while on the surface the restoration might appear already successfully completed. The proposed differences in effective hydraulic conductivity of the alluvial sediments in different parts of the floodplain (option two and three) highlight the importance of pre-studies that identify the specific natural conditions before the restorations (Kondolf and Micheli, 1995; Woolsey et al., 2007; Pander and Geist, 2013). Focusing only on the hydrogeomorphology of the surface waters or individual target species in restoration practice might be insufficient to restore the functional properties of the river ecosystem (Kondolf et al., 2006; Woolsey et al., 2007). If groundwater-stream water interactions are understood as substantial features of the system to be restored, this has to be taken into account in the restoration and monitoring practice, as well as in the evaluation of restorations.

3.3 Impact of alluvial structures on small-scale nutrient heterogeneities in near-surface groundwater

Franziska Pöschke[1,2], Jörg Lewandowski[1,2], Gunnar Nützmann[1,2]

Ecohydrology 2015, 8, 682-694

[1] Institute of Freshwater Ecology and Inland Fisheries, Ecohydrology Department

[2] Humbodt University Berlin, Geography Department

Published in: Ecohydrology

Pöschke, F., Lewandowski, J., Nützmann, G. 2015. Impact of alluvial structures on small-scale nutrient heterogeneities in near-surface groundwater. Ecohydrology. 8. 682-694

http://dx.doi.org/10.1002/eco.1535

Copyright © 2014 John Wiley & Sons, Ltd.

Abstract

Spatially heterogeneous and temporally variable nutrient concentrations (P, N) in near-surface aquifers are common and are driven by different factors such as climate, topography, vegetation, sediment compositions, and water level fluctuations. Nonetheless, the identification of discrete areas where similar concentrations patterns can be expected is still difficult, especially in patchy systems such as riparian zones of lowland rivers. To address this challenge, a floodplain aquifer of the River Spree (Germany) has been investigated by sampling groundwater with high vertical and horizontal resolutions. Vertical nutrient distributions measured by multi-level samplers with a 10 cm resolution indicate a biogeochemical layering of the aquifer. High concentrations in the upper 2 m can be attributed to a local redox gradient, which is induced by water level fluctuations and biological turnover processes, while the layer below is mainly influenced by medium-scale to large-scale groundwater flow patterns. High concentration in the upper part of the aquifer enforces groundwater sampling with a high horizontal resolution of 3 m from the near-surface groundwater. The results compared with highly resolved elevation and sediment data indicate that geomorphological features and water level fluctuations control the thickness of the unsaturated zone and the redox gradient. The strength of the gradient and the amount of degradable organic matter determine the intensity of nutrient release by chemical reactions and biological turnover.

3.3.1 Introduction

Eutrophication of surface waters is still a major world-wide problem. In the past decades, there has been an increasing awareness of groundwater as nutrient source for surface waters because point sources have been gradually eliminated (Driescher and Gelbrecht, 1993; EEA, 2005; US EPA, 2007) and retention capacities of unsaturated soils and aquifers are exhausted. Thus, an improved understanding of origin and fate of nutrients in aquifers is urgently required. In contrast to many contaminants, nutrients are naturally present in pristine systems and their release and storage is heterogeneously distributed in space and time even without anthropogenic impacts (Bjerg and Christensen, 1992; Takatert et al., 1999; Lewandowski and Nützmann, 2010; Schot and Pieber, 2012). In the past, a number of different factors have been identified, which influence the groundwater nutrient composition: climate, topography (Pinay et al., 1989; Tiemeyer et al., 2007; Courtwright and Findlay, 2011), vegetation (Wassen et al., 2002), sediment characteristics (Takatert et al., 1999), and water level fluctuations (Burt et al., 2002). For most aquifers, a combination of factors rather than a single one is driving the groundwater composition and its variations. It can be assumed that with an increasing number of factors and an increasing variability of them, the prediction of groundwater composition becomes more complicated. Böttcher and Strebel (1988a, 1988b, 1988c) as well as Bjerg and Christensen (1992) found that concentrations of different biogeochemical parameters changed within only a few metres in horizontal direction. Furthermore, groundwater velocity, capillary fringes, and redox gradients might cause a vertical heterogeneity within an aquifer (Spalding and Exner, 1980). For example, in humid regions under natural conditions, the concentrations of redox-sensitive substances, such as phosphate and iron, decrease with sediment depths (Schüring et al., 2000), whereas more conservative substances increase because of leaching processes in the upper soil. In comparison to the often observed spatial heterogeneity, the temporal variance of the groundwater composition is usually small (e.g. Bjerg and Christensen, 1992; Lewandowski and Nützmann, 2010; Schot and Pieber, 2012).

One of the most complex natural ecosystems is floodplains in lowland regions. Because of the enormous power of flowing water in these highly dynamic, contracting, and expanding ecosystems, a lot of complex morphological structures develop during centuries. Thus, there is much small-scale patchiness (Amoros and Bornette, 2002; Charlton, 2008), e.g. wet swales filled with organic matter (OM) is located immediately adjacent to a sandy and dry bar. Furthermore, riparian zones are collection points of different types of waters (e.g. anaerobic groundwater and oxygen-saturated surface waters). Thus, floodplains are assumed to be highly effective zones of mass retention (Grimm et al., 2003).

The aims of the present study are to quantify the variability nitrogen and phosphate concentrations in a typical lowland floodplain aquifer and to identify the major drivers of the observed concentration

patterns. Therefore, we investigated different small-scale spatial dimensions in the floodplain aquifer of the lowland river Spree in Germany. Lewandowski and Nützmann (2010) already found a high spatial and a negligible temporal heterogeneity of both nutrients at the floodplain scale. We hypothesize that the spatial variations of the nutrient concentrations in the groundwater are a result of the small-scale variability of topography, water level fluctuations, sediment structure, and vegetation as shown in Figure 3.3-1.

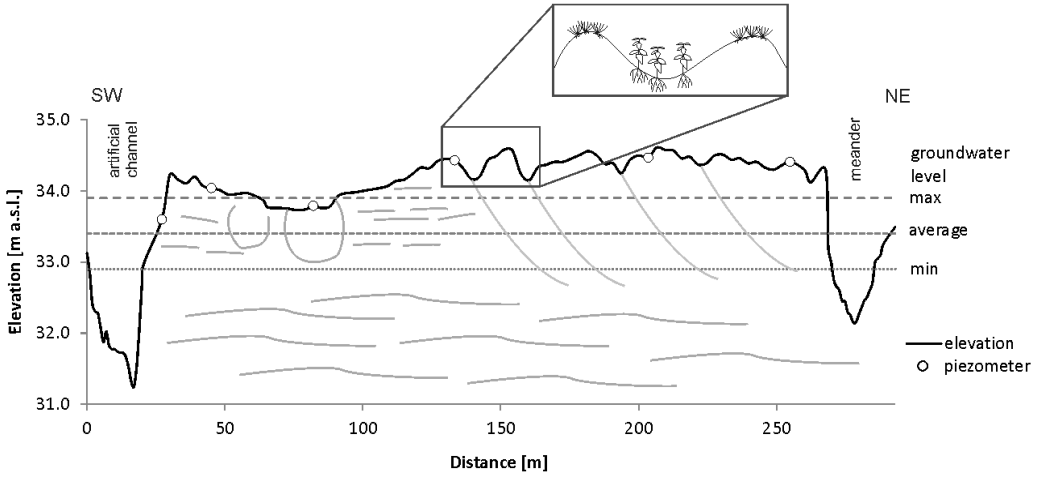

Figure 3.3-1: Conceptual model of the study site visualizing topography (scalable) and subsurface stratification of the floodplain (not to scale). As a result, microhabitats with different plant communities have formed (modified from Lewandowski et al., 2009).

3.3.2 Material and Methods

Study Site

The study site is located in a floodplain of the river Spree in north-eastern Germany (N52°22’06’’, E13°48’25’’). During the Pleistocene, the area was part of the Berlin–Warsaw glacial valley; a layer of glacial sediments such as gravel and coarse sand was deposited. This layer was superimposed by fluvial sediments during the Holocene. The substrate of the fluvial accreted layer is characterized by medium to fine sand containing lenses of silt and peat (Driescher, 1999). Both layers form an unconfined aquifer of about 20m thickness (Lewandowski et al., 2009). The valley is surrounded by ground moraines in the north and in the south (Driescher and Gelbrecht, 1999); the study site is situated close to the northern moraine. Similar to the glacifluvial sediments in the floodplain, the sediments of the moraines have a high permeability. Therefore, groundwater and surface waters are well connected in that area. The regional groundwater flow direction is from the northeast/ east to the south-west/west, i.e. from the moraine to the valley following the topographic gradient of the valley (Nützmann et al., 2013). However, the hydraulic gradients are very low (<0.1 ‰). This implies a low

groundwater flow velocity of about 10^{-7} to 10^{-6} m s^{-1} (Nützmann et al., 2013). Because the floodplain is the deepest point in the landscape (34.2 m a.s.l. ± 0.44 m), the groundwater table is quite close to the surface (33.4 m a.s.l. ± 0.5 m) (Lewandowski et al., 2009).

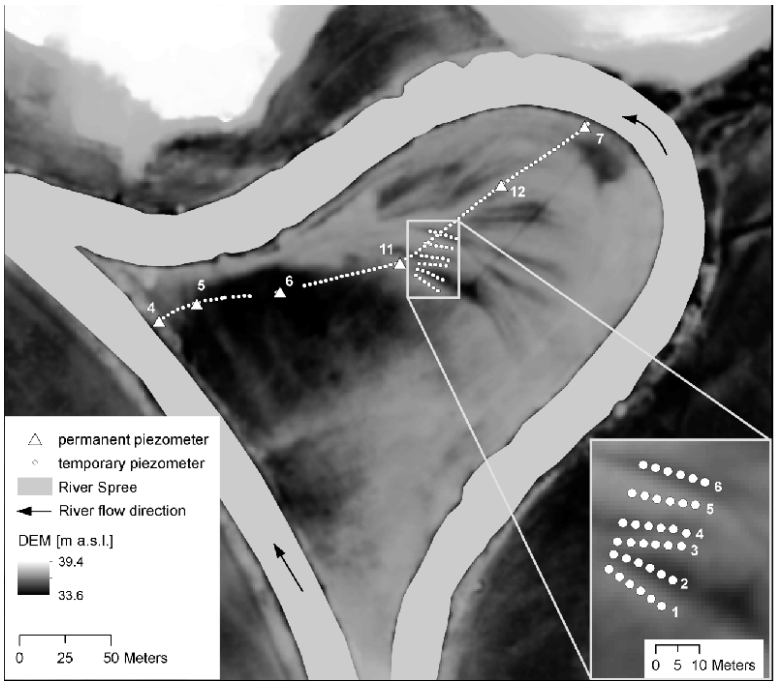

Figure 3.3-2: Digital elevation model (DEM) of the island and position of the temporary and permanent piezometers; multi-level sampler (sampled in April 2009, August and October 2011) are located at the same positions as the permanent piezometers. The first horizontal campaign of the temporary piezometers along the transect of permanent piezometers were sampled in October and November 2008. The second horizontal campaign on the ridge and swale structure was conducted in July 2010.

Nowadays, floodplain and river are affected by anthropogenic impacts. The study site is used as agricultural meadow. This included digging of an additional stream bed to shorten the course of the river (cut through in 1960) and the closure of the meander. By that river flow, velocity was increased and flooding periods of the agriculturally used floodplain shortened, while the groundwater level was decreased. Subsequently, a mud layer developed in the inactive meander. Consequently, the exchange between meander water and groundwater was reduced (Lewandowski et al., 2009). In 2009, the mud was removed and the meander was reopened as a stream restoration measure. The artificial channel was closed by a dam; an overflow during flood events is still possible. Hence, the studied floodplain section has characteristics of an island bordered by an artificial channel and a meander bend (Figure 3.3-2).

Since 2006, hydraulically and geochemical investigations are conducted within the floodplain and the hyporheic zone of the river Spree. Therefore, a transect of permanent piezometers was installed into the floodplain and the river to capture hydraulic gradients and geochemical processes within the area (Fehler: Referenz nicht gefunden). For detailed description refer to Lewandowski et al. (2009) and Lewandowski and Nützmann (2010).

Digital Elevation Model

Following the classification of Nanson and Croke (1992), the floodplain of the river Spree can be characterized as a medium-energy and non-cohesive floodplain of a meandering river. Because of the displacement of the meander, a formation of microtopography is possible in those floodplains. However, differences in elevation of such floodplains are only about 1m (Hickin, 1974). Hence, the identification of small structures necessitates a digital elevation model (DEM) with a high spatial resolution. The DEM was generated by an ordinary kriging (OK) operation on the basis of rectified LIDAR data (source: Landesvermessungsamt und Geobasisinformation Brandenburg). The data have a spatial resolution of 1m and an accuracy of 0.3m in both horizontal and vertical dimensions.

Ground penetrating radar

Ground penetrating radar (GPR) was used for the identification of the characteristics of subsurface sediments and stratigraphy of the study site. This technique allows the estimation of the current subsurface structures (Annan, 2006) as well as of the floodplain's formation processes. GPR is an electromagnetic reflection method based on electromagnetic reflection properties of materials, in particular their conductivity and permittivity (Annan, 2006). The reflection properties of different grain sizes as well as the principles of the method are illustrated in Davis and Annan (1989).

The GPR survey and the subsequent image processing were done by a private company (GMB GmbH) in September 2009. The investigation was conducted with the SIR 2000 (GSSI, USA), and a measurement frequency of 200 MHz was applied. This high frequency allows a detailed observation of the underground, because of its short wave length. The used frequency provides an observation depth of about 8m below the ground. GPR profiles were recorded in the direction of the meander movement for parallel transects with a distance of approximately 25 m to each other. This results in five vertical profiles. Additionally, one profile along a transect of permanent piezometers (Lewandowski and Nützmann, 2010) was measured. Because of the relatively large distance of the GPR profiles to each other, only a two dimensional interpretation of the radargrams was possible. The analysis of the radargrams was done with the software

REFLEXW (Sandmeier Scientific Software, Germany). Different factors have to be considered during interpretation: the double running times (antenna-object-antenna), the different spreading velocity depending on sediment grain sizes, and the non-vertical emission of electromagnetic pulses. Furthermore, the radargrams had to be validated by sediment data. For that purpose, drill logs of permanent piezometers were used.

Biogeochemical investigation

The identification of the small-scale vertical nutrient distribution patterns was realized by six multi-level sampler (MLS) according to Graham (2009) along the transect of permanent piezometers (Figure 2). The MLS consisted of 24 ports with a distance of 10 cm between them. Therefore, their deepest port reached a maximum depth of 3m below the ground. They were installed in November 2008. The sampling was done for all samplers in April 2009, as well as in July, August, and October 2011. All 24 tubes were sampled simultaneously with a multi-channel peristaltic pump (Ismatec IPC24, 9 ml min^{-1}). This guarantees an exclusively horizontal flow toward the MLS ports (Graham, 2009). The first 20 ml of each port was discarded to avoid sampling of tube water (Graham, 2009). Afterwards, water samples were collected (20 ml), immediately filtered (0.45 µm), and acidified with 2M HCl to pH 2 on-site. The samples were analysed for soluble reactive phosphorus (SRP), ammonium (NH_4^+), and dissolved iron (Fe^{2+}) following the miniaturized photometrical method of Laskov et al. (2007). For data analysis, the samples were assigned to two vertical layers. The first (upper) layer is affected by groundwater level fluctuations, and the second (lower) one is not. The layers were statistically compared to identify significant differences.

Earlier groundwater investigations at the transect of permanent piezometers revealed a low temporal variability of nutrient concentrations (Lewandowski and Nützmann, 2010, 2011), which is also supported by the MLS findings. Therefore, a single groundwater sampling is adequate to capture the spatial distribution of nutrient concentrations. Temporary piezometers were installed in the upper layer identified by MLS investigations with a distance of 3m along the transect of permanent piezometers in autumn 2009 (n = 86, first sampling campaign). The transect covered all types of sediments and microtopography that were present at the study site (Fehler: Referenz nicht gefunden). An additional investigation was conducted in summer 2010. The focus of that second campaign was to study the impact of microtopography. Therefore, piezometers were placed along three ridges and three swales. On each ridge and swale, six temporary piezometers were installed with a distance of 3m between the adjacent piezometers of a single ridge or swale (n = 36) (Figure 3.3-1). Groundwater sampling from the temporary piezometers was always done in about 70 cm below the groundwater table. The drills were done manually with a piston sampler set (Eijkelkamp), and a steel pipe was installed (1.3 cm in

diameter, four slits with a length of 20 cm and a width of 0.5 mm). The groundwater was pumped with a peristaltic pump (Eijkelkamp, 0.3 l min^{-1}). Before sampling, the pumped water was discarded for 20 min to guarantee constant water quality and to reduce impacts of disturbances as a result of the drilling (Lewandowski and Nützmann, 2010). After sampling, the drill hole was closed again. To characterize the geochemical composition, physical and chemical parameters of the groundwater were determined. Redox potential, pH, temperature, and electrical conductivity were measured on-site (WTW ConOx, Schott Blue Line 31 Rx). In order to investigate nutrient distribution patterns, concentrations of SRP, NH_4^+, and NO_3^- were analyzed. Besides SRP, NH_4^+, and NO_3^-, also concentrations of dissolved iron (Fe^{2+}) were determined because P cycling is closely coupled to the fate of the redox-sensitive iron. Sampling and analyses were conducted according to standard methods as described by Lewandowski and Nützmann (2010).

The data were statistically analyzed with open source statistic software R (R Development Core Team, 2014). Biogeochemical data were tested for their dependency on geomorphological structures. Furthermore, correlations between the different nutrients and iron were calculated to receive information about the dominant processes of nutrient release and storage. Only 76 of the 86 samples of the first sampling campaign along the transect of permanent piezometers were included into the analysis because 10 samples did not meet the prerequisite for statistical analyses. The criterion for the inclusion into the analysis was a sampling depth of 32.7 m a.s.l. ± 0.3 m to guarantee a similar sampling depth within the upper groundwater layer identified by MLS investigation. In the second sampling campaign, all 36 samples were considered.

3.3.3 Results

Digital Elevation model

The DEM illustrates the microtopography of the island (Figure 3.3-2). Along the whole island, there is a difference in elevation of about 1m (33.4 to 34.4 m a.s.l.) from the artificial channel to the meander. Along the bank of the straight artificial channel, there is a ridge, which is a relict from channel construction. Adjacent to the ridge is the deepest area of the island, which stretches about 100m long perpendicular to the transect of permanent piezometers. Typical meander scroll bar formations – a succession of former point bars (Lobeck, 1939) – are located from the middle of the island to the meander bend. These are characterized by a sequence of ridges and swales, which differ in surface elevation (about 0.4 m) and width (5 to 15 m). In middle of the island, the ridges stretch over the total width of the island. Adjacent to the meander, the microtopography is only visible in the northern part of the island. This belongs to the increased flow velocity of the river with the increased bending of the

meander. At the head of the meander, the water flow becomes too high for point bar accumulation. After the water passed the bend, the flow velocity allows the accretion of eroded material and point bar formation starts (middle to tail section).

Ground Penetrating Radar

Different GPR reflection properties can be recognized in the GPR images: Coarse grain sizes, such as sand and gravel, are characterized by a discontinuous reflection, which is distorted by diffraction. In the GPR image, this is visualized by a light yellow to violet coloration. Clay and silt are depicted in white and light grey colours. Because these sediments adsorb most of electromagnetic radiation (Davis and Annan, 1989), it is not possible to detect the stratification below them. In contrast, peat layers that have the same coloration in the image as clay and silt have do not reflect electromagnetic radiation but are penetrable for electromagnetic pulses. Therefore, deeper stratifications and grain size compositions below peat layers are detectable. To verify the assumptions of the reflection properties, the GPR profiles were compared with drill logs of the six permanent piezometers, which are shown in Figure 3.3-3. In general, both drill logs and GPR profiles show an increasing grain size in downward direction. It is to mention that the upper 50 cm of the GPR profile cannot be taken into account because the reflection is influenced by the transition from unsaturated to saturated conditions (Davis and Annan, 1989). In general, the areas with peat (logs 6 and 7) and silt (log 11) could be detected quite well, whereas the separation of different types of sand is not clearly distinguishable. Figure 3.3-4 gives an overview of the positions of six GPR profiles and illustrates the sediment stratification of the island. There is a significant change in the sediment layering, and the corresponding border is marked with red dots in Figure 3.3-4 B. The south-western part (Figure 3.3-4 C) of the island is dominated by vertical accretions, which have been accumulated during flood events. Close to the artificial channel (in 0 - 30 m distance), coarse sediments dominate, probably because of the construction of the channel. This is also indicated by the higher surface elevation according to the DEM. In 30 - 100 m; distance to the channel, there is an increased content of finer sediments and OM. Additionally, there are swales filled with organics (in 40 - 50 and 70 - 90 m distance). Between 100 and 140 m distance to the channel, a lens of silt and clay was detected in about 1.5 m below ground. The north-eastern part of the floodplain (Figure 3.3-4 D) is dominated by lateral accreted fluvial sediments (sand, gravel, OM) as a result of erosion processes in the former riverbed.

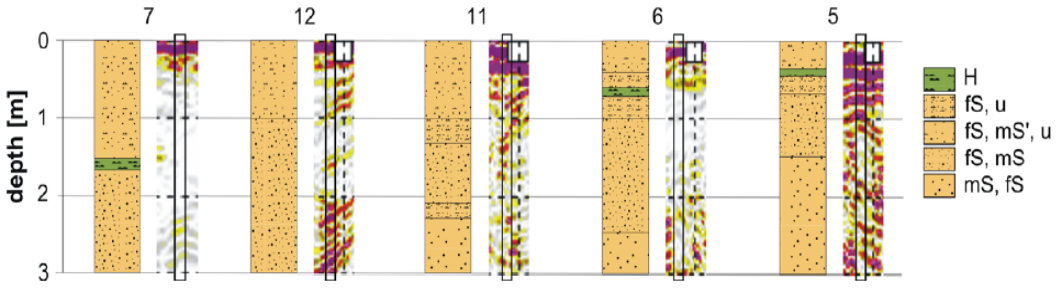

Figure 3.3-3: Validation of GPR profiles by drill log cores. The core profiles illustrate the main grain size of the soil horizon (H = peat; u = silt; fS = fine sand; mS = medium sand). In the GPR profiles, coarser grain sizes are colored from yellow to violet (sand and gravel fraction). Silt and peat are colored white to light grey. Silt and peat can be distinguished by the layers below: Below peat layers, sediment stratification is visible whereas below silt and clay is not. The pictures illustrate a 2 m wide GPR profile, and the black bordered boxes show the position of the cores. The location of the GPR profiles is shown in Figure 3.3-4.

Also, in Figure 3.3-4 C and D, the vertical subdivision of the floodplain becomes visible (black line in Figure 3.3-4 C and D). As mentioned in the preceding texts, the upper part consists of fluvial deposits of about 4m thickness. Below, glacifluvial deposits dominate. As it is typical for this kind of deposits, they consist of slightly inclining layers of gravel and sand (van Overmeeren, 1997; Hyndman and Tronicke, 2006).

As a result of the GPR and DGM information, four horizontal zones were identified, which have different properties in sediment composition and elevation. The characteristics of the zones are summarized in Table 3.3-1.

Table 3.3-1: Sediment and topographical characteristics of the four different zones within the floodplain

Zone	Sediment	Topography
I	Anthropogenically deposited sediment of shortcut constructions	Decreasing from south to north
II	Vertically accreted sediments; old river channel filled with organic matter	Flat and deepest zone of the floodplain
III	Vertically accreted sediments; silty layer	Increasing from south to north
IV	Laterally accreted sediments; inclined layers of sand and organic matter	Ridge and swale topography (meander scroll bars)

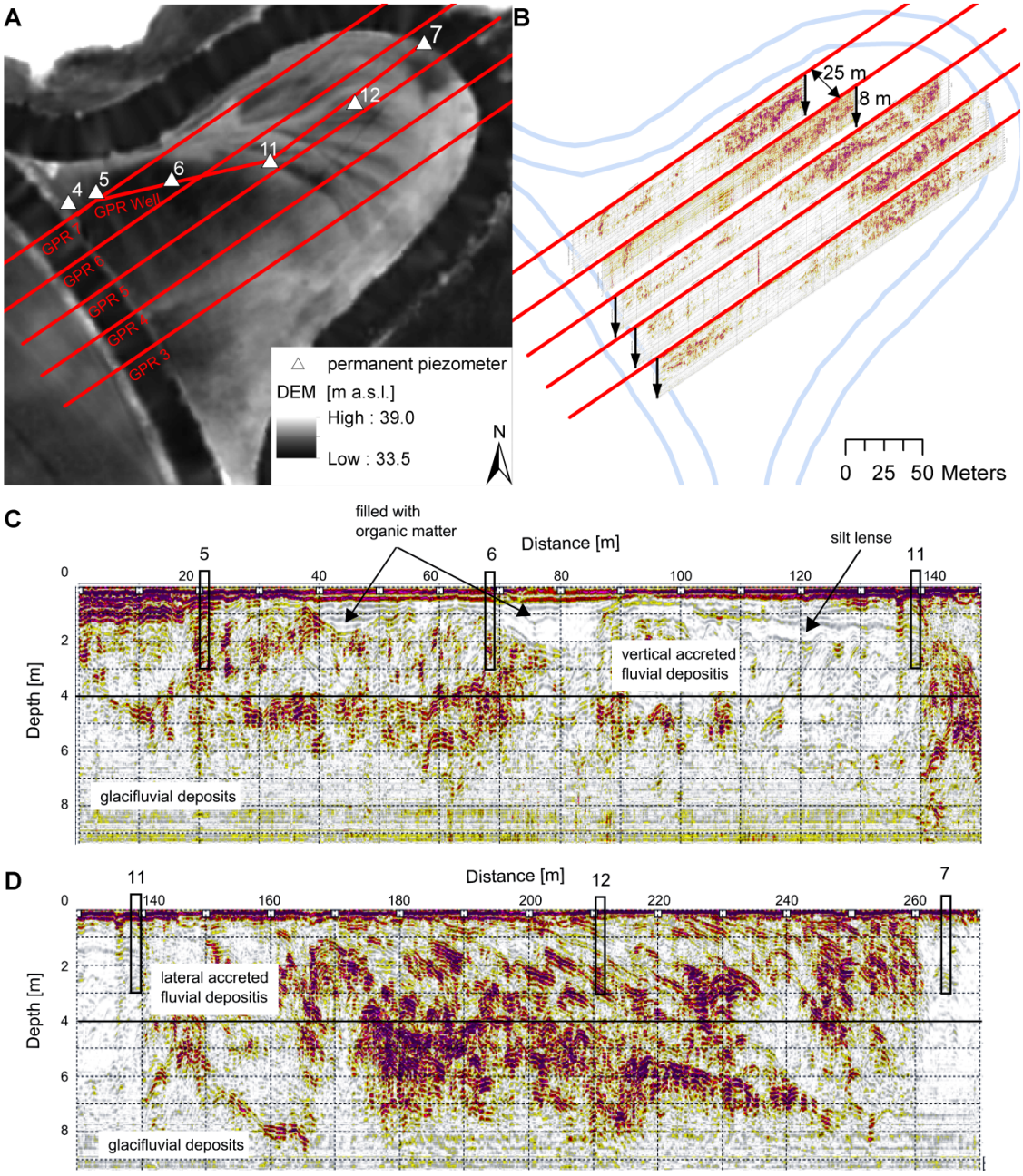

Figure 3.3-4: Results of the GPR survey. Figure (A) illustrates the position of the GPR profiles, which are shown in (B). The red points are located at the positions of changing stratification of the fluvial sediments. (C) and (D) show the GPR profile along the transect of permanent piezometers. Because of the length of the profile it was cut into (C) and (D). Three fundamentally different stratification types of the floodplain can be distinguished. Beside the previously mentioned changes of stratification of the fluvial sediments, the third type can be found in depths below 4 m, which are glacifluvial sediments.

Biogeochemical investigation

Vertical investigation with MLS. The highly resolved vertical groundwater investigations from MLS at six different positions along the transect indicate large variations of SRP, NH_4^+, and Fe^{2+} concentrations of up to one order of magnitude between the sites as well as in vertical direction at a single site (Figure 3.3-5). Temporal variability is in general low, i.e. the observed pattern of vertical nutrient distributions has been similar at the different sampling dates. However, it has to be noticed that for samples taken from above the average groundwater level (33.4 m a.s.l.), a temporal heterogeneity could not be excluded because there are indications for significant variations in nutrient concentrations. However, results from above the mean groundwater level (33.4 m a.s.l.) were not included into further analysis as a result of an insufficient number of samples. Additionally, it has to be mentioned that the identified vertical layering of the nutrient concentrations was found in the fluvial deposits and depends on the influence of the groundwater level fluctuation.

In average, SRP and NH_4^+ - N concentrations are higher in the upper 1.5m of the aquifer (SRP: 0.9 mg l^{-1} ± 0.5 SD; NH_4^+ - N: 0.9 mg l^{-1} ± 0.4) than below (SRP: 0.3 mg l^{-1} ± 0.1; NH_4^+ - N: 0.6 mg l^{-1} ± 0.2). Fe^{2+} showed no systematic difference between the upper and the lower layer (15.5mg l^{-1} ± 10.5 vs 15.2 mg l^{-1} ± 12.6). The two layers were statistically compared (Mann–Whitney U test) for all MLS and all sampling dates. There are significant differences between the upper and lower layer for SPR ($p = 3.3\times10^{-18}$), NH_4^+ - N ($p = 2\times10^{-4}$) and no significance for Fe^{2+} ($p = 0.12$). Because of the large difference in group size between the upper (n = 493) and lower layer (n = 190), a random selection of concentrations from the upper layers were used for the statistic tests to ensure the results. Additionally, the statistically analysis was conducted for each sampler separately. The results are shown in Table 3.3-2. There were found highly significant differences between the upper and lower layer for SRP for the MLS 4, MLS 5, MLS 11, and MLS 7 and significant differences for MLS 12 but not for MLS 6. The ammonium concentrations also differ significantly for MLS 4 and MLS 7. Vertical differences for dissolved iron could only be identified for MLS 4, MLS 6, and MLS 7.

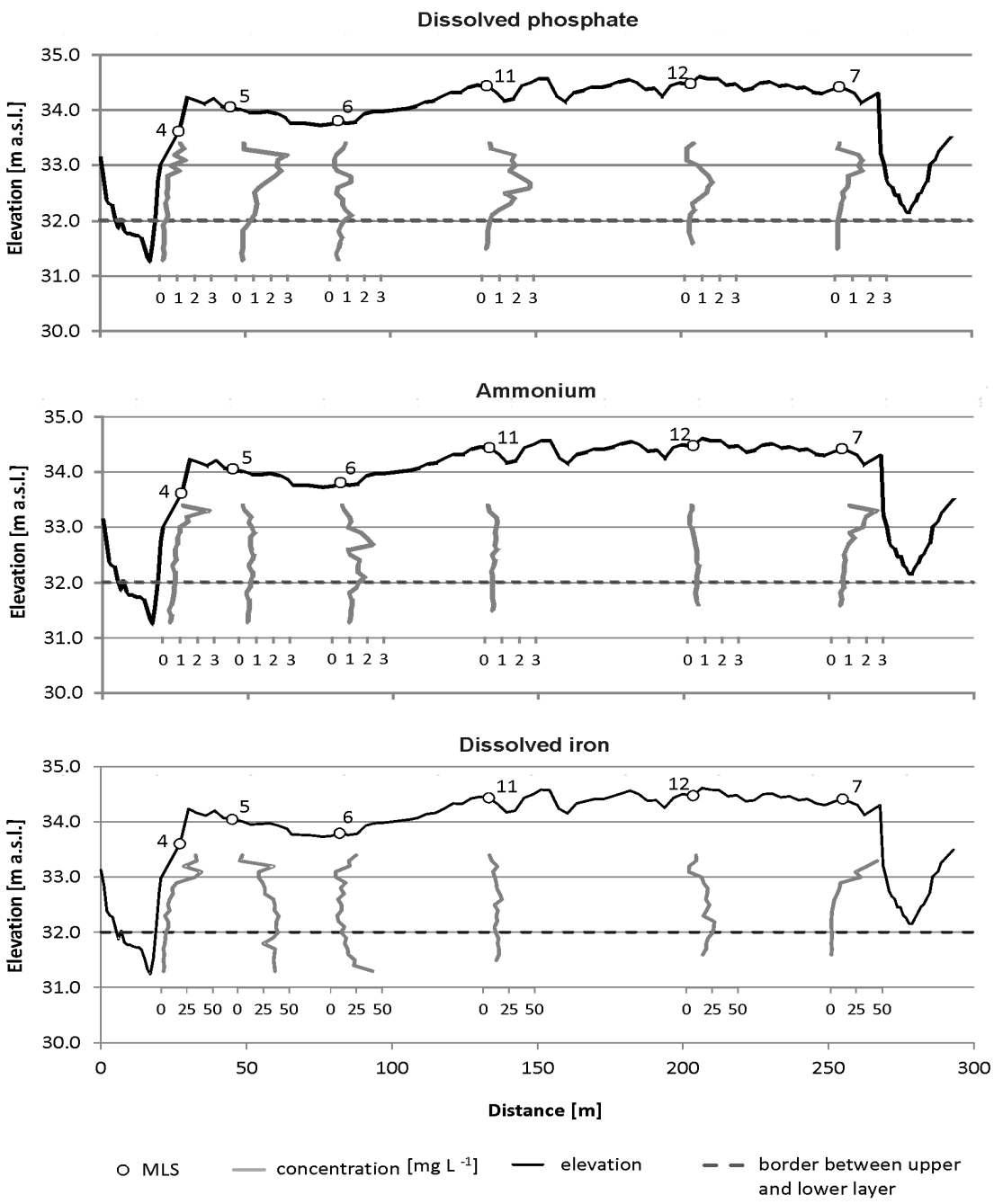

Figure 3.3-5: Median (n = 5) concentration depth profiles of dissolved phosphate, ammonium, and dissolved iron and their location along the transect of permanent piezometers. The dashed line shows the border between the identified upper layer, which is influenced by water level fluctuations and the lower layer, which is not.

First horizontal sampling campaign with temporary piezometers. The two sampling campaigns with temporary piezometers focused on the upper aquifer layer identified by MLS investigation above 32 m a.s.l. Because of the onsite measurements, the upper groundwater can be classified as pH neutral, with

reducing conditions and decreasing electrical conductivities from west to east (> 1000 µS cm^{-1} close to artificial channel to about 300 µS cm^{-1} close to meander bend, Fehler: Referenz nicht gefunden). The small-scale variation of the on-site parameters is very heterogeneous. pH values range between 6 and 7 below the meander scroll bars. Electrical conductivities vary about < 100 µS cm^{-1} within the 3 m distance between neighboring temporary piezometers (Figure 3.3-6). The concentrations of SRP, NH_4^+, and Fe^{2+} are also very heterogeneous, whereas nitrate concentrations were always below the detection limit (< 0.05 mg l^{-1}). This confirms the findings of Lewandowski and Nützmann (2010). Because the results of the GPR and the DEM showed fundamental changes of horizontal sediment distribution and topography, the transect of the first campaign was subdivided into four different zones as shown in Table 3.3-1 and Figure 3.3-6.

In the first zone (I) (n = 12), largest differences were detected for SRP (0.4 – 2.2 mg l^{-1}) and dissolved iron (6.5–74 mg l^{-1}). However, both show the same pattern, which results in a significant Spearman's correlation index of 0.8 ($p<0.01$). The variation of ammonium (0.5 - 1 mg NH_4^+ - N l^{-1}) is less intense within zone I and has no significant correlation with SRP. The second zone (II) (n = 7) has higher variations of NH_4^+–N (0.4–1.6 mg l^{-1}) and Fe^{2+} (10–30 mg l^{-1}) than variations of SRP (0.2–0.7mg l^{-1}). Nevertheless, a correlation was found for phosphate and dissolved iron ($R_S = 0.7$, $p < 0.1$).

In zone III (n = 15), SRP (0.1–0.4 mg l^{-1}) and NH_4^+–N (0.2–0.7 mg l^{-1}) are low and varying in a small range, whereas Fe^{2+} is the most varying compound in this zone (4–30 mg l^{-1}). The correlations between phosphate and ammonium as well as between phosphate and iron are close and significant ($R_S = 0.7$, $p < 0.01$).

Zone IV (n = 42) is characterized by the largest heterogeneity of nutrient concentrations. All parameters are varying in a wide range from almost zero up to 4.5 mg l^{-1} (SRP), 2mg l^{-1} (NH_4^+ - N), and 72 mg l^{-1} (Fe^{2+}), respectively. In general, there is no clear correlation between the different ions.

A Kruskal–Wallis test has been conducted to test if the differences between the four zones are significant. The test indicates that the concentrations of SRP ($H(3) = 36.4$, $p = 5.5 \times 10^{-8}$), NH_4^+ ($H(3) = 14.46$, $p = 0.0023$), and Fe^{2+} ($H(3) = 13.49$, $p = 0.008$) are significantly different for the four groups. A detailed view on the data distribution in the single groups is illustrated in Fehler: Referenz nicht gefunden. Post hoc tests by Siegel and Castellan (1988) indicate that the SRP concentrations between the zones I - III, II - IV, and III - IV are significantly different, whereas there is no significant difference of SRP between the zones I - II, I -IV, and II - III. Ammonium concentrations are only significantly different between zones II - III, and the concentrations of dissolved iron are significantly different between zones I - III and III - IV (Table 3.3-2).

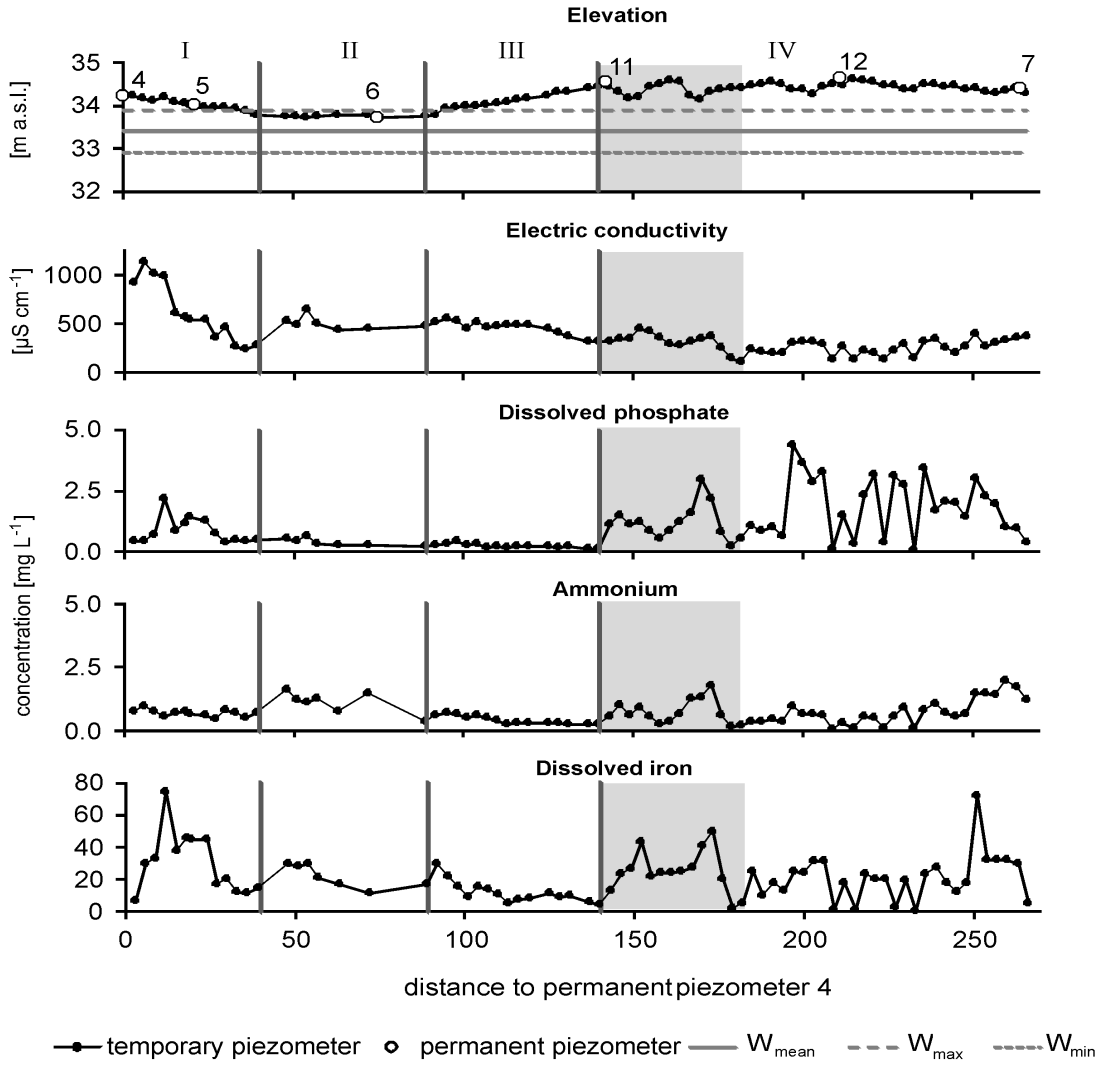

Figure 3.3-6: Concentration patterns determined by the linear investigation with temporary piezometers (first campaign) along the transect of permanent piezometers. Zone marked in grey illustrates locations of temporary piezometers in the second campaign (Figure 3.3-8). Zones I - IV have been identified as stratigraphically different zones based on DEM and GPR.

Table 3.3-2: Results of the Mann–Whitney U tests between the upper and lower layers of the MLS investigations. W is the test statistic, p the probability and r the magnitude of the effect size. Statistically significant differences between the upper and the lower layers are colored in grey.

	SRP			NH_4^+			Fe^{2+}		
	W	**p**	**r**	**W**	**p**	**r**	**W**	**p**	**r**
MLS 4	2343	$2.8 \cdot 10^{-12}$	0.67	2030	$8 \cdot 10^{-7}$	0.47	2347	$2.3 \cdot 10^{-12}$	0.67
MLS 5	2254	$1.1 \cdot 10^{-11}$	0.66	1575	0.026	0.22	1110	0.37	0.08
MLS 6	1063	0.36	0.1	1117	0.17	0.14	556	$8 \cdot 10^{-4}$	0.35
MLS 11	1643	$2 \cdot 10^{-8}$	0.56	1126	0.13	0.15	651	0.02	0.23
MLS 12	951	0.057	0.19	399	0.002	0.32	554	0.09	0.17
MLS 7	1270	$2 \cdot 10^{-7}$	0.54	1116	$2 \cdot 10^{-4}$	0.4	1240	$8 \cdot 10^{-7}$	0.51

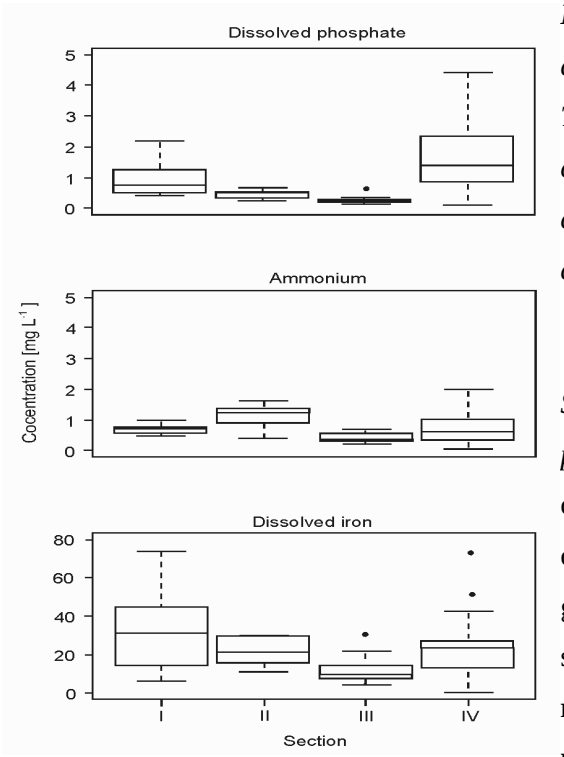

Figure 3.3-7: Concentration distribution of phosphate, ammonium, and dissolved iron for the four sections. The differences are significant between the SRP concentrations of section I–III, II–IV and III–IV. NH_4^+ differences are only significant between Sections II–III and Fe^{2+} between I–III and III–IV.

Second horizontal sampling campaign with temporary piezometer. Based on a visual comparison of nutrient concentrations with the topography of zone IV, a correlation of the concentrations with the geomorphological features is indicated. This finding is systematically tested with the second campaign along a ridge–swale structure, with positions of temporary piezometers relatively close to each other. Figure 3.3-8(left graphs) illustrates the results of SRP, ammonium, and dissolved iron as a mean for three swale transects and three ridge transects (n = 6, Figure 3.3-2). Also, in this case, all nitrate concentrations are below the detection limit. Figure 3.3-8 A visualizes the mean elevation of each transect. Phosphate and ammonium have minimum concentrations in the aquifer below the first transect (0.3 mg SRP l^{-1} and 0.3 mg NH_4^+ - N l^{-1}). Maximum concentrations were measured below the transect 6 (3.0 mg SRP l^{-1}

and 1.6 mg NH_4^+ - N l^{-1}). Dissolved iron is increasing from 5 to 35 mg l^{-1} at transect 6. Hence, there is a gradient for all parameters, which is assumed to be a result of increasing contents of OM from transects 1 to 6. The amount of OM was not determined during the investigation; however, the gradient was visually recognized during the drillings. To identify the impact of the surface elevation on the groundwater composition, this gradient of OM content needs to be eliminated from the data. The elimination is done by adopting a linear regression line to each biogeochemical parameter and using the residuals to test if the concentration of phosphate, ammonium, and dissolved iron differ significantly between the ridges and the swales. Because the residuals were normally distributed, a t-test with two independent variables was performed. Phosphate ($t(32.4) = -2.64$, $p = 0.01$) and ammonium ($t(33.7) = -2.46$, $p = 0.02$) differ significantly between the ridges (lower concentrations) and the swales (higher concentrations) while dissolved iron is not significantly different ($t(31.3) = 1.1$, $p = 2.8$) (Figure 3.3-8 E, F, and G).

The Spearman's correlation indices between the ions measured in the second campaign are high. Phosphate and ammonium have an R_S of 0.82 ($p < 0.001$). For phosphate and dissolved iron as well as for ammonium and dissolved iron, R_S is 0.63 ($p < 0.001$). Correlations differ for separate evaluations of ridges and swales (Table 3.3-3).

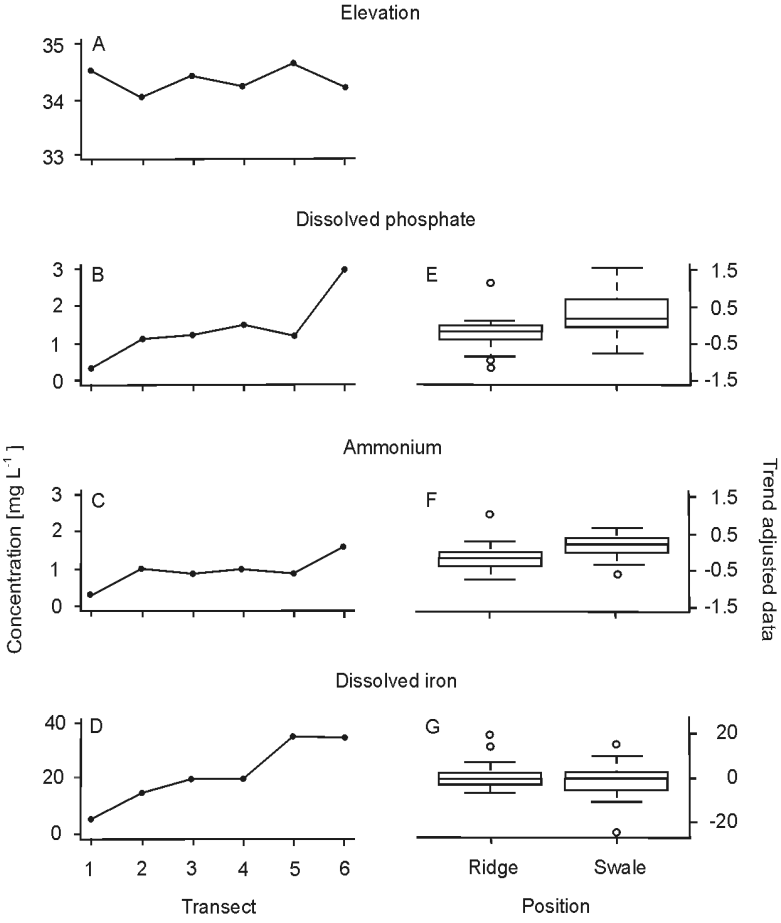

Figure 3.3-8: Results of the investigation of groundwater below ridges and swales with temporary piezometers (second campaign). Panels A–D show the average (n = 6) for each ridge (n = 3) or swale (n = 3), respectively (compare locations shown in Figure 3.3-2). Panels E–G show the boxplots for the trend adjusted data. The differences between ridges and swales are significant for phosphate and ammonium, whereas there is no significance for dissolved iron.

Table 3.3-3: Spearman's correlation coefficients for concentration of soluble reactive phosphate, ammonium, and dissolved iron for the temporary piezometer located in the swales and on the ridges (second campaign). (p < 0.001; ** p < 0.01)*

	Total (n=36)	**Ridges** (n=18)	**Swales** (n=18)
SRP : NH_4^+	0.82*	0.90*	0.6*
SRP : Fe^{2+}	0.63*	0.69**	0.6**
NH_4^+ : Fe^{2+}	0.63*	0.74*	0.72*

3.3.4 Discussion

The investigation of groundwater nutrient concentrations indicates that there are at least two vertical layers with different nutrient distributions. The upper layer is characterized by high and heterogeneous concentrations, whereas below the concentrations are spatially more homogeneous (Figure 3.3-5). Nützmann et al. (2013) already described a hydraulic division of the aquifer, with the upper 15 m of the aquifer indicating a local flow system and the deeper parts belonging to the regional flow system. However, the identified biogeochemical layers are both located in the local flow system; the upper layer is of only 2 m thickness and characterized by maximum concentrations between the average and the minimum groundwater table depth. Because the investigated species are redox-sensitive, it suggests itself that changes in the redox chemistry are causing the layering. The deeper layer is free of oxygen and nitrate. This goes along with findings from Lewandowski and Nützmann (2010) who found that O_2 and NO_3^- concentrations are completely depleted within a flow path of a few meters in the groundwater approaching the floodplain from the moraine plateau. Additionally, there is less easily degradable material in the deeper layer than in the upper layer. This implies little release of phosphate and ammonium by biological degradation processes (Uusi-Kämppäa et al., 1997; Reddy et al., 1999; Rivett et al., 2008). Also, the second source of phosphate release, the dissolution of ironbound phosphate, is less important because the permanent saturation leads to a decreased availability of iron in general. Both processes are relevant in the upper layer because there is much reactivity and an annual change in the redox conditions. These changes can be attributed to water level fluctuations in the upper part of the aquifer and the delivery of easy degradable organic material from the soil surface (Lewandowski et al., 2009). The temporal stability of both layers is reasonable because of the very low groundwater flow velocities of about 10-6 m s-1 in horizontal direction and 10^{-6} to 10^{-7} m s^{-1} in the vertical direction (Nützmann et al., 2013).

Because of the stability of the layers thicknesses and the homogeneity of the deeper layer, the upper two meters of the aquifer represent most of the spatial heterogeneity of the nutrient concentrations observed by Lewandowski and Nützmann (2010). Therefore, a horizontally highly resolved sampling was conducted along the transect of permanent piezometers. The results show a quite heterogeneous distribution of nutrients even within a flow path of only 3m (Figure 3.3-6). Additional GPR and DEM investigations allow a linkage between the nutrient concentrations, microtopography, and sediment characteristics. A difference in altitude of 1m is already important for local leaching and storage processes. The topography is crucial for the local thickness of the unsaturated zone, and therefore, it decides about different timescales for nutrient turnover (Courtwright and Findlay, 2011; Tiemeyer et al., 2007). On the local scale, the most important sediment characteristics are the grain size composition and the amount of OM. According to topography and grain size composition, the upper aquifer was divided horizontally in four different zones (Table 3.3-1, Figure 3.3-6).

In general, the GPR investigation revealed that the floodplain was formed by two different fluvial processes. The area from the artificial channel up to the middle of the island is formed by vertical accretions, whereas lateral accumulation dominates the second part of the floodplain. Vertical accretion occurs during flood events when the river inundates into its floodplain and sediments are deposited on the ground. The resulting topography is shallow and even, and the sediments are less coarse (Bridge, 2003; Charlton, 2008). In the investigated floodplain, this results in two slightly inclined slopes and a flatter and less elevated area between them. These are forming three of the four zones (I to III), which determine the nutrient concentrations in the upper aquifer. The first ridge (zone I) is close to the artificial channel and is the result of the construction of the channel. This can also be seen in the unlayered and destroyed sediment structure in the underground (Figure 3.3-4 C). It is followed by a swale (zone II), which forms the deepest part of the island. Here, relict channels filled with OM were identified by GPR. In this zone, the groundwater level is close to the surface or even above the surface during high water level periods. Therefore, a special habitat formed here, where moisture adopted plants are dominating (Lewandowski and Nützmann, 2010). In direction to the meander, the elevation increases from 33.8 m a.s.l. in the swale to 34.5 m a.s.l. within a horizontal distance of 60m (zone III). The distinctive sediment property is a silt layer in about 1m depth, which accumulated during flood events in areas with very low flow velocities. The groundwater sampling was conducted below the silt.

The adjacent zone IV reaches from the middle of the island to the meander and is characterized by an undulating topography. This belongs to the alternation of successive levees (ridges) and backswamps (swales), which were formed during the movement of the meander (Hickin, 1974), and this features are named meander scroll bars (Lobeck, 1939). The sediment in this area consists of slightly inclined layers of sand and OM (Figure 3.3-4). The mean difference in elevation between ridges (34.6 m a.s.l.)

and swales (34.2 m a.s.l.) amounts only to 0.4 m. However, this is sufficient for the formation of different habitats because the availability of groundwater is the restrictive factor for the vegetation development. Hence, on the ridges the plant communities are more adapted to drier conditions than in the swales.

The comparison of zone I and IV of the first campaign shows similar high and heterogeneous phosphate and iron concentrations. The sediments of both sections consist of fine to medium sands: The sediments in zone I were accumulated anthropogenically during channel construction and in zone IV by the river. Both zones have similar surface elevations. Nevertheless, in zone I, the source for phosphate seems to be the dissolution of iron, which is indicated by the high correlation between dissolved iron and SRP (R_S = 0.8), whereas in zone IV, no dominant process could be identified. However, by taking a detailed look at both zones, one could identify a gradient in surface elevation. The land surface elevation of zone I is on average 34 m a.s.l., whereas the elevation of zone IV is 0.4m higher. Furthermore, the topography of zone IV is quite undulating. Hence, the average elevation is not an adequate representation for this zone. Therefore, the second horizontal campaign was conducted to investigate the influence of the alternating ridges and swales. Below the ridges, ammonium and dissolved phosphate are significantly correlated indicating that the release of both nutrients is the result of the degradation of OM (mineralization). In contrast, below the swales, phosphate release from mineralization of OM and dissolution of iron(III) compounds are equally important. The reason for this could be the thickness of the unsaturated zone. Even during high water levels, the ridges have an unsaturated zone of at least 0.5m, whereas this is less than 0.1m below the swales. Hence, there is an increased stability of iron(III) compounds as a result of the higher oxygen availability below the ridges and therefore a higher binding capacity for phosphate than below the swales. High nutrient concentrations were observed below the swales. Besides the dissolution of iron(III) compounds and subsequent P mobilization, it can be assumed that there is an increased biogeochemical turnover below the swales. As mentioned before, there is a difference in plant communities of ridges and swales. The annual production of plant material is much higher in the swales, and therefore, the delivery of easily degradable material is also increased fuelling biological turnover processes below swales.

This conclusion is also supported by zones II and III, where surface elevation is similar to that of zone I. However, the sediments in these zones are well sorted and less coarse. For phosphate and dissolved iron, the median concentrations and the variation of the concentrations are lower than those of zones II and III. Because zone II is the zone with the deepest surface elevation along the transect, the thickness of the unsaturated zone is almost zero during medium and high groundwater levels (Figure 3.3-6). Hence, the duration of complete saturation of the sediments is very long, and the biological turnover is decreased. However, it has to be considered that these conclusions for zone II are only based on seven samples (Figure 3.3-6). In contrast to zone II, the low concentrations of phosphate, dissolved iron, and

ammonium in zone III are caused by a layer of silt in a depth of about 1.5m below ground that diminishes the delivery of nutrients into the aquifer from the surface.

The ammonium concentrations of the four zones differ much less along the transect than the concentrations of phosphate and dissolved iron do (Figure 3.3-6). However, zone II reveals two peaks of high ammonium concentrations (Figure 3.3-6). These peaks occur below the two swales that are filled with OM (Figure 3.3-4). As mentioned above, zone II has the lowest elevation in the floodplain. Because the groundwater level is very close to the surface elevation even in summer, biomass production is not water limited. Hence, we observed that this area is a favored grazing place for the stock cattle and thus excrements accumulation. We assume that this results in the locally high ammonium concentrations.

3.3.5 Conclusion

The study showed that in floodplain aquifers with low hydraulic gradients and resulting low flow velocities, spatially heterogeneous nutrient concentration might establish. Moreover, this heterogeneity could be found in vertical as well as horizontal dimension. The vertical heterogeneity is the result of water level fluctuations, which lead to the establishment of a vertical layering of nutrient concentrations. The upper layer (about 1.5 m) is influenced by the change of water saturation of the sediment. This leads to the establishment of different redox zones, which set off different chemical reactions and biological processes. Furthermore, there is a permanent delivery of easy degradable OM from the surface supporting nutrient release and storage. The conditions in the lower layer are more constant. There are permanent reducing conditions and low delivery of organics. This implies more stable and lower nutrient concentrations. Furthermore, we found that the vertical layering of the nutrient concentration is not related to the vertical layering of the sediment or the local or regional groundwater flow pattern.

Besides the water level fluctuation, the upper layer is impacted by variations of surface elevations, of sediment grain size distributions and of vegetation patterns. The horizontal heterogeneity results in four zones caused by differences in sediment composition, surface elevation, vegetation, and the thickness of the unsaturated zone, respectively. This induces the establishment of different redox gradients on a small scale, which are responsible for the stability of abiotic nutrient sorption and biological turnover processes. In general, there is no strict separation of the factor surface elevation and sediment distribution possible because they are both results of the same geomorphological processes and thus, mutually dependent. Moreover, if one factor is known, this allows conclusion on the other one. Even though nutrient concentrations in the upper groundwater layer are high, it cannot

be concluded that the floodplain is the source of high nutrient loads for the river. The groundwater flow velocity is very low (Nützmann et al., 2013), and the sediments in the upper layer consist of finer material than below. Hence, this improves the retention capacity and reduces nutrient transport (Burt et al., 1999). Furthermore, little is known about the nutrient retention at the interface between the aquifer and the river Spree, i.e. even if a significant amount of nutrients is transported toward the surface water body, it might be possible that these nutrients are immobilized at the immediate interface. Hence, no conclusion can be drawn on the impact of the upper groundwater on the surface water.

3.4 The hole in the aquifer - effects of groundwater leakage on the local groundwater flow system of a lake

Franziska Pöschke[1,2] , Gunnar Nützmann[1,2], Peter Engesgaard [3], Jörg Lewandowski[1,2]

[1] Leibniz-Institute of Freshwater Ecology and Inland Fisheries, Dept. Ecohydrology, Berlin, Germany

[2] Humboldt-University of Berlin, Geographical Institute, Berlin, Germany

[3] University of Copenhagen, Dept. Geosciences and Natural Resources Management, Copenhagen, Denmark

Abstract

Groundwater is an important source of compounds in lake mass balances and impacts on surface water quality. In that context a lot of studies were focusing on the direct transition zone between groundwater and surface water and identified this zone as highly effective in terms of storage and turnover. However, most of these studies neglect that groundwater originates from different flow systems (local, intermediate, regional). Thus, besides chemical and biological processes there is also a physical mixing of different water qualities within the transition zone. Hence, the size of the catchment, the concentrations at the source and transformations along the flow path are important to determine the load which enters the surface water. The subsurface basin of Lake Stechlin is of complex nature and water level measurements in groundwater wells with different filter depths show potential diverging flow paths. In order to explore the groundwater flow systems and her potential contributions to the lake's mass balance we estimate the extension of the Lake Stechlin subsurface basin with a simple steady-state 2D vertical modeling approach. It turned out, that the lake is only fed only by a local groundwater recharge. However, the subsurface catchment of the lake contributes to regional discharge. That implies that not the total groundwater recharge which formed in the catchment can be considered for lake water balances. Furthermore, the contribution to regional flow systems also implies a decrease of extension of the local flow system and a prolongation of flow paths within the local flow systems. This is plays an important role concerning water traveling and chemical reaction times.

3.4.1 Introduction

Lakes are used by humans for many purposes, e.g. water supply, recreational activities, fishery etc.. Therefore, there are high demands regarding to lake water quality. Hence, management strategies for lakes depend on a reliable elaboration of the water and substance balance; however this is still a challenge, especially when groundwater has large impacts on the mass balance (Rosenberry et al., 2015). In general, there are two approaches to estimate the volume of lacustrine groundwater discharge (LGD): (1) measurement of groundwater ex- and infiltration directly in the lake sediments and (2) calculating budgets relying on the catchment size. The first allows a direct estimation of fluxes; however, the upscaling of local groundwater ex- and infiltration measurements for the whole lake is difficult due to the spatio-temporal heterogeneity of fluxes (e.g. Fleckenstein et al., 2009, Kidmose et al., 2011, Meinikmann et al., 2013). Furthermore, there is recently no consistent measurement method for flux quantification (Rosenberry et al., 2015).

In contrast, the second approach is more reliable regarding the total volume which entering the lake, but cannot give evidences regarding the area, where the subsurface water is entering the surface water body. However, the requirement for the second approach is an accurate estimate about the subsurface area, which is discharging into the lake. In surface hydrology this area can be described by the topography (e.g. Winter et al., 2003). In subsurface hydrology this parameter alone is not sufficient, especially in low land areas (Winter et al., 2003). For instance, Tóth (1963) illustrated the formation of nested flow systems (local, intermediate, regional) along a topographic gradient of the water table. That implies that the discharge area to a surface water body increases with distance to the watershed (Figure 3.4-1). Beside the amount of water entering a lake, the chemical composition of the lakes is more similar to that of the groundwater the more they are situated at the lower end of the landscape (Webster et al., 1996, Kratz et al., 1997, Ala-aho et al., 2015). Hence, chemical composition of the groundwater and surface water can also be used for identifying different groundwater origins (Menció et al., 2012, Ala-aho, et al., 2015).

This could lead to the assumption that the estimation of catchment sizes for lakes at the upper end of the landscape should easier since only local flow systems are present. However, Winter (1983) could illustrate with a hypothetical model the time dependency of the local flow system, which is mainly depending on the climatic conditions. Higher groundwater recharges lead to the formation of groundwater mounds, which than contribute to the groundwater discharge towards the lake. For instance, this could be proven by Anderson and Munter (1981) for Lake Snake (USA) and Holzbecher (2001) for Lake Stechlin. Furthermore, variations of geological settings and sediment distributions within the aquifer and lake also lead to variations of local groundwater flow systems (Winter et al. 1998).

So far, there is no study, which consider that surface water and their groundwater catchment in a head areas of lowlands belongs to the recharge area of the regional flow system (Figure 3.4-1)). Hence, there are two hydraulic gradients present in head water systems: the gradient towards the lake and the one towards the depth (Figure 3.4-1). This downward flux was neglected, since in a layered aquifer system the higher hydraulic conductivity of the aquifer directly connected to the surface water was assumed to dominate the subsurface flow processes. However, in hydrogeology leaking aquifers are a well-known phenomenon (Bear, 1988), which is mostly considered for the delivery rate for wells in a specific aquifer (e.g. Hemker, 1999; Jiang et al., 2013). However, until know it was not taken into account for the determination of the subsurface catchment of a lake.

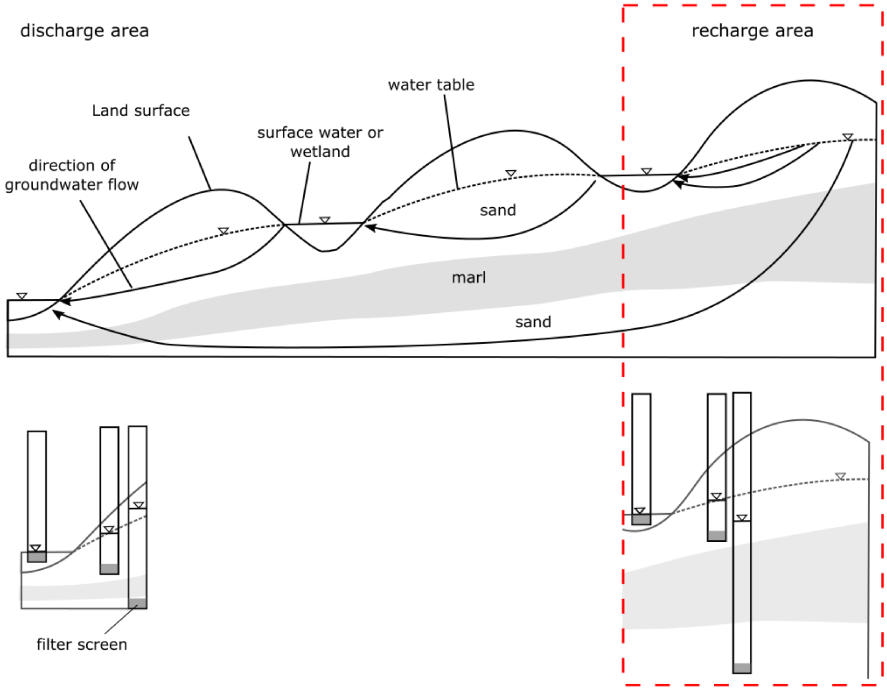

Figure 3.4-1: Concept of nested flow systems and layered aquifer systems in low land areas. The focus of the present study is set on the local flow systems in recharge areas in the head areas of low land landscapes.

In the present study, we hypothesized that the contribution to the regional flow system in a head water side has an impact of the size of the local flow system of a lake. Since this is very hard to prove with field measurements, we set up a numerical groundwater model. The chosen test site is situated in the NE German lowland head waters. The natural protected area of Lake Stechlin is equipped with about 60 stations of water level observations stations, which were measured monthly since 1957. There are 20 surface water gauges and about 40 groundwater wells, whereas the most are filtered in the upper unconfined aquifer, which are hydraulically well connected with the lakes. However, there are some

wells filtered in the second aquifer. However, the hydrogeological conditions in the area are very dynamic. Holzbecher (2001) found that there is a horizontal variation of the watersheds between the different lakes, which make an application of a 3D model very complicated. Therefore, it was assumed that a simple 2D vertical cross section model should be sufficient to test the hypothesis. Hence, a transect of groundwater wells was chosen, where the general groundwater flow direction from the catchment into the lake does not change over time and a groundwater level measurement in a deeper aquifer was available (Figure 3.4-2). Furthermore, different scenarios were calculated to get some insights about the extent of the groundwater leakage and its effect on the catchment size and the groundwater flow path.

3.4.2 Material and Methods

Study Site

Lake Stechlin (N53° 9' 8.212" E13° 1' 43.388") is situated in the south of the Mecklenburg Lake District in NE Germany (Figure 3.4-2). The area was formed by the last glaciation period in northern Europe (Weichsel) and is characterized by a slight undulating topography, closed drainage basins and highly permeable sediments. The recharge is dominated by the groundwater flow (95 %) (Merz and Pekdeger, 2011).

The lake itself is situated in a depression of a former melt water channel, which was cut into the sediments of an outwash plain and blocked by dead ice after the removal of the inland ice sheet (Ginzel and Kaboth, 1999). Lake Stechlin is embedded into a layered aquifer system, which is terminated by a Mesozoic clay layer (~ 140 m below sea level). The clay separates the subsurface freshwater from the saltwater (Kaboth et al., 2008). The sandy outwash plain forms the upper unconfined aquifer of a thickness up to 50 m and a hydraulic conductivity $k_f \sim 10^{-4}$ ms^{-1} (Ginzel and Kaboth, 1999; Samek, 2000). This aquifer is hydraulically well connected to the lake. The second aquifer is separated from the upper one by ground moraine from the previous glaciation (thickness: 10 – 50m, $k_f < 10^{-6}$ ms^{-1}) (Kaboth et al., 2008).

The size of the subsurface catchment of Lake Stechlin is determined by the surrounding lakes and the climatic conditions (Holzbecher, 2001). The author could illustrated, that catchment size increases in its horizontal extension during periods of increased precipitation and vice versa. The average size is about 12 km^2.

The climatic conditions can be characterized as warm and temperate (Richter, 1997). The long- term average precipitation (1981 – 2010) for a broader area is about 560 mm a^{-1} (Deutscher Wetterdienst,

2014). Estimations of the average groundwater recharge calculation for the area reaching from 68 mm a^{-1} to 130 mm a^{-1} (Richter, 1997; Ginzel and Kaboth, 1999; Nützmann et al., 2003; Solzbacher, 2013).

The whole catchment area of the lake belongs to a natural protected area since 1938. Therefore, the catchment is covered by 95 % by forest, which is dominated by mixed forests of beeches (*fagus sylvatica*) and pine (*pinus sylvestris*) (Feierabend and Koschel, 2011).

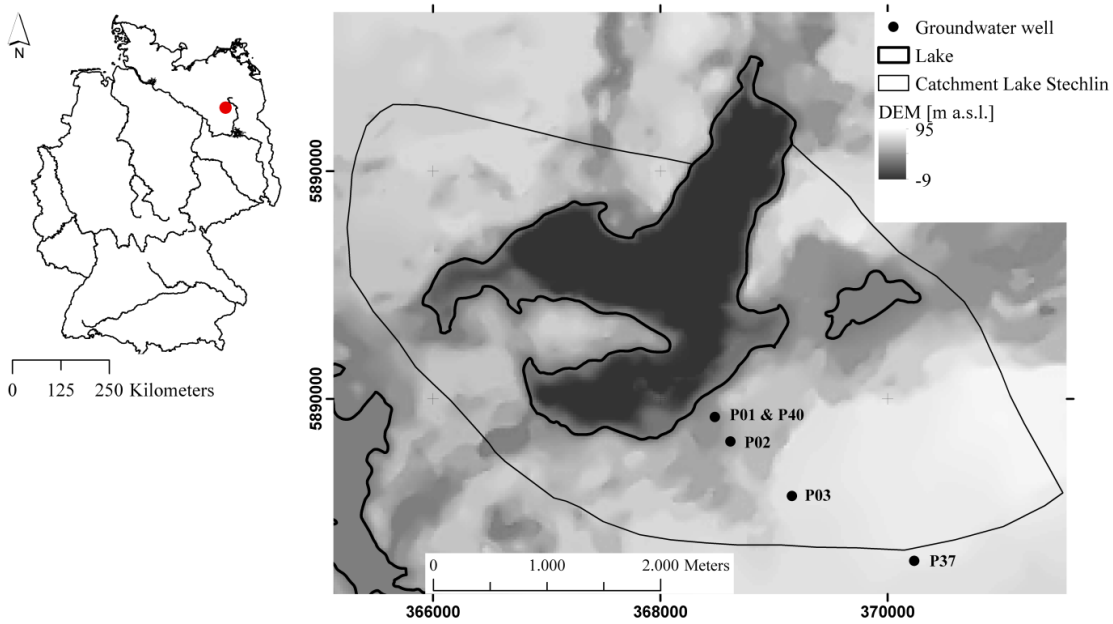

Figure 3.4-2: The left side illustrates the location of the study site within Germany (red dot).The right side gives an over view of the elevation groundwater catchment and bathymetry of Lake Stechlin. The black dots mark the position of the groundwater wells used for the conceptual model and the numerical simulation.

Conceptual model

The geological and geomorphological conditions along the investigated transect (Figure 3.4-2) are a result of the last Mid-European glaciation periods. The sediment of the upper unconfined aquifer was accumulated during the last glaciation (Weichel) in the outwash plain of the glacier. Hence, the sediment composition is quite homogeneous and consists of medium to coarse sands (Ginzel and Kaboth, 1999). Below there is a Saalian till layer ($k_f < 10^{-6}$ m s^{-1}) (Kaboth et al. 2008), which separates the upper aquifer from deeper ones. However, due to the large gradient into deeper aquifers (compare water level of well P01 to the lake level; Figure 3.4-3), it can be assumed that this layer is not impermeable (Ginzel and Kaboth, 1999). The topography along the transect is decreasing from south-east (92 m; catchment border) to north-west (59 m; lake shore) There is a steep step in elevation in 800 m distance from the shore. This indicates the extension of the former melt water channel, which cuts

the outwash plain at this location. The former melt water channel is also reflected in the extension of the aquifer. The till layer is about 50 m a.s.l. in the most parts of the catchment of Lake Stechlin and reaches an elevation of about 25 m a.s.l. below the lake itself. This indicates that parts of the till layer were removed by the melt water.

The hydrogeological conditions of the upper aquifer are reflected in the time series of the groundwater levels of the wells P37, P03, P02 and P40. These indicate, that the groundwater flow is driven by to main factors: (1) the groundwater recharge through a large unsaturated zone (P37 and P03) and (2) the anthropogenically controlled hydraulic head of the lake and its annual water level fluctuations (P02, P40) (Figure 3.4-3). The aquifer of the south-eastern part of the transect (P37 and P03) is characterized by a large unsaturated zone (30 m) and a small saturated zone (10 m). The extent of the unsaturated zone leads to a highly dampened time series of the groundwater level fluctuations, which exhibits only long-term fluctuations and no interannual variations of groundwater levels. Assuming an evenly distributed till layer over the entire area, the ground moraine below this part of the transect is at least 25 m thick. This is different for the north-western part of the transect (P02, P40), which represents the melt water channel. Here the ratio of unsaturated zone (< 10 m) to saturated zone (~ 30 m) is reversed. The groundwater is closely coupled to the lake water fluctuations and the thickness of the till layer is decreased and might even be completely eroded in some parts.

The existence of a connection between the upper and the lower aquifer can be concluded from the time series of well P01 (Figure 3.4-3). This well is situated directly adjacent to well P40 but its filter screen is located below the till layer. However, both wells show the same fluctuations which clearly indicates that there is a connection between both aquifers. Furthermore, the water level of P01 is much lower than that of P40 and the lake level. This leads to the assumption that there is a groundwater flow towards the deeper aquifer. This interpretation can be supported by further groundwater level measurements in a multi-level well Hy Ngw 1/ 2009 which reaches down to the Mesozoic clay layer (Table 3.4-1). That well which is located close to P40 and P01 indicates a strong hydraulic gradient towards the deeper aquifers than towards the lake.

Table 3.4-1: Water levels at 05/12/2014 of the deep well Hy Ngw 1/2010 at filtered at different depth. The well is situated close to the wells P01 and P40 (compare Figure 3.4-2).

Well	**Position of the filter [m below surface]**	**Water level [m a.s.l.]**
Hy Ngw 1/2010 OP	4 - 31	59.99
Hy Ngw1/2010 MP	80 - 86	58.93
Hy Ngw 1/2010 UP	164 – 168	57.64
Hy Ngw 1/2010 UP (T)	226 – 231	57.40
Average of Lake Stechlin		59.60

Beside the direct comparison of water levels in a single time step, cross-correlations give some information about how the different time series are temporally dependent. For instance, the cross-correlation between well P03 and P01 indicates a time lag of nine month, whereas between P03 and P40 the time lag is eleven month (Table 3.4-2). This is an additional hint, for a faster groundwater movement towards the deeper aquifer than towards the lake.

Another indication for a contribution to the regional groundwater flow is the fact, that there was a drastic decrease (about 2 m) of the groundwater level of P37 and P03 (within 20 years). Since the water level of Lake Stechlin is more or less constant over that period, it can be assumed that the decrease would not have been so large if the groundwater flow only enters the lake. The same decrease was also observed for other lakes and groundwater wells in the same geographical region (Kaiser et al. 2015).

Table 3.4-2: Cross-correlations of the water levels and time lags (month) of selected wells and the lake

	Lake		P01		P40	
	R^2	**Time lag**	**R^2**	**Time lag**	**R^2**	**Time lag**
P37	0.64	20	0.84	11	0.81	11
P03	0.67	19	0.87	9	0.84	11
P02	0.84	0	0.96	0	0.98	0
P40	0.88	0	0.96	0	-	-
P01	0.85	0	-	-	0.96	0

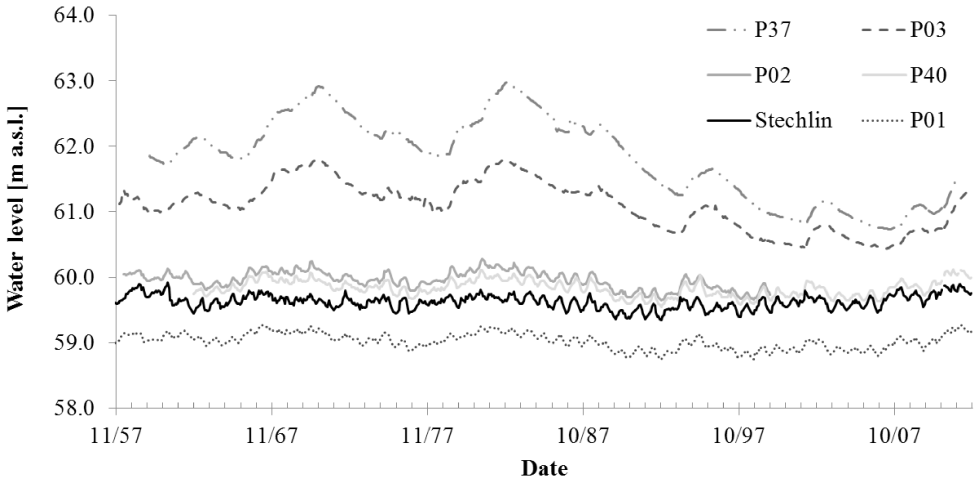

Figure 3.4-3: Water level of Lake Stechlin and five groundwater wells from November 1957 to October 2012. The wells P37, P03, P02 and P40 are filtered in the upper unconfined aquifer. Well P01 is filtered below a glacial till layer. For the location of the wells compare Figure 3.4-2.

In classical hydrogeology, differences in hydraulic gradients are explained by the variability in hydraulic conductivities within the catchment (Hölting and Coldewey, 2009). Hence, this is the fitting parameter for numerical groundwater models in the most cases. That this is not sufficient for the investigated transect can be shown by a simple 1D analytical solution. That model calculates the steady state groundwater level h at a specific point x that establishes based on the length of the system (L ~ 3000 m), the groundwater recharge (N ~ 100 mm a^{-1}) (Solzbacher, 2013), the constant lake level (h_1 = 59.61 m) and a specific hydraulic conductivity (k_f = variable):

$$h = \sqrt{\frac{2N}{k_f}\left(Lx - \frac{x^2}{2}\right) + h_1^2}$$

Equation 3.4-1

Variations of the hydraulic conductivity illustrate that the system is very sensitive to this value (Figure 3.4-4). Hence, an implementation of sediment heterogeneities to improve the fit of the observation points will results in a small scale heterogeneity which is cannot be validated with the available drill logs.

Based on the information presented above, a conceptual model of groundwater flow along the transect in the catchment of Lake Stechlin was developed (Figure 3.4-5). It is assumed that groundwater leaking into deeper aquifers occurs between the border of the melt water channel and the lake´s shoreline (dotted line). Nevertheless, nothing is known about the real extension of the leakage area, which can be rather small or covering the whole area.

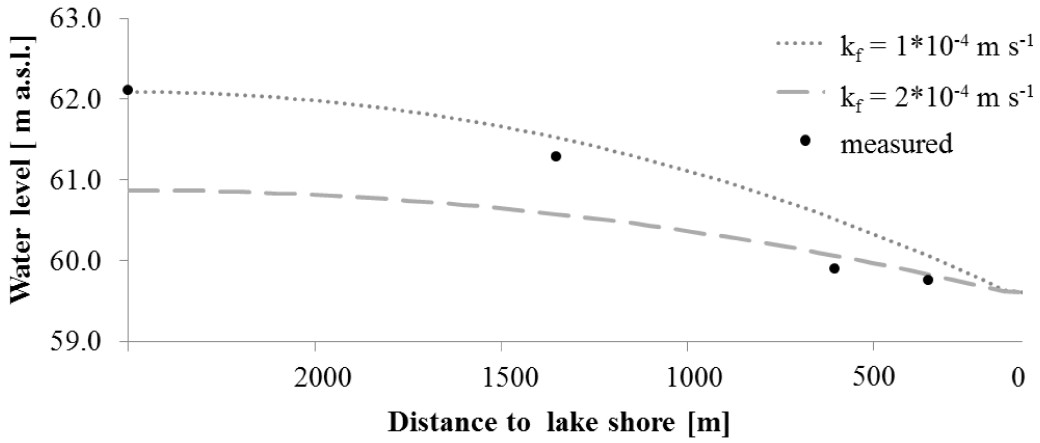

Figure 3.4-4: Groundwater levels that would establish along a flow path from the catchment to the lake for a fixed lake head of 59.6 m a.s.l., a groundwater recharge of 100 mm a^{-1} and different hydraulic conductivities (k_f). Measured average groundwater levels (1962 – 1999) are shown and compared to groundwater levels calculated based on equation 1 assuming steady state conditions. The figure illustrates that the system is very sensitive to small changes in hydraulic conductivities.

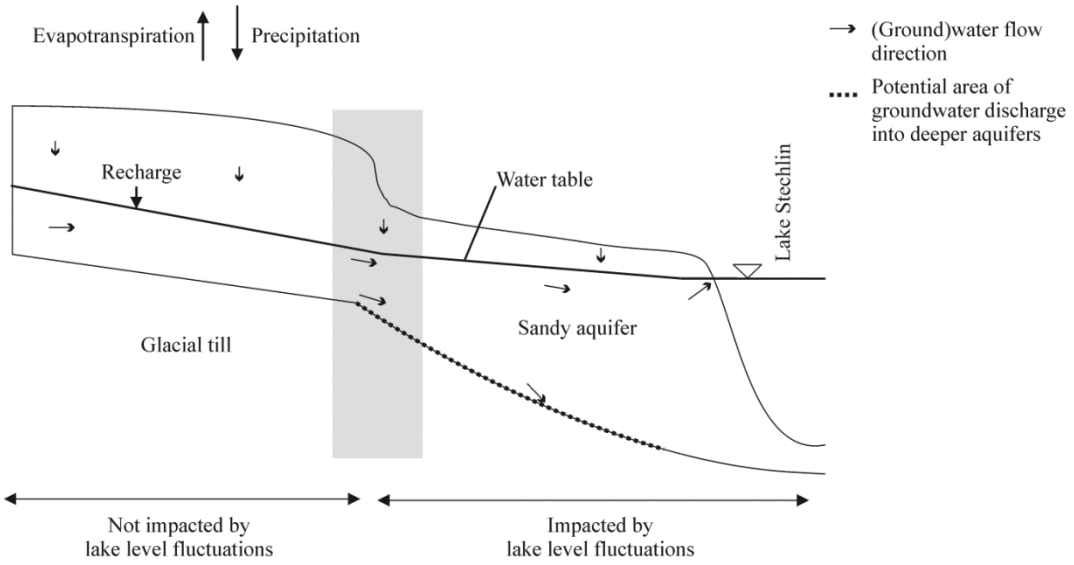

Figure 3.4-5: Conceptual Model for the groundwater flow towards Lake Stechlin and the deeper aquifers. The grey box indicates the area where is an expected change between groundwater level fluctuations. The groundwater level close to the lake is impacted by the lake level fluctuations; the groundwater on the left side is not.

Numerical groundwater model

A 2D numerical groundwater model was established with FEFLOW (Figure 3.4-6) (Diersch, 2014) to test the hypothesis that the groundwater catchment of Lake Stechlin contributes to regional groundwater flow. The overall aim was to get a general estimate of the impact of aquifer leakage on the local groundwater – lake interaction and therefore the simulation was conducted under steady state conditions. This resulted in simplifications for the model set up, the initial conditions and the calibration.

The model domain was set up for the upper aquifer, since the geologic and hydraulic information about the layered aquifer system are not sufficient. The top of the model domain was determined by a digital elevation model with a spatial resolution of 25 m. The position of the bottom was estimated by drill logs of the wells and additional information originating from geological cross sections (Ginzel and Kaboth, 1999). The aquifer is unconfined and the unsaturated zone needs to be considered. Since this zone is thick in the south-east of the transect, this would result in a large computational effort. However, the thickness does not play any role under steady state conditions. Therefore, the thickness of the unsaturated zone was reduced to the maximum observed water level plus one meter. The calculations of the Richards- Equation was conducted with default van Genuchten parameter (α = 1.33 $1m^{-1}$ and n = 1.64).

The hydraulic conductivity was varied according to the estimates of the 1D model (1×10^{-4} m s^{-1} and 2×10^{-4} m s^{-1}).

A long term groundwater recharge of 100 mm a^{-1} was applied as Neumann boundary condition on the top of the model domain. Solzbacher (2013) used different methods for the calculation of groundwater recharge in the catchment of Lake Stechlin such as, BAGLUVA (Glugla et al., 2003), water table fluctuation method (Einsele, 1975) and chloride mass balance (Eriksson and Khunakasem, 1969). The study of Solzbacher (2013) ended with different averages. Thus an average value of all methods was chosen for modeling.

The average lake water level (59.6 m a.s.l.) over a period of 37 years (1962 – 1999) was used as a Dirichlet - boundary condition at the lake bottom. The leakage into deeper aquifers was modeled by a Neumann boundary condition. Since the extension of the leakage area is unknown, three different areas were defined where the water is allowed to leave the system: Leakage area 1 is the smallest and is situated between well P02 and P40 (black line in Figure 3.4-6). The second area (red line in Figure 3.4-6) represents the melt water channel. Leakage area 3 (dark grey line in Figure 3.4-6) is the area where a loss of groundwater over the whole bottom length of the model towards the deeper aquifers occurs.

For each hydraulic conductivity four different scenarios were considered (Table 3.4-3): without drainage and with the tree different drain areas (see Figure 3.4-6). For each scenario the leakage flux was calibrated, until the root mean square error between model and observed groundwater heads reached its minimum.

For calibration the modeled groundwater head was compared with the average observed groundwater levels for a period of 37 years (1962 – 1999).

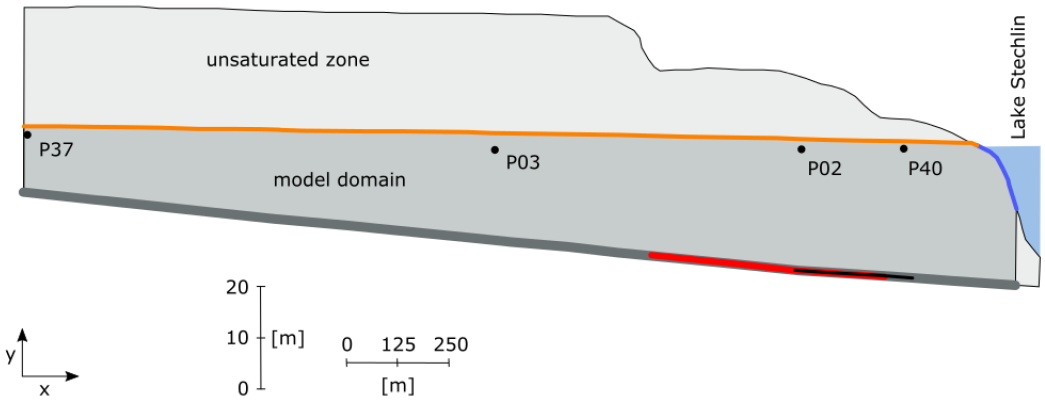

Figure 3.4-6: 2D vertical cross-sectional FEFLOW model for a groundwater transect at Lake Stechlin. The dark grey area indicates the area used for the numerical simulation; the white grey area is the total extension of the system, which shows also the thick unsaturated zone. The black points show the position of the observation points. The lake water level was used as fixed head boundary condition (blue line) of 59.60 m a.s.l., the average groundwater recharge (100 mm a^{-1}) was applied at the top of the model domain (orange line). At the bottom there were different groundwater leakage areas, which were used in different model scenarios: the leakage area 1 (black), 2 (red) and 3 (dark grey). Please note the different horizontal and vertical scales.

Table 3.4-3: Overview over the eight simulation scenarios which consider different hydraulic conductivities and different leakage areas. The leakage fluxes listed in the table are the fluxes which produced the best fit between observed and simulated groundwater levels.

Model scenario	**Hydraulic conductivity [10^{-4} m s^{-1}]**	**Leakage area**	**Leakage flux [mm a^{-1}]**
I	1	-	-
I a	1	1	700
I b	1	2	300
I c	1	3	40
II	2	-	-
II a	2	1	100
II b	2	2	50
II c	2	3	10

3.4.3 Results

All models scenarios ran numerical stable and resulted in a balanced budget. The root mean square error (RMSE) between the measurements and model runs varies between 0.16 and 1 between the scenarios (Table 3.4-4).

A sufficient good adjustment of the simulated to the observed values can be achieved by a calibration of the hydraulic conductivity as well as by the variation of the subsurface drainage towards deeper aquifers (Table 3.4-4).

For all scenarios II a PEST calibrated hydraulic conductivity ($2 \cdot 10^{-4}$ m s^{-1}) was used as basis for the calculations. This resulted in a good fit for all wells except for well P02, which was overestimated (~ 0.3 m) (scenario II). The implementation of a subsurface drainage (II a – c) does not lead to a significant improvement of the adjustment of well P02. Only high amounts of drainage would lead to a good fit of P02 which in contrast results in a drastic underestimation of the other wells. Hence, a subsurface drainage is only of minor importance for these scenarios.

Table 3.4-4: Results of the eight different model scenarios. Positive deviations between simulated and measured groundwater levels indicate an overestimation while negative values indicate an underestimation. Furthermore, the Root Mean Square Error is shown to compare the performance of the different model runs. The budget columns show the volume of water entering the lake or the deeper aquifers.

Model scenarios	**Deviation simulated - measured**				**RMSE**	**Budget**	
	P37	**P03**	**P02**	**P40**		**Flux into the lake [m^3 a^{-1}]**	**Flux into the deeper aquifer [m^3 a^{-1}]**
I	1.43	1.11	0.81	0.28	1.00	232	-
I a	0.77	0.41	0.06	-0.17	0.45	35	197
I b	0.45	0.07	-0.03	-0.01	0.24	62	169
I c	-0.05	0.05	0.34	0.07	0.18	136	97
II	-0.11	0.01	0.33	0.07	0.18	232	-
II a	-0.17	-0.05	0.27	-0.03	0.16	204	28
II b	-0.21	-0.10	0.25	0.03	0.17	204	28
II c	-0.34	-0.15	0.27	0.04	0.23	206	24

In contrast, a hydraulic conductivity of $1 \cdot 10^{-4}$ m s^{-1} leads to an overestimation of all observed water levels (scenario I). In this case, the establishment of the subsurface outflow can reduce the RSME and the deviation between simulated and measured water levels (Table 3.4-4). Implementing the leakage area 1, the RMSE can be reduced to about the half to 0.45. However, since P37 and P03 have the highest deviations the small leakage area is not sufficient for fitting the water levels at this part of the transect without having significant impacts on the groundwater level close to the lake. The second leakage area results in a good fit of P03, P02 and P40, but still overestimates P37 about 0.45 meter. Considering the whole bottom as a leakage area, leads to a similar and even slightly better fit as for scenario II; again P02 is overestimated about 0.3 m.

In the following comparison only scenario II, Ib and Ic are considered, which performed best. According to the characteristics of the leakage area, there is a change in the extension of the subsurface catchment, the flow pattern, the flow velocity and the groundwater volume entering the lake. In the case of scenario II the whole catchment is contributing to the lacustrine groundwater discharge (LGD). The highest groundwater flow velocities are reached close to the lake and the largest volume is entering the lake (Table 3.4-4).

Table 3.4-5: Comparison of observed and simulated groundwater exfiltration at the near-shore areas.

		Min Exfiltration [m^3 d-1]	**Max Exfiltration [m^3 d-1]**
Measured			
	Seepage-Meter	0.003	0.005
	Temperature depth profiles	0.001	0.009
Simulated			
	I	0.03	0.04
	I b	0.006	0.009
	I c	0.018	0.02
	II	0.03	0.09
	II a	0.02	0.03
	II b	0.02	0.03

Assuming subsurface leakage of groundwater over the whole bottom of the upper aquifer leads to a reduction of the catchment in horizontal extension (Figure 3.4-7). Groundwater recharged close to the watershed does not reach the lake but discharges into the deeper aquifer. In the case of scenario I c only 60 % of the generated recharge is reaching the lake. Consequently, both the lacustrine groundwater discharge and the local maximum of LGD are decreased (Table 3.4-4 and Figure 3.4-7).

The catchment area as well as the LGD rates are decreasing about one third in scenario I b. There is also a change in the distribution of flow velocities (Figure 3.4-7). The comparison of the LGD rates calculated for I b with LGD rates measured in 2012 and 2013 by seepage – meters (method described by Lee, 1977) and temperature depth profiles (method described by Schmidt et al., 2006) (Table 3.4-5) show a good agreement. The LGD rates of the other scenarios are about on magnitude higher.

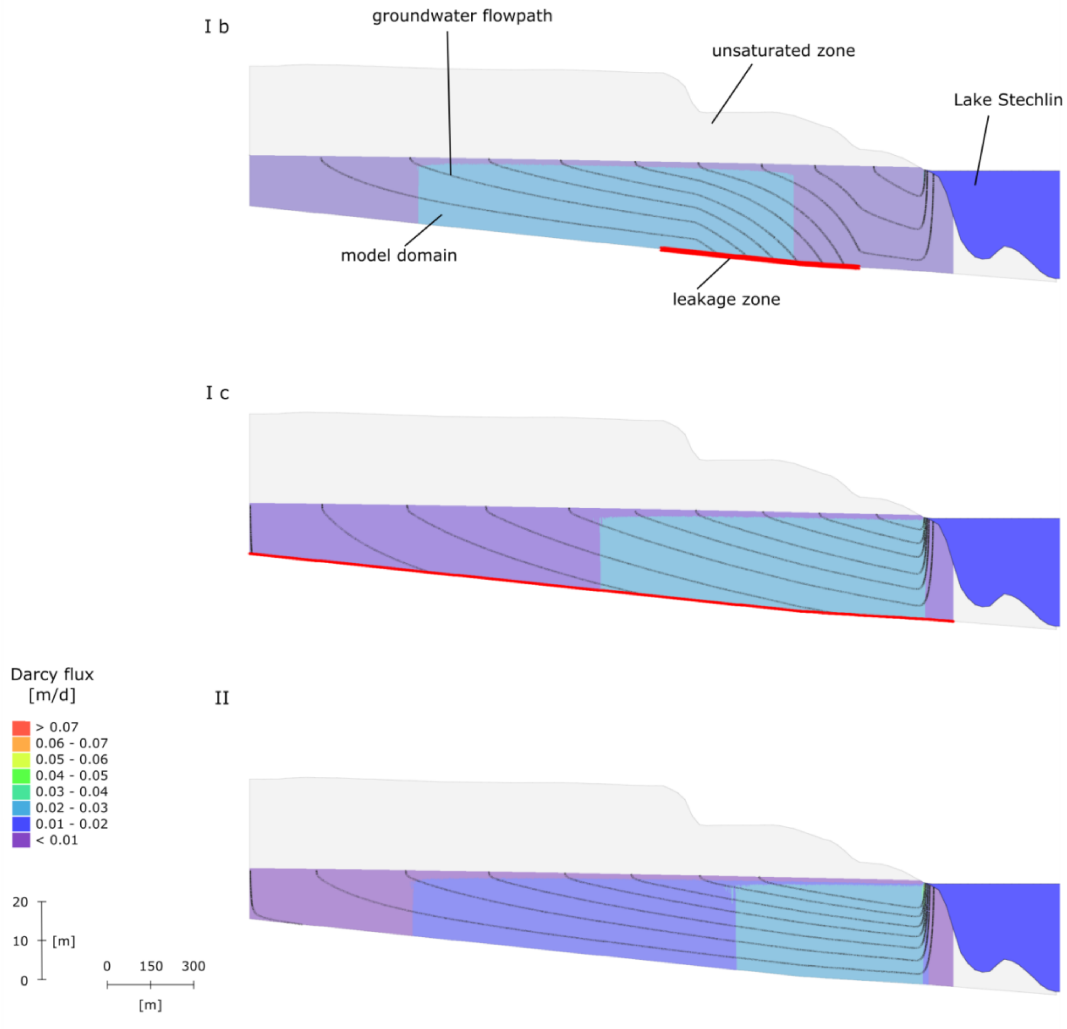

Figure 3.4-7: Flow paths and distribution of Darcy flow velocities for simulation I b, I c, and II. The red line shows the area water is leaking into the deeper aquifers.

3.4.4 Discussion

A simple two dimensional vertical groundwater modeling approach was used to test the hypothesis that a small unconfined aquifer contributes to both the local system of Lake Stechlin and to a regional flow system. Therefore, eight different simulation scenarios were compared, which were varied regarding hydraulic conductivity and by using different leakage areas (Figure 3.4-6). First of all, model runs pointed out that the system reacts very sensitive to small changes in the hydraulic parameter and to the establishment of different leakage areas. That complicates the identification of a distinct factor, which drives the establishment of the measured groundwater levels.

Scenario II ($k_f = 2 \cdot 10^{-4}$ m s^{-1}, no leakage) results in a good agreement between measured and simulated water levels for three wells (P37, P03 and P40). However, this scenario is not able to reflect the decrease of the hydraulic gradient, which occurs between P03 and P02. Assuming a contribution of the catchment to a regional flow system, it is probable that this will take place between wells P02 and P40 (scenario II a). However, the establishment of the leakage area does not lead to a significant improvement of the fit of well P02. This is also valid for scenarios II b and II c. Nevertheless, there is a small improvement of the RMSE when implementing leakage areas (scenario II a and b) with a loss into a deeper aquifer. This loss is small, but not unrealistic. Glacial till layers have a low hydraulic conductivity, but are not impermeable. Following Darcy's law the hydraulic conductivity and the gradient are inversely proportional (Hölting and Coldewey, 2009). As a consequence the low hydraulic conductivity leads to a large gradient between the aquifer systems which were observed in the present case (Table 3.4-1). This would imply a reduction of groundwater discharge towards the lake of about 10 % (Table 3.4-4).

Scenario I based on a hydraulic conductivity of $1 \cdot 10^{-4}$ m s^{-1} which results in a large overestimation of the water levels of all wells. In contrast to scenario II, an establishment of leakage areas leads to a significant improvement between measured and simulated water levels (Table 3.4-4). The extension of the leakage area plays a significant role. In cases I a and b the leakage areas can be described as a geological window where the water is able to leave the system due to higher hydraulic conductivities or the absence of the aquitard. However, according to the fact, that there is a larger overestimation of the water levels of the wells P37 and P03 in comparison to wells P02 and P40 the leakage area of scenario b led to better fits than the area used in sencario a. As a consequence of the geological window, the catchment area is contributing to the LGD to Lake Stechlin would diminish to less than 35 % of the original catchment size. This reduction is about 30 % when an overall permeable layer is assumed (I c). It has to be mentioned, that scenario I c and II are leading to almost equal deviations between measured and simulated groundwater levels.

In 2012 and 2013 point measurements of groundwater exfiltration into the lake were conducted with seepage meters and temperature depth profiles. The measurements were done in the same area as

where the modeling transect is situated. The determined LGD rates are about 10 to 90 l m^{-2} d^{-1} depending on the distance from the shoreline. These measured LGD rates are up to one magnitude lower than the modeling results. Of course, there are impacts on LGD rates at the immediate sediment – water interface (e.g. clogging) and which are not considered in the model. However, it can be that these impacts are of minor importance since the sediments in the littoral do not differ from the aquifer material. In general, the scenarios II estimate higher LGD rates than scenarios I (Table 3.4-4), which is the result of the higher hydraulic conductivity. That indicates that the lower hydraulic conductivity is more reliable and subsurface discharge needs to be considered.

However, the present approach does not allow making a clear statement of the location of the leakage area and the LGD volume. Scenario I b has the best agreement with the measured LGD n rates, but this would imply that most of the groundwater recharge occurring in the catchment does not reach the lake. Furthermore, this scenario assumes a geological window of sediments with higher conductivity. This might be proven by additional drillings between wells P03 and P02, which could clarify if the window is present or not. For more detailed information about the extension of the window, geophysical approaches can be used.

A more realistic scenario is I c. This has lower exfiltration rates and assumes a generally broader leakage area, which is more probable due to the sediment composition of glacial till. Also a reduction of the groundwater discharge towards the lake of 30 % seems to be in a more realistic range. This could be justified with the fact that geological windows are rare. In the case of the present study it can be expected that a window of a that size which was chosen in the study would lead to a more similar water level between well P01 and P40. However, there is a clear gradient between both wells, which implies a less permeable layer in between both.

Beside the size of the catchment, considering groundwater leakage also induces a change in groundwater flow path towards the lake. The groundwater flow is deflected towards the depth (Figure 3.4-7). This implies longer traveling times and also longer reaction times for substances which were transported via the groundwater.

The study could give a first impression about the importance of considering groundwater leakage to regional flow systems on the groundwater-lake interaction. However, a proper quantification would require additional information about a broader area, like the identification of the regional hydraulic gradient, detailed information about the geological settings of the aquifer system, reliable leakage coefficients and water level measurements in the different aquifers.

3.4.5 Conclusion

The present study illustrate with a simple modeling approach that the leakage of groundwater into deeper aquifers need to be considered when studying lacustrine groundwater discharge towards surface water bodies in head water areas in lowlands. Therefore, a two dimensional numerical groundwater model was set up for a transect. Eight scenarios were simulated which consider different hydraulic conductivities and different sizes of areas where groundwater leakage can occur. All scenarios deliver a similar good fit to the measured groundwater levels along the transect. However, the comparison with measured LGD rate with seepage meters and temperature depth profiles have a better match, when the subsurface groundwater leakage is considered.

The leakage of groundwater into deeper aquifers has to main effects for the groundwater - surface water interaction: (1) the groundwater recharge, which is generated in the catchment, does not necessarily contributing to the lake water balance. The volume of groundwater reaching the lake decreases within a range of 10 – 60 %, depending on the size of the leakage area and the amount of leaking water. (2) In all cases, where leaking was simulated, there was a distraction of the flow paths towards the depth. Hence, the flow paths are longer in comparison to the assumption, that all the water is entering the system. This needs to be taken into account also for the investigation of travel times and chemical reactions times of substances, which are transported by the groundwater.

3.5 Localization of lacustrine groundwater discharge (LGD) by airborne measurement of thermal infrared radiation

Jörg Lewandowksi [1,2], Karin Meinikmann[1,2], Thomas Ruhtz[3], Franziska Pöschke[1,2], Georgiy Kirillin[1]

Remote Sensing of the Environment, 2013, 138, 119 – 125

[1] Institute of Freshwater Ecology and Inland Fisheries, Ecohydrology Department

[2] Humbodt University Berlin, Geography Department

[3] Free University, Institute for Space Science

Published in: Remote Sensing of Environment

Lewandowski, J., Meinikmann, K., Ruhtz, T., Pöschke, F., Kirillin, G. 2013. Localization of lacustrine groundwater discharge (LGD) by airborne measurement of thermal infrared radiation. Remote Sensing of Environment. 138. 119-125.

http://doi.org/10.1016/j.rse.2013.07.005

Copyright © 2013 Elsevier.

Abstract

Although lacustrine groundwater discharge (LGD) might be important in water and nutrient budgets, it has often been neglected due to the required effort to measure LGD and due to intense spatial heterogeneity of LGD limiting the validity of measurements. Therefore, fast, easy applicable methods for a first snapshot of the LGD pattern are required and might be the basis for choosing relevant and representative sampling sites. In the present case study, which is actually the first application of an airborne measurement of thermal infrared radiation (TIR) to identify LGD pattern for entire deep freshwater lakes, the measurement was substantiated with thermal profiles in sediments and awater-table map. We found that measurement of TIR is a powerful tool to identify LGD pattern in lake-related studies provided that there is a lack of warm surface inflows. A TIR image taken in March 2012 shows that warm groundwater entering the relatively colder lake water in some near-shore areas is visible as a plume floating on top of the lake water. Prerequisites for the application of TIR to detect LGD pattern are the positive buoyancy of the groundwater relative to lake water and weak mixing in the water column. We propose a dimensionless scale for identifying groundwater floating conditions based on weather conditions. Attributing a surface thermal anomaly to LGD depends on careful consideration of other factors that could produce similar patterns and careful consideration of lake physics.

3.5.1 Introduction

Lacustrine groundwater discharge (LGD) is an important component in water balances of some lakes (Harvey et al., 2000). Even if its contribution to the water balances is small, it might be important to nutrient balances since nutrient concentrations in groundwater are often much higher than in other components of the water balance and in the lake water itself (Vanek, 1987). During the last decades much effort was spent on localization of discharge zones and quantification of LGD as well as the development of measurement and modeling tools for that purpose. Due to intense small-scale spatial heterogeneity of LGD (Kishel and Gerla, 2002; Ommen et al., 2012), the large area covered by the interface and its difficult accessibility for direct measurements all methods have limitations. In principle, there are three different types of methods for the identification of LGD: (1) Spatially explicit methods measuring LGD rates at a single point or over a small area (e. g. seepage meters Lee, 1977, sediment temperature depth profiles Schmidt, et al., 2006), (2) integrating methods quantifying the whole groundwater import into the lake (e. g. radon balances (Kluge et al., 2007), stable isotope approaches (Dincer, 1968; Hofmann et al., 2008; Krabbenhoft et al., 1994), annual groundwater recharge in the entire subsurface catchment, mostly determined by modeling or calculation of the water budget) and (3) methods for identification of discharge pattern without quantification of LGD (e. g. fiberoptic distributed temperature sensing (FO-DTS, Selker et al., 2006a), geophysical approaches around the lake perimeter (Ong et al., 2010), airborne measurements of thermal infrared radiation (TIR) (present study)).When interested in nutrient budgets integrating methods alone are not sufficient. Nutrient budgets are calculated by multiplication of LGD rates and nutrient concentrations in discharging water. Due to the large spatial heterogeneity of nutrient concentrations in groundwater, segmented approaches are much more reliable than integrating approaches: local discharge rates should be multiplied with the corresponding nutrient concentrations instead of multiplying total discharge rates with mean nutrient concentrations (Ommen et al., 2012). Thus, fast methods for pattern identification could be useful to localize the most relevant and representative zones for further more time-consuming investigations. With the present study we tested whether airborne TIR measurements are a suitable tool for pattern identification.

Airborne and ground-based TIR measurements have been used in several studies to detect groundwater discharge or hyporheic exchange flow in streams and rivers (Schuetz and Weiler, 2011; Torgersen et al., 2001). Fast mixing of groundwater discharge and stream water results in the visibility of discharging groundwater at the stream surface as small temperature increase or decrease compared to the river water not impacted by groundwater discharge. The volume of the stream water is relatively small so that the discharge of groundwater or hyporheic water with its temperature different than stream water results in a significant deviation of the impacted stream water compared to the not impacted stream water. The fundamental differences of lake–groundwater interactions compared to

stream–groundwater interactions are the absence of hyporheic exchange flows in lakes, smaller groundwater discharge rates, less turbulent mixing of the water body and a larger volume-ratio of the water body to the discharging groundwater. Thus, analogies of groundwater discharge to streams and lakes that would be relevant for airborne TIR measurements are minor.

Airborne TIR measurements have been used in several studies to detect submarine groundwater discharge (SGD) in coastal zones (Danielescu et al., 2009; Duarte et al., 2006; Garcia-Solsona et al., 2010; Johnson et al., 2008; Peterson et al., 2009; Shaban et al., 2005) and in studies of saline lakes (Lee, 1969;Whiting, 1975). In saline systems, there is a large density difference between discharging fresh groundwater and saline water due to different salinities. Thus, the less dense groundwater will always float on top of the sea water and if there are some temperature differences between groundwater and sea water the groundwater can be detected with airborne TIR measurements. In freshwaters, lake water and groundwater have similar salinities and thus no salinity-induced floating of groundwater occurs. However, under certain circumstances temperature differences might cause small density differences that result in the same groundwater buoyancy as previously observed in saline systems.

To the best of our knowledge the present study is the first application of an airborne TIR measurement to identify LGD pattern for an entire deep freshwater lake. There are studies of Cook et al. (1991) who used a handheld infrared camera to detect LGD along the shore line (line scan survey) of a Scottish lake; a study of Anderson et al. (1995) who also used a handheld infrared camera to visualize surface water temperatures and to detect cold springs along a geologic fault zone, water circulation and an influent plunging plume; and an airborne TIR study of Rundquist et al. (1985) in a shallow lake in the Nebraska sand hills to detect groundwater discharge. The two latter studies investigated LGD in relatively shallow water bodies where mixing processes similar to the ones described above for streams might occur and cause visible surface anomalies despite the absence of floating characteristics of the groundwater discharge. In both studies groundwater relatively colder, and thus, heavier than lake water (of approximately 20 °C) was observed at the lake surface. Also, some authors (e. g. Hook et al., 2003) used satellite images to determine lake surface temperatures but data were not used to identify LGD pattern.

We hypothesize that at low lake water temperatures under relatively calm weather conditions; warmer groundwater discharge might float on top of the water body and can be detected by TIR measurements. The aim of the present study is to test the method and identify conditions favoring application of TIR to detect LGD.

3.5.2 Material and Methods

The method was tested at Lake Arendsee (max. depth 49 m, mean depth 29 m, surface area 5.13 km^2) which is a highly eutrophic (total phosphorus concentration approximately 200 µg P L^{-1}) seepage lake located in north eastern Germany. The littoral zone along the shore is very narrow except an approximately 200 m broad shallow zone (10 m water depth) at the Northern shore of the lake (Hupfer et al., 2000). The use of TIR to localize LGD is discussed and evaluated based on physical considerations, a water temperature depth profile taken with a YSI probe (Model 6600 V2/4) on 20 March 2012 at the deepest point of the lake, continuously measured water temperatures in 1.5 m depth, and weather data collected by a weather station (EcoTech Bonn, Germany) on an unmanned raft.

The TIR data were collected on 22 March 2012 from 10:59 to 11:03 local time during an airborne mission with a Cessna 207 T operated by the Free University Berlin with two transects above Lake Arendsee. The TIR camera (VarioCam HR, head 600) was installed on a stabilized platform (GSM 3000) together with an inertial navigation system (IGI Aerocontrol). The stabilized platform was controlled by the inertial system and the corresponding altitude and navigation data were collected by this system. The camera has a resolution of 640 × 480 pixels, a focal length of 30 mm and was used with a frame rate of 1 image per second synchronized and triggered by the GPS–PPS pulse of the navigation system. The very low lens distortion of the camera and the stabilized platform made it possible to mosaic the data rapidly with a common imaging program (Gimp) without major photo- and geometric correction. For this procedure only a limited number of 6 pictures were used to cover the whole lake and to compile the resulting image. A more sophisticated mosaic would include more time consuming laboratory calibrations, measurements of the camera distortion and a bore site calibration flight. That was not the scope of the study aiming at a first snapshot of the LGD pattern and would also contradict to the advantage to have a fast and easily applicable method. The flight was performed at an altitude of approximately 1500 m with a velocity of approximately 50 m s^{-1}. The resulting image was rotated by 104° and scaled from a spatial pixel resolution of approximately 1.6 m × 1.2 m to 1.5 m × 1.5 m. For the temperature calibration the specific data of the manufacturer of the TIR camera were used. The absolute temperatures of the TIR image should be considered with care but for the present application only relative temperature differences are important.

In addition to the above-mentioned physical considerations we also used information about the study site to discuss the collected TIR images and as basis for Figure . We summarize that information here since the original sources are reports in German and similar gray literature. Results of our own below-mentioned investigations are not published yet since the time-consuming and manpower-intensive ground-based investigations are still ongoing with the TIR image of the present study being a helpful tool for selecting the best sites for further investigations. Based on 40 wells, previous studies and

hydrogeological maps we determined groundwater contour lines and the delimitation of the subsurface catchment (Figure). Groundwater in the catchment is flowing in northern directions towards the lake (perpendicular to the contour lines in Figure) with a steep hydraulic gradient along the south-south – eastern shoreline. There, relatively high LGD rates are expected while in the east and west of the lake less LGD is assumed due to a smaller extent of the subsurface catchment and lower groundwater gradients. Aquifer sediments along the southern shoreline originate from different Pleistocene stadials which had been deposited on Miocene material. Borehole profiles indicate an increasing thickness of the Pleistocene layers from about 10 to > 35 m in eastern direction along the southern shoreline. In some parts, an aquitard separates the sediments into two aquifers. However, this aquitard is not consistently present, and thus, a general hydraulic connection between the different geologic sediments can be assumed. Values for hydraulic conductivity (k_f) in the upper parts of the aquifer (less than 11 m below surface) show an increase in eastern direction, from $1.4 \cdot 10^{-4}$ in the south-west to $4.9 \cdot 10^{-4}$ in the south-east. Further eastwards, k_f decreases again.

In the north and north-west lake water infiltrates into the aquifer and in the north-east the subsurface catchment is extremely small so that nearly no LGD is expected to occur along the northern shore. Local LGD rates calculated from curvature of temperature depth profiles (Schmidt et al., 2006) in the lake sediments (dots in Figure along the shoreline) support in principle the aforementioned description of LGD pattern. Temperature depth profiles are based on the temperature difference between groundwater (e.g. 10 °C) and lake water (e.g. 4 °C). At high groundwater discharge rates temperatures of upwards flowing groundwater remain high while the groundwater approaches the sediment surface. Only on the last decimeters to centimeters heat conduction and diffusion result in a relatively sharp decrease of the temperatures from 10 °C to 4 °C. At lower groundwater discharge rates conductive and diffusive heat transport processes affect deeper sediment layers so that the curvature of the profiles is more flat. We also applied FO-DTS (Selker et al., 2006a) to investigate LGD in deeper zones of the lake. Results suggest that no significant LGD occurs far away from the shore. Theoretical considerations, modeling exercises and the local hydrogeology also support a focusing of LGD to near-shore zones (e. g. Kishel and Gerla, 2002; Pfannkuch and Winter, 1984; Shaw and Prepas, 1990).

3.5.3 Results

Figure 3.5-1 shows the TIR image of Lake Arendsee taken on 22 March 2012. For its interpretation some background information described in the Material and methods section, such as the delimitation of the subsurface catchment water table contour lines and near shore groundwater discharge rates is additionally shown in the same figure. Surface water temperatures in areas impacted by LGD are close to 7 °C which is more than 1 °C warmer than the rest of the lake surface (Figure 3.5-1) and exceeds the temperature of maximum density of freshwater (4 °C). A lake water depth profile taken on

20March 2012 shows a difference between the top and the bottom of the water body of only 0.26 °C and 1 µS cm^{-1} with a temperature at the lake bottom of 4.12 °C and an electrical conductivity of 483 µS cm-1, i.e. the lake had been completely mixed short before the measurement campaign. Groundwater temperatures in 10 groundwater observation wells close to the shore were 10.5 ± 0.3 °C (arithmetic mean ± standard error) and electrical conductivities were 643 ± 69 µS cm-1. Calculated electrical conductivities based on water compounds agreed well: 727 ± 77 µS cm^{-1}. Total dissolved solids (TDS) were approximately 302 ± 36 mg L^{-1} compared to approx. 220 mg L^{-1} of the lake water. There was no rain in the days before the flight and the measurement day was warm and cloudless which resulted in fast warming of the lake surface due to solar radiation (Figure 3.5-1).

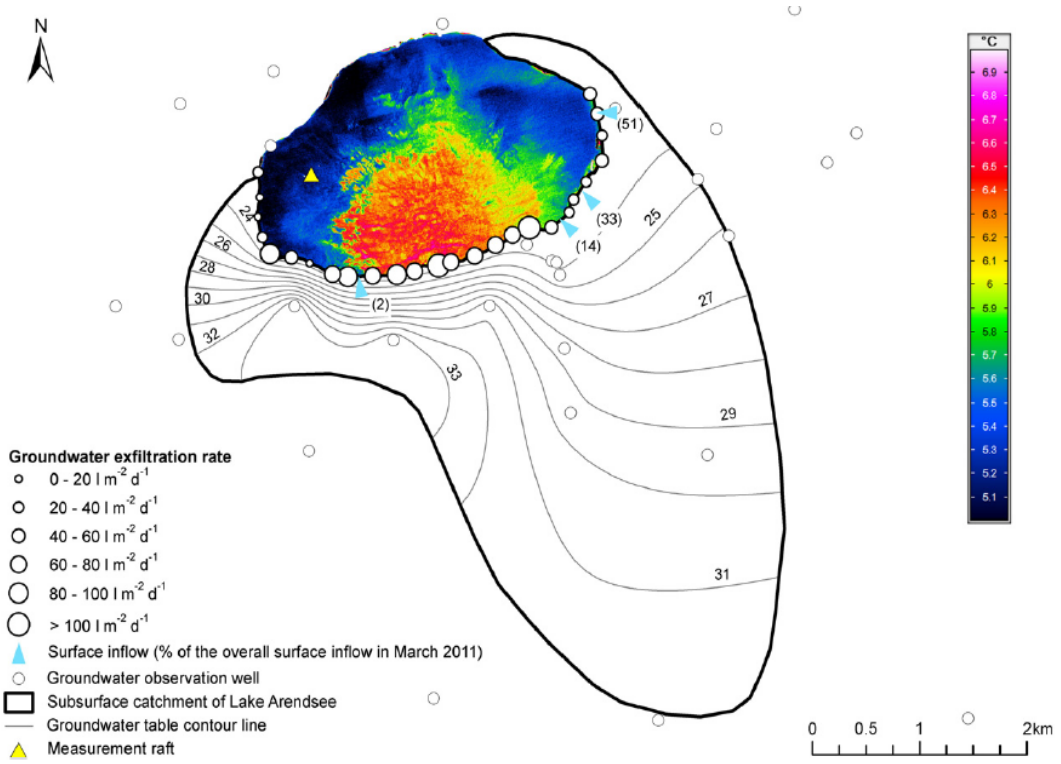

Figure 3.5-1: Thermal infrared image of Lake Arendsee taken on 22March 2012. Groundwater entering the lake in near-shore zones in the south of the lake floats as thin warm layer on top of the water body and spreads out onto open waters. Water table contour lines in the catchment of Lake Arendsee and delimitation of the catchment were determined based on 32 groundwater observation wells. Size of near-shore circles indicates rates of groundwater discharge in that shore section based on sediment temperature depth profiles (Schmidt et al., 2006) taken at the end of July and the beginning of August 2012. Blue triangles indicate location of the 4 small ditches entering the lake and the numbers in parentheses indicate the percentage of the overall surface water inflow entering the lake via that ditch in March 2011 (no measurements conducted in March 2012).

3.5.4 Discussion

The TIR image shows an area of warmer surface water spreading from the southern shoreline onto the lake (Figure 3.5-1). Dispersion of the warm slick is driven by advection due to residual currents and by turbulent diffusion. Both mechanisms are dampened alongshore by boundary friction. Therefore, diffusion is stronger in the direction normal than parallel to the shoreline (Ozmidov, 1990). The area of maximum LGD along the southern shoreline in the TIR image agrees well with our previous knowledge of zones where major LGD occurs. This is a first indication that the TIR image is a good approximation of the LGD pattern derived from ground-based methods. For the data interpretation it is not really necessary that the absolute values of the measured temperatures are correct since only the relative differences are of interest. Therefore, a labor intensive and time consuming calibration of the flight data is not required as long as data for the whole lake surface can be collected nearly instantaneously.

During the day at which the TIR image was taken and some days before, lake water temperatures measured in 1.5 m water depth were slowly approaching 5 °C. The warmer groundwater (10 °C) discharging into the lake was less dense than lake water even though TDS concentrations were slightly higher (approx. 60 mg L^{-1}) in groundwater compared to lake water. Density difference based on temperature and TDS: 236 ± 53 mg L^{-1} (n = 10); density difference based on temperature, TDS and changed volume due to dissolved ions: 183 ± 53 mg L^{-1} (n = 10, calculation according to Dietz et al., 2012) respectively 190 ± 53 mg L^{-1} (n = 10, calculations according to Boehrer et al., 2010). Therefore, LGD is immediately forced to the lake surface by denser lake water. During the ascent some mixing might have occurred and the contact with surrounding water resulted in some cooling of the groundwater. Nevertheless, it was still warmer than the rest of the water body and thus, floated on the top of the water body. From there the warmer less dense water gradually spread as a plume on the lake surface.

We can rule out the possibility that the observed temperature anomaly in Figure is caused by shortwave solar radiation. If shortwave solar radiation had been the driver of the increased surface water temperatures on a cloudless day heating would be evenly distributed on a lake with the size of Lake Arendsee or it might be increased in the shallow areas at the northern shore (compare Material and methods section and Hupfer et al. (2000) for a bathymetric map of Lake Arendsee). However, Figure shows no signal in the northern shore section of the lake. Nevertheless, it might be advantageous to conduct future flight missions pre-dawn to relieve all uncertainty associated with shortwave solar radiation.

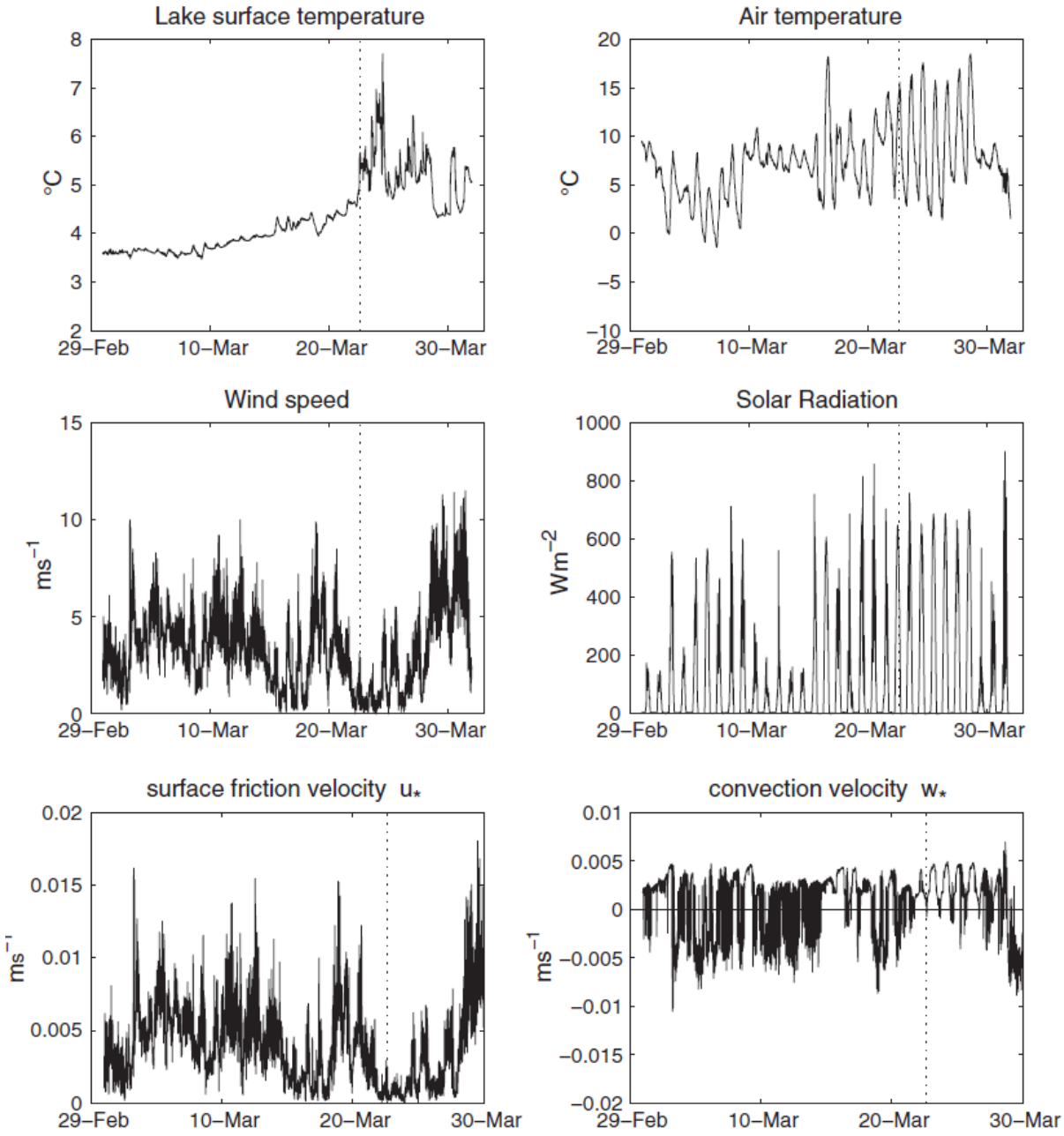

Figure 3.5-2: Water temperatures (T_{Water}) of Lake Arendsee in 1.5 m water depth and weather conditions over Lake Arendsee (air temperature $T_{Air,}$ wind velocity and radiation) in March 2012. Vertical dashed lines designate the date of the TIR survey.

Some authors report temperature anomalies in lakes due to surface inflows (Schott, 1979). However, it can be ruled out that warm surface water entering the lakes through four drainage ditches is the major source of the observed temperature pattern since the drainage ditches enter the lake outside of the plume area or at its edges (Figure 3.5-1). Also, it is impossible that upwelling of the bottom lake water

by wind or seiches causes the observed lateral variations of surface water temperature since temperature differences between the upper water layers and the bottom water were only 0.26 °C. Only the immediate water surface is in some areas much warmer. Another explanation combining shortwave solar radiation and wind would be that the wind might have mixed and destroyed the warmer surface layer along the eastern, western and northern shore. However, there is no reasoning or indication for such wind pattern. Besides, the weather was quite calm before the flight (mean wind velocity in the last 14 h was 0.8 m s^{-1}). Shading can also be excluded as cause of the observed TIR temperature pattern due to the flat topography and the large size of the lake. Trees can cause some shading at the southern shore, but there water surface temperatures were highest. Also, the sky above Lake Arendsee was cloudless during the flight mission so that shading by clouds could not have any impact on the TIR image.

As described in the Material and methods section ground-based labor-intensive methods such as the measurement of the curvature of temperature depth profiles in the sediment showed amajor groundwater discharge at the south-southeastern shore (Figure 3.5-1). The size and shape of the catchment, hydraulic gradients (groundwater contour lines), and k_f data reported in the Material and methods section also support that the major LGD occurs in this shore section (Figure 3.5-1).

The present study demonstrates a strong potential of airborne TIR imaging for investigation of groundwater inflow in lakes. However, the success of the method depends on the combination of external factors, which should favor buoyancy of groundwater and maintaining of temperature differences between groundwater and lake surface. A basic prerequisite for this is the positive buoyancy of the subsurface inflow, strong enough to reach the surface without being completely mixed with the lake water. A measure of the ratio of inflow buoyancy to the mixing forces is the densimetric Froude number *Fr*, which may be defined as

$$Fr = \frac{u_*}{\left(g * \frac{\Delta\rho}{\rho_w} * h_{LGD}\right)^{1/2}} = \frac{u_*}{u_g} \qquad \textit{Equation 3.5-1}$$

or its counterpart, the Richardson number *Ri*, used often in the studies on buoyancy flows

$$Ri = \frac{u_g^2}{u_*^2} = \frac{1}{Fr^2} \qquad \textit{Equation 3.5-2}$$

Here, u_* is the characteristic scale of shear velocity, which is the measure of turbulent momentum flux (Reynolds stress), g is the acceleration due to gravity, $\Delta\rho$ is the density difference between the groundwater and the lake water of density ρ_w, h_{LGD} is a height scale relevant to the LGD, and u_g^2 has the physical meaning of the internal gravitational wave speed based on the buoyancy $b=g\,\Delta\rho\,\rho_w^{-1}$:

$$u_g = (b * h_{LGD})^{1/2}$$ *Equation 3.5-3*

Fr becomes imaginary at negative buoyancy of the groundwater $b < 0$, whereas *Ri* is defined for both positively buoyant ($Ri > 0$) and negatively buoyant ($Ri \leq 0$) flows. Hence, a necessary (but not sufficient) condition for groundwater to reach the lake surface is the positive buoyancy of the groundwater, i.e. $\Delta\rho > 0$, $b > 0$, and $Ri > 0$. In addition, turbulent mixing should be weak to allow the groundwater to reach the surface without being completely mixed within the water column. Equation can be combined with Equation 3.5-2 as

$$\frac{u_*^2}{b} < C_1 * h_{LGD}$$ *Equation 3.5-4*

where C_1 is a dimensionless constant subject to empirical estimation. The wind friction velocity at the lake surface is a major source of the lake mixing (Wüest and Lorke, 2003) and can be adopted for u_* in Equation 3.5-4. An appropriate choice for the LGD height scale h_{LGD} could be the vertical extension of the LGD area or the lake depth at the point of LGD. For Lake Arendsee an appropriate choice for the LGD height scale is the mean lake depth (29 m).

Another factor affecting strongly the mixing of the groundwater with the lake water is the vertical heat (or, more precisely, buoyancy) flux across the lake–atmosphere interface. If the downward heat fluxes is positive it depresses wind-driven turbulence and prevents mixing of the warm floating groundwater with the surrounding colder lake water. The balance between the wind mixing and the stabilizing buoyancy flux is expressed by the Monin–Obukhov length scale L_{MO} (Monin and Obukhov, 1954)

$$L_{MO} \sim \frac{u_*^3}{B}$$ *Equation 3.5-5*

Where $B=g\alpha Q$ is the buoyancy flux at the lake surface. Here, Q is the surface temperature (heat) flux and α is the coefficient of thermal expansion for the surface water. An upward heat flux destabilizes the lake water column and produces strong convective mixing, which homogenizes the water temperature. The Deardorff's (1970) convective velocity scale w_* quantifies the intensity of convective motions

$$w_* = (-h_{mix} * B)^{1/3}$$ *Equation 3.5-6*

where h_{mix} is the thickness of the surface mixed layer. The two criteria 3.5-5 and 3.5-6 can be combined for both positive and negative surface buoyancy flux *B* as,

$$0 < \frac{u_*^3}{w_*^3} < C_2$$ *Equation 3.5-7*

or

$$0 < \frac{L_{MO}}{h_{mix}} < C_2 \qquad \textit{Equation 3.5-8}$$

Where C_2 is another dimensionless constant. The lower boundary is set here to 0 since convection in lakes has generally a higher potential for vertical mixing of water masses than the wind-driven turbulence at the background of the stabilizing buoyancy flux. Thus, we suggest that tracing of groundwater at the lake surface is impossible as long as the surface buoyancy flux is directed into the atmosphere and produces convective mixing in the upper lake water.

A simple interpolation formula combining Equation 3.5-4 and Equation 3.5-7 provides a criterion G for groundwater floating at the lake surface

$$0 < G \ll 1 \qquad \textit{Equation 3.5-9}$$

where G is a dimensionless number defined as

$$G = \frac{u_*^3}{C_1 * w_*^3 + C_2 * u_* * b * h_{LGD}} \qquad \textit{Equation 3.5-10}$$

Equation 3.5-9 is equivalent to Equation 3.5-4 at infinitesimal w_*; if, in turn b vanishes, Equation 3.5-9 turns into Equation 3.5-7.

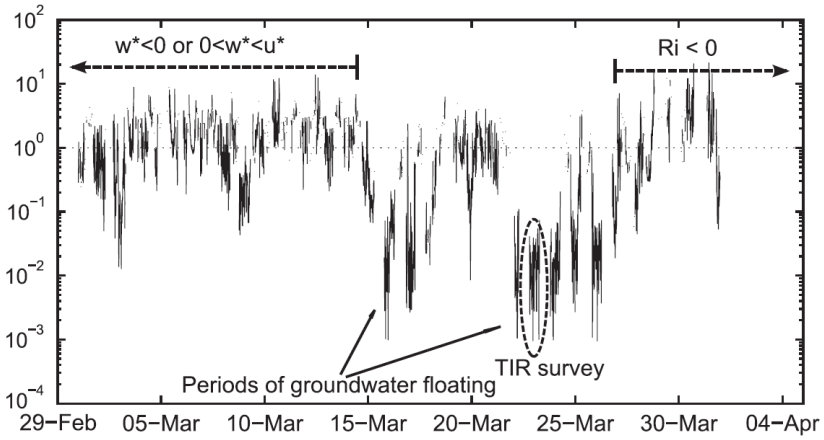

Figure 3.5-3 : The groundwater floating criterion G (Equation 3.5-10) in Lake Arendsee in March 2012. u_* is the friction velocity at the lake surface, w_* is the convective velocity scale, and Ri is the Richardson number. The gaps correspond to the periods of negative G, when no groundwater floating is possible independent of the absolute value of G.

The qualitative balance between buoyancy and mixing expressed by Equation 3.5-10 can be used for quantification of the groundwater floating, if the constants C_1 and C_2 are defined. Their thorough estimations require more detailed field data than we possess. However, the first-guess estimations can be derived directly from our dataset. Intrinsic for scaling analysis, the constant of proportionality in a dimensionless criterion is close to 1, if the chosen scales are representative for the mean balance between the governing forces (Barenblatt, 2003). Indeed, reported values of C_1 vary in the range 0.1 to 10 (Padman et al., 1996), so that we assume $C_1 = O(1)$ in what follows. Because the LGD height scale h_{LGD} is not clearly defined, the observation data can be used for backward estimation of scale $C_2 h_{LGD}$. The same considerations of the approximate balance between the governing forces as above suggest that $u_*^3 w_*^{-3}$ and $u_*^2 (C_2 b\, h_{LGD})^{-1}$ should vary within the same orders of magnitude (compare Equation 3.5-4, Equation 3.5-7 and Equation 3.5-9). Substitution of $u_*, w_* and\ b$ from the observational data from Lake Arendsee for March 2012 into both terms shows that the condition is equivalent to $C_2 h_{LGD} \sim 10^{-3}$. After tentative adopting of this value, the variability of G within the month allows to clearly identify the periods of potential groundwater floating events in Lake Arendsee (Figure 3.5-3): in the first half of March the mixing dynamics was dominated by strong winds ($G > 1$) and by convection due to heat loss into the atmosphere ($G < 0$, blank areas in Figure 3.5-3). Several events of low wind and strong heating between March 16 and March 26 produced periods with G values between 10^{-2} and 10^{-3}, one of which coincided with the period of our TIR survey on March 22. Later, stronger winds and colder nighttime air temperatures (Figure 3.5-2) result in G values above one and below zero, respectively. In a longer perspective, the overall tendency of lake surface heating should produce the negative buoyancy of the groundwater relative to the surface waters, so that the floating of groundwater in summer becomes impossible ($Ri < 0$ and $G < 0$).

The balance between buoyancy and mixing considered above suggests that the favorable conditions for groundwater floating, at least in temperate climates, should appear twice a year, in spring and in autumn, when (i) lake water densities are higher than the groundwater density, and (ii) mixing produced by the heat and momentum fluxes at the lake surface is weak. However, in autumn measurement windows might be extremely small or non-existent since water bodies cool down much slower than the atmosphere so that heat fluxes from the water surface to the atmosphere might hinder groundwater floating on top of the lake water. The condition (ii) usually varies at rather short time scales, depending on the synoptic situation. The dimensionless criterion G may be useful in this sense for planning airborne surveys based on short term weather forecasts and on current lake water temperatures.

3.5.5 Conclusion

Airborne measurement of TIR is a useful technique to identify groundwater discharge not only in marine systems (SGD) but also in freshwater lakes (LGD). In the present case study lake temperatures, the high amount of LGD, the LGD pattern and weather conditions before the campaign were favorable for the application of the method. We hope that the present study promotes further TIR investigations by different research groups. Simultaneous ground-based measurements of the thickness of the warmer surface layer and the temporal development of the plume are necessary for providing justification and refinement of constants used in the theoretical criterion given as Equation 3.5-9. In the future, the method might be applied to get a first fast snapshot of the LGD pattern and might be a useful basis for planning the application of ground-based measurement techniques. In case that a study aims at the determination of nutrient loads a combination of hydrological and biogeochemical investigations is required. For example, in the present case study, the TIR image (Figure 3.5-1) revealed, that the major LGD occurs in the south-southeastern shore section where the small town of Arendsee is located. Thus, further hydrological and biogeochemical investigations should focus on this area. Based on the results of a thermal infrared image it is possible to conduct time-consuming, labor-intensive ground-based investigations more specifically in the most relevant and representative zones instead of the more or less random approach applied nowadays. Our aim is to stimulate the use of airborne thermal infrared by different scientists in different case studies since we are quite sure that a broader application of the method would be a large step forward in understanding of groundwater–lake interactions. However, attributing surface thermal anomalies to LGD depends on careful consideration of other factors that could produce similar patterns such as above-ground inflows, solar radiation, and wind as well as careful consideration of lake physics.

3.6 Upwelling of deep water during thermal stratification onset - A major mechanism of vertical transport in small temperate lakes in spring?

Franziska Pöschke[1,2], Jörg Lewandowski[1,2], Christof Engelhardt[1], Konrad Preuß[3], Martin Oczipka[3], Thomas Ruhtz[4], Georgiy Kirillin[1]

Water Resources Research, 2015, 51, 9612 – 9627

[1] Institute of Freshwater Ecology and Inland Fisheries, Ecohydrology Department

[2] Humbodt University Berlin, Geography Department

[3] University of Applied Science, Faculty of Spatial Information

[4] Free University, Institute for Space Science

Published in: Water Resources Research

Pöschke, F., Lewandowski, J., Engelhardt, C., Preuß, K., Oczipka, M., Ruhtz, T., Kirillin, G. 2015. Upwelling of deep water during thermal stratification onset - A major mechanism of vertical transport in small temperate lakes in spring? Water Resources Research. 51. 9612–9627.

DOI: 10.1002/2015WR017579

Copyright © 2015 John Wiley & Sons, Ltd.

Abstract

Using airborne thermal infrared imaging and horizontally-resolved *in-situ* temperature monitoring at the lake surface we estimated strength and duration of regular wind-driven upwelling of dense deep water to the lake surface in two small (in terms of Rossby radius) temperate lakes during the initial phase of summer thermal stratification. The onset and duration of the upwelling events correlated well with the balance between stratification (in terms of Schmidt Stability) and wind forcing, as expressed by Lake and Wedderburn Numbers: The period of regular upwelling appearances lasted 7-15 days, identified by Schmidt stabilities around 30 J m^{-2} and Lake Numbers between 0 and 1, and resulted in persistent temperature gradients of up to 2 °C across the lake surface. Our results suggest that spring upwelling should inevitably take place in all freshwater temperate lakes with mean temperatures crossing the maximum density value of freshwater on annual cycle, whereas duration and intensity of the upwelling would vary depending on lake morphometry and weather conditions. Our results suggest major contribution of upwelling in nutrient supply to the upper waters, oxygenation of the deep water column, and air-lake gas exchange, in particular, the release of the sediment-produced methane into the atmosphere.

3.6.1 Introduction

The seasonal cycle of thermal stratification affects all transport processes in freshwater lakes and is therefore crucial for the lake ecological state and water quality. The stratification regime is closely related to the lake surface temperatures crossing the freshwater maximum density value (TMD) of ~ 4 °C At surface temperatures above the TMD, the heat input from the atmosphere produces vertical density stratification with negative downward temperature gradients across the water column, while at temperatures below the TMD the inverse stratification with downward temperature increase is formed by heat release from the lake surface. In the transition between both stratification regimes the water temperature crosses the TMD that leads to a complete vertical mixing of the water column (overturn) (Hutchinson, 1957). During overturns, the transport of momentum, heat, and mass is assumed to be essentially vertical, driven by convective mixing, which homogenizes the water column. In contrast, vertical transport during the stratified periods is limited by the potential energy of the stratification damping the mixing kinetic energy of the wind stress (Spigel and Imberger, 1980). If thermal stratification is strong, the mixing energy is confined to the upper layer (epilimnion) of the lake, while exchange of energy and substances with the deeper layers (meta- and hypolimnion) is restricted. The geographical position of a lake and the climatic conditions determine the seasonal mixing regime of lakes (Hutchinson, 1957): freshwater lakes in temperate, boreal, and (sub-) Arctic regions with mean depths varying in the approximate range of 10^1–10^2 m are typically *dimictic* with two continuous stratification periods in winter and summer divided by two relatively short overturn periods in spring and in autumn. The deeper *monomictic* lakes have higher thermal inertia preventing cooling below TMD in winter and have therefore only one stratification period; the shallower *polymictic* lakes are destratified in summer by wind mixing and short-term surface cooling events, and do not have any regular seasonal stratification pattern.

Apart from vertical mixing produced by the wind-driven shear at the lake surface and by convection due to surface cooling (or surface warming at temperatures below the TMD), an indirect path of water exchange between epi- and hypolimnion is created by transformation of the wind kinetic energy into the potential energy of the free surface tilt and the counter directed slope of the isotherms in the stratified meta- and hypolimnion (Mortimer, 1952). If the slope of isotherms is strong enough, the lower boundary of the epilimnion arrives at the lake surface, bringing the stratified waters into direct contact with the atmosphere and facilitating its mixing with the epilimnion waters in the lateral direction, not restricted by the gravity force. By analogy with the coastal upwelling at the ocean shelf, the effect is called upwelling (Schladow et al., 2004) and may eventually lead to complete destruction of the vertical thermal stratification. Similar to the coastal ocean, upwelling brings nutrient-rich deep waters to the lake surface (Webster, 1990; MacIntyre et al., 1999). Hence, upwelling events have

significant impact on distribution of nutrients and plankton development in lakes. A criterion for the upwelling appearance in stratified lakes can be defined as (Imberger and Patterson, 1990):

$$Ri * h/(L/2) \leq 1 \qquad \textit{Equation 3.6-1}$$

where Ri is the Richardson Number which describes the ratio between stratification and wind shear, and with the former being subject to further definition based on the lake morphometry and vertical density stratification. The term $h/(L/2)$ is the geometric aspect ratio of the lake defined as the ratio of the lake half-length $(L/2)$ and the depth of the upper boundary of meta- or hypolimnion h.

$Ri * \frac{h}{\frac{L}{2}} = 1$ corresponds to the critical slope of isotherms bringing the meta/hypolimnion to the lake surface at the upwind shore of a rectangular lake (see Imberger and Patterson, 1990; Stevens and Imberger, 1996 for details). From Equation 3.6-1, upwelling is more probable for lakes with larger horizontal dimensions L. Observations in large lakes, with horizontal dimensions larger than or comparable to the barotropic Rossby radius (Gill 1982) $R_O = f^{-1}(gH)^{1/2}$, where f is the Coriolis parameter, g is the gravity acceleration and H is the mean depth of the lake, support an important role of upwelling in the coastal circulation (Haffner et al., 1984; Schladow et al., 2004; Plattner et al., 2006; Troitskaya et al., 2014). In these lakes the aspect ratio h/L does not exceed 10^{-3} (using the order-of-magnitude estimation of the epilimnion depth as 10^1 m), and transient upwelling events have been encountered, driven by strong wind events and affecting primarily the littoral areas without destroying the mean stratification in the central parts of lakes. The large cluster of smaller lakes with $L \ll Ro$ can be suggested to be too small for upwelling to develop there for significant time periods. Assuming that stratification strength Ri is similar in all lakes of the temperate climatic zone, upwelling in small and shallow (*polymictic*) lakes ($L \ll Ro$ and $H<h$) prevents development of seasonal stratification. Small *dimictic* lakes ($L \ll Ro$ and $H>h$) can be suggested to be free from upwelling events. These considerations lie behind the usage of the criterion (Equation 3.6-1) as a threshold separating dimictic and polymictic lakes (Gorham and Boyce, 1989; Padisák and Reynolds, 2003).

The condition of Ri being essentially small to fulfil the criterion (Equation 3.6-1) is however satisfied in any dimictic lake at a certain stage of seasonal stratification cycle, viz. during the transition from the overturn to the summer stratification, suggesting upwelling events could have an important ecological relevance at the initial stage of the productive period in spring. While convective mixing oxygenizes the hypolimnion during overturns, upwelling can additionally contribute/ accelerate this effect. Moreover, upwelling can provide a direct pathway of the nutrient-rich deep water to the euphotic layer, accelerating significantly primary production in the lake.

No detailed observations of upwelling development in small dimictic lakes have been performed to date, although conditions satisfying Equation 3.6-1 were reported in relatively small lakes at low *Ri* (Stevens and Lawrence, 1997). Also, altered temperature (Coman and Wells 2012, Bocainov et al. 2014), oxygen (Robertson and Imberger 1994) and nutrient (MacIntyre and Jellison 2001) regimes of the littoral zone in those lakes were attributed to the upwelling events at low stratification and (or) extremely strong winds (Simpson et al. 2014). Evidence was also reported of the epilimnion water tilted down to the lake bottom by wind ('downwelling') during inverse (winter) stratification without ice cover in small lakes (Kirillin et al., 2009).

Apart from the straightforward method of upwelling detection by spatially-resolved vertical temperature soundings, the thermal infrared (TIR) satellite imaging has proven as an effective method of upwelling detection in large lakes, using horizontal temperature gradient on the lake surface with colder water at the windward site and warmer water at the leeward site of the lake as a direct indication for upwelling: Steissberg et al. (2005) described an upwelling event in Lake Tahoe determined from the satellite images of skin surface temperature verified by depth-resolved *in-situ* temperature measurements at several points. The relatively coarse resolution of satellite images makes the method not applicable to small water areas, being another reason for the lack of information on upwelling events in relatively small lakes.

In the present study we combined airborne TIR imaging with horizontally-resolved *in-situ* monitoring of the lake surface temperatures to estimate development of the surface temperature pattern in two small temperate, dimictic lakes in eastern Germany. The study was conducted in spring 2013 between the ice break up and the establishment of the summer stratification. The study pursued two aims: (1) estimating the likelihood, duration, and frequency of upwelling events, during the summer stratification formation with projections on the ecological significance of the phenomenon; (2) testing the performance and compatibility of both skin infrared and *in situ* surface temperature measurements.

3.6.2 Material and Methods

Study sites

The study sites Lake Arendsee and Lake Stechlin are situated in the North German Lowlands (Figure 3.6-1). Morphometric parameters of each lake are given in Table 3.6-1. Both lakes are dimictic, and have similar depths (mean depth in Lake Arendsee and in Lake Stechlin are 29 m and 22 m respectively). The regional climate is warm and temperate (Köppen, 1936) with the average air temperature for 1981-2010 about 9 °C (DWD, 2014). The general weather situation is dominated by west winds, especially in spring and autumn.

The thermal regime of Lake Arendsee as well as Lake Stechlin is dimictic. The beginning of the summer stratification is similar for both lakes and starts in the middle of April. It lasts in average for 240 days (Engelhardt and Kirillin, 2014). Both Lake Arendsee and Lake Stechlin are fed mainly by groundwater (Holzbecher and Nützmann, 2000; Meinikmann et al., 2013). The average groundwater catchment is about 15 km² for Lake Arendsee (Meinikmann et al., 2013) and 11 km² for Lake Stechlin (Ginzel and Kaboth, 1999). See Bernhardt and Kirillin (2013), Kirillin et al. (2013a, b) and Engelhardt and Kirillin (2014) for further information on the hydrological regime and thermal stratification in both lakes.

The main difference between both lakes is caused by their origin: Lake Arendsee was formed by a collapse of a salt dome (Leineweber et al., 2009). Hence, it is characterized by an almost circular shape; steep in-lake slopes close to the shoreline and a flat bottom (Figure 3.6-1). In contrast, the shape of Lake Stechlin is determined by two glacial melt water channels, which were protected against sedimentation by dead ice (Krey, 1985). Therefore, Lake Stechlin consists of elongated and narrow bays. The northern bay has very steep in-lake slopes close to the shore and the deepest point of the lake is located in this basin. The western and the southern bay are shallower and the in-lake slopes are less steep (Figure 3.6-1).

Table 3.6-1: Characterization of Lake Arendsee and Lake Stechlin

	Lake Arendsee	**Lake Stechlin**
Position	N52° 53' 29.494"	N53° 9' 8.212"
	E11° 28' 34.241"	E13° 1' 43.388"
Maximum depth [m]	49	69
Mean depth [m]	29	22
Surface area [km²]	5.1	4.25
Trophic status	eutropic	oligo-mesothropic

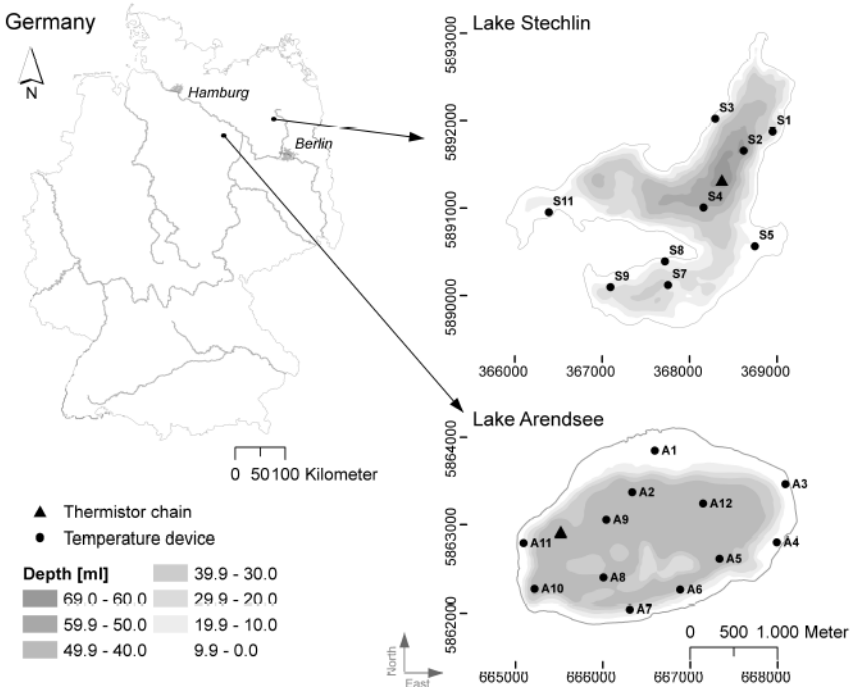

Figure 3.6-1: Location of study sites, positions of lateral temperature measurements (black circles) and thermistor chains (black triangle). The data are projected in UTM 32 WGS 84 for Lake Arendsee and UTM 33 WGS 84 for Lake Stechlin, respectively.

Surface temperature measurements

The measurements of the horizontal surface temperature distribution on the lake surface followed two approaches: snapshotting by airborne thermal infrared (TIR) of the skin layer (upper first millimeter of the water column) and surface temperature monitoring of the upper first centimeter of the water column at several points distributed over the lake surface (Figure 3.6-1). The TIR delivered a spatially high resolved temperature pattern, whereas the *in-situ* monitoring allowed continuous tracing of the temperature pattern variability over a period of several days.

Four overflights were performed for each lake in April 2013: one on 24 April (8:19 h Lake Arendsee; 9:10 h Lake Stechlin) and three on 28 April (8:20, 9:37, and 11:56 h Lake Arendsee). The airborne mission was conducted with a Cessna 207 T by the Institute of Space Science of the Free University of Berlin. The images were taken from the altitude of about 765 m at the average flight velocity of 55 m s^{-1}. To cover the whole lake surface two flights were performed over Lake Arendsee and three over Lake Stechlin. The TIR camera (VarioCam HR, head 600) had a resolution of 640 x 380 pixels and a focal length of 30 mm. The camera was installed on a stabilized platform (GSM 3000) which was controlled by an inertial navigation system (IGI Aerocontrol). The pictures were taken every second. The inertial system also collected altitude and navigation data. On 24 April a total of 2000 images at

Lake Arendsee and 2090 images at Lake Stechlin were recorded during each flight. After conversion from the proprietary file format to standard tiff files, every tenth image was selected for mosaicking. Within the mosaicking process, a slight blending was done by using a multi-resolution spline algorithm to avoid hard seam lines. However, erroneous reflections from the water surface and distortions caused by e.g. waves were reduced too and an accurate continuous mosaic was calculated. The mosaic then was georeferenced using ground control points at the shore.

The *in-situ* point measurements were conducted with TR-1060 temperature loggers (Richard Brancker Research Ltd., Canada; accuracy ± 0.002 °C; resolution: < 0.00005 °C). The positions of the loggers were determined with the ArcGIS tool 'create random points' (ESRI, 2012) to ensure approximately equal coverage of the lake surface. The temperature loggers were installed in the first centimeter of the water column by fixing cylindrical floats to the probe housings (Figure 3.6-2). The loggers were attached to buoys moored at the previously selected positions. Twelve loggers (A1-A12) were installed in Lake Arendsee and eleven (S1-S11) in Lake Stechlin (Figure 3.6-1). The temperatures were recorded every 20 seconds from 23 to 29 April in Lake Arendsee and from 23 to 30 April in Lake Stechlin. Three loggers A02, S06 and S10 failed to keep the horizontal position in the surface layer and their data were excluded from the subsequent analysis. Spatial interpolation was carried out to determine the horizontal temperature pattern, with 11 and 9 interpolation points for Lake Arendsee and Lake Stechlin, respectively. Two *in-situ* data sets were used for subsequent analysis: (1) averages over each flight period and (2) daily averages. The former was used for the direct comparison with the airborne TIR images and the latter for the estimation of the temporal evolution of the lake surface temperature pattern. The daily averaging was chosen to exclude diurnal temperature fluctuations. Additionally, the spatial mean over all logger positions was subtracted from the daily averaged single logger records to exclude the gradual surface heating from the horizontal temperature patterns.

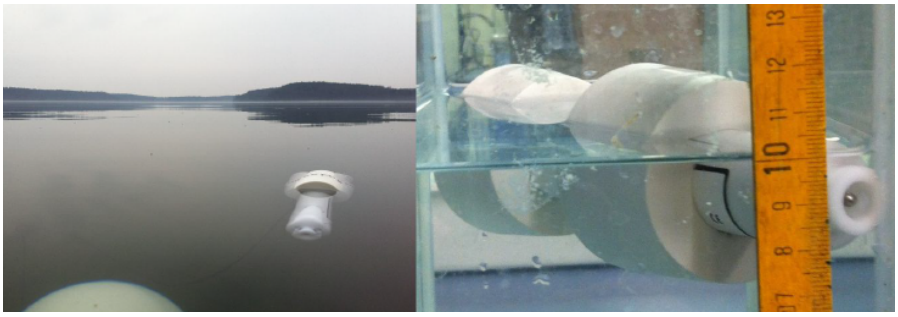

Figure 3.6-2: Set up for the in-situ horizontal temperature investigation. Floating material was fixed at the end of the data logger to ensure that the temperature sensor is placed one centimeter below the water surface (scale on the right picture is in cm).

Five methods were tested for interpolation of the point temperature measurements on the entire lake surface - Ordinary Kriging, Co-Kriging, Universal Kriging, Universal Co-Kriging and Inverse distance weighting (Cressie, 1991) - all demonstrating similar performance. The Ordinary Kriging approach was adopted in the following analysis, performed with R (R Core Team, 2014) using the packages automap (Hiemstra et al., 2008) and gstat (Pebesma, 2004).

Temperature depth profiles and meteorological data

As a source of information on thermal stratification development, vertical profiles of the water temperature were measured by thermistor chains located close to the deepest point of each lake (Figure). In Lake Arendsee the chain consisted of 15 temperature-oxygen loggers (D-Opto Probe, Zebra Tech., NZ; temperature accuracy ±0.1 °C) measuring once per hour. The uppermost 10 loggers were placed every 2.5 m at depths from 2.5 to 25 m below the surface, with a coarser vertical resolution of 5 m below 25 m. The temperature depth profiles in Lake Stechlin were measured by a Lake Environmental Sensing Platform (LakeESP, PME Ltd., USA) measuring at 42 depths with vertical resolution of 0.5 m in the upper 12 m of the water column and in the 2 m thick bottom boundary layer, reducing to 1-5 m in the bulk of the water column. The sampling time of loggers was one minute.

Two temperature (CTD)-transects were taken in Lake Arendsee on 28 April with a portable CTD-Profiler (RINKO-Profiler; JFE Advantech Co., Ltd., Japan; temperature resolution 0.001 °C, accuracy ± 0.01 °C). In total, 12 profiles with a vertical resolution of ~10 cm were taken every 300 m from the southern shore to the northern and eastern shore, respectively.

Meteorological data - wind speed, wind direction, barometric pressure, air temperature and solar radiation - were measured at Lake Arendsee every 10 minutes at 2 m above the surface from a floating platform equipped with a weather transmitter (Vaisala WXT520; Vaisala Oyj, Finland) and located close to the deepest location 226 of the lake. For Lake Stechlin data from a lakeshore weather station run by the German Environmental Agency (UBA) were used, collected at 30 min intervals, whereas wind direction and speed were measured at 35 m height by Ultrasonic Anemometer 3D. Wind speeds for both lakes were later transformed to 10 m heights using the MATLAB package AIR-SEA (Pawlowicz et al., 2001).

Stratification indices and upwelling criteria

Basic definitions. Approximating the lake by rectangular basin with the long axis *L* and a two-layered vertical density (temperature) distribution with density difference between the layers $\Delta\rho$ and thickness of the upper (thinner) layer z_e, the Richardson Number in Equation 3.6-1 can be expressed as (Imberger and Patterson, 1990):

$$Ri_w = \frac{g' z_e}{u_*^2} \qquad \textit{Equation 3.6-2}$$

Where $g' = g\Delta\rho/\rho_0$ is the reduced gravity, g is the acceleration due to gravity, ρ_0 is the mean density of the water column, and u_*^2 is the wind friction velocity defined as

$$u_* = \sqrt{\frac{\rho_a}{\rho_0} C_D U_{10}^2} \qquad \textit{Equation 3.6-3}$$

Here, U_{10} is the wind velocity at 10 m above the water surface ρ_a/ρ_0 is the air-water density ratio and C_D is the drag coefficient which is given, e.g., by Hicks (1972):

$$C_D = 1 * 10^{-3} \; for \; U_{10} < 5 \; ms^{-1}$$

$$C_D = 1.5 * 10^{-3} \; for \; U_{10} > 5 \; ms^{-1}$$

The multiplication of Ri_W with the lake aspect ratio yields the Wedderburn number (Thompson and Imberger, 1980):

$$W = Ri_w * z_e / (L/2) \qquad \textit{Equation 3.6-4}$$

with the lake length *L* [m]. If $W >> 1$, the wind is unable to tilt the interface between the two layers to produce an upwelling. If $W << 1$, the wind shear stress is expected to destroy density stratification completely. Around the threshold value of $W \sim 1$ a temporary upwelling can be expected (Imberger and Patterson, 1990).

Extending the situation from a two-layered case to a real density profile involves the Schmidt Stability S expressed by (Schmidt, 1928):

$$S = \frac{g}{A_0} \int_0^{z_D} (z - z_V) \rho_z A_z dz \qquad [\text{J m}^{-2} \text{ or kg s}^{-1}] \qquad \textit{Equation 3.6-5}$$

where ρ_z and A_z are the vertical distributions of the water density and horizontal cross-sectional area of the lake, respectively; A_0 is the surface area of the lake, z_D is the maximum depth, and z_v is the center of volume of the lake, defined as

$z_V = \frac{1}{V}\int_0^{z_D} A_z dz$; V being the lake volume. The Schmidt stability is the measure of energy required to mix completely a stratified lake with arbitrary vertical density distribution taking into account the volume development of the lake basin. Substituting of S as stratification measure into mixing balance (Equation 3.6-2) yields the 'Schmidt-based' Richardson Number $Ri_S = S(\rho_0 z_V u_*^2)^{-1}$, which, when multiplied with the same aspect ratio as in Equation , turns into the criterion of the upwelling, alternative to the Wedderburn Number — the Lake Number L_N:

$$L_N = Ri_S * \frac{2z_e}{L} = \frac{2Sz_e}{L\rho_0 u_*^2 z_V} \qquad \textit{Equation 3.6-6}$$

For rectangular basin geometry and two-layered density distribution, L_N is equivalent to the Wedderburn Number (Equation 3.6-4) (assuming $z_e << z_D$, see Stevens and Imberger (1996) and Coman and Wells (2012) for detailed discussions). Note that a slightly different definition of L_N is often used (e.g. Imberger and Patterson, 1990; Stevens and Imberger, 1996; Read et al. 2011), with z_e replaced by the total thickness of the epilimnion and metalimnion (z_e+z_m), while keeping z_e as a vertical length scale in the Wedderburn Number (Equation 3.6-4). In that case, the vertical density distribution is tentatively assumed as three-layered and W and L_N are treated as criteria for partial 'metalimnetic' upwelling and 'full' upwelling, respectively (Imberger and Patterson, 1990; Stevens and Imberger, 1996).

Application of upwelling criteria to observed temperatures. The vertical density distributions were calculated from temperatures using the freshwater equation of state (Chen and Millero, 1986) with the help of LIMSTATE density calculation routine (Pawlowicz, 2008). Several parameterizations of the friction u_* for neutrally stratified atmospheric boundary layer, as included into the AIR-SEA calculation package (Pawlowicz et al. 2001) were tested, all providing negligible differences. No atmospheric stability correction was performed. Density distributions with the surface-bottom density difference < 10^{-3} kg m^{-3} (roughly corresponding to the temperature sensors accuracy) were assumed completely mixed with $W = L_N = 0$. For the rest of the density (temperature) profiles, the position of the epilimnion bottom z_e was determined from the condition of maximum vertical gradient $\max(\delta T/\delta z)$, and the bottom of the metalimnion (z_e+z_m) was set based on the maximum curvature of the temperature profile $\max(\delta^2 T/\delta z^2)$. W and L_N were calculated based on both z_e and (z_e+z_m) as vertical length scales, providing essentially the same outcomes with deviations < 10%. Only the

numbers based on z_e are presented in the following analysis. The horizontal length scale *L/2* was approximated by the square root from the lake surface area $A_0^{1/2}$.

3.6.3 Results

Comparison of surface temperatures from TIR and in situ measurements

On 24 April the skin temperatures measured by the TIR were about 1.3 °C (± 0.2 °C, here and below the range is given as standard deviation) higher than the *in-situ* measurements in Lake Arendsee, and about 0.8 °C (± 0.2 °C) higher than the bulk temperature values in Lake Stechlin, respectively. The persistent warm bias in the TIR measurements can be interpreted as a 'warm skin' effect producing temperature difference between the lake surface and bulk of the upper mixed layer, see, e.g. Murray et al. (2000). However, since the deviation is in the declared range of accuracy of the TIR imaging (± 1.5 °C), the existence of the skin effect cannot be tested based on available data.

The spatial resolution of the *in-situ* logger measurements was much coarser than those of the TIR imaging: In average there was one logger on 500 m², whereas one pixel of the TIR image represents 2 m². However, the general horizontal lake surface temperature pattern was detectable with both approaches. On 24 April both methods indicated a temperature increase from West to East (Figure 3.6-3) which shifted from North to the South on 28 April (not shown). The higher spatial resolution of the TIR image provided a more detailed temperature pattern and allowed revealing interpolation artefacts in the *in-situ* measurements (Figure 3.6-3): The TIR image of Lake Arendsee shows a warm local spot around logger A12 and, since the logger is placed directly within this spot, its dimensions were overestimated by the interpolation. In turn, the TIR image of Lake Stechlin revealed a cold spot in the western bay east of logger S11, which was overlooked by the *in-situ* measurements and interpolation.

Thus, the temperature patterns analyzed below relies on a 312 compromise between the airborne snapshots with high spatial resolution but lacking the temporal resolution, and the horizontal patterns based on sparsely distributed *in-situ* measurements, tracking the temporal development but subject to interpolation artefacts. The latter becomes larger with the larger spatial temperature variability especially evident in Lake Stechlin (Figure 3.6-3). While the interpolation misses the morphometrically determined small-scale details in the surface temperature distribution, the overall interpolated lake-wide pattern can be considered as sufficiently reliable, as it is shown below by analysis of the deviation from the spatial mean.

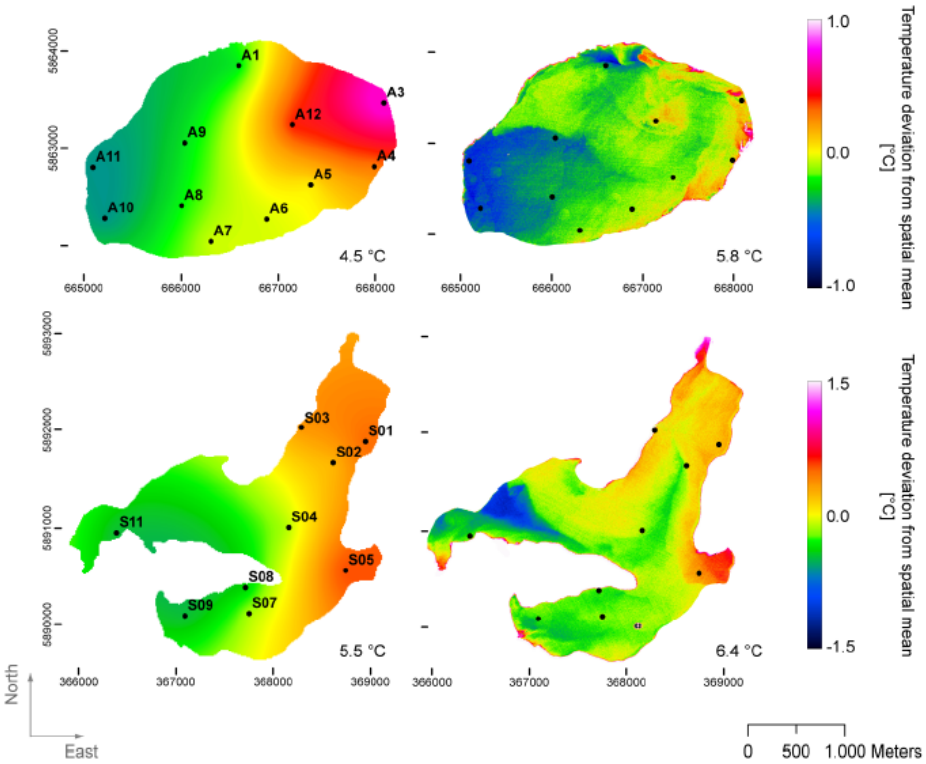

Figure 3.6-3: Comparison of interpolated temperatures of sensors floating on the lake surface (left column) and the TIR image (right column) on 24 April 2013. Images were taken for Lake Arendsee at 8:16 - 8:21 h (upper row) and for Lake Stechlin at 9:06 - 9:15 h (lower row). The data are projected in UTM 32 (WGS 84) for Lake Arendsee and UTM 33 (WGS 84) for Lake Stechlin, respectively. The figure illustrates the deviation of the temperature from a spatial mean during the time of flight, which is written in the right lower corner of each panel.

Temporal variations of the surface temperature pattern

During the entire study period from 23 to 30 April, which includes the two dates of both TIR surveys, the surface temperatures in Lake Stechlin were above the maximum density value (TMD) of 4 °C, indicating development of thermal stratification in the lake. In Lake Arendsee, the surface temperatures dropped below 4 °C in the nights of the 23 and the 24April at five positions (A1, A9, A10, A11, and A12), suggesting a short-term development of a ‘thermal bar’-like horizontal front (Zilitinkevich et al. 1992) between the NE and SW parts of the lake at the very beginning of the measurements period. Horizontal fronts associated with the effect of TMD on water density are short-leaving phenomena, except in great lakes with littoral areas exceeding several tenths of kilometers (Zilitinkevich et al. 1992). Our dataset is insufficient to analyze this effect in details, since the surface temperatures stayed above the TMD over the entire lake afterwards. Therefore, we concentrate in the further analysis on spatial deviations from the daily mean lake-averaged surface temperatures (Figure

3.6-4). Daily averaging filtered out the diurnal variability associated with solar heating and lake-atmosphere heat exchange. The horizontal lake surface temperature distribution in both lakes did not reveal significant variations on shorter sub-daily scales, supported also by airborne measurements. The TIR images from 28th April (not shown) demonstrated the same temperature pattern within two hours, except a uniform heating of the surface water by solar radiation.

The eight days period can be conditionally subdivided into two different periods based on changes in air and surface water temperatures. The first four days are characterized by an increase in average air temperature from 10 °C to 14 °C. In the same time the average water temperature of the lake surface increased from 4.7 °C to 7.8 °C in Lake Arendsee and from 5.4 °C to 7.8 °C in Lake Stechlin (Figure 3.6-4), respectively. In the night from 26 to 27 April the air temperatures dropped below the water surface temperatures with subsequent surface cooling of about 1.1 °C in both lakes. The rest of the second period was characterized by a slower increase of mean lake surface temperatures from 6.7 °C to 6.9 °C in Lake Arendsee and from 6.7 °C to 7.9 °C in Lake Stechlin, respectively.

West winds prevailed during the study period. The surface temperature distribution in both lakes was unambiguously related to the wind direction and speed (shown as arrows of different size and direction in Figure 3.6-4) with a colder surface at the windward side and a warmer surface at the leeward side of the lake. The slight changes in the wind direction between SW and NW resulted in associated changes in the orientation of the horizontal temperature gradients, following the changes in the wind direction with a lag of up to 24 hours. Hence, the instantaneous surface temperature pattern was partially affected by winds of the previous day. In the following the lake surface temperature interpolation and wind will be illustrated for both lakes separately. The wind data are represented by the daily means and the standard deviations, the latter illustrating the wind speed variations during a day.

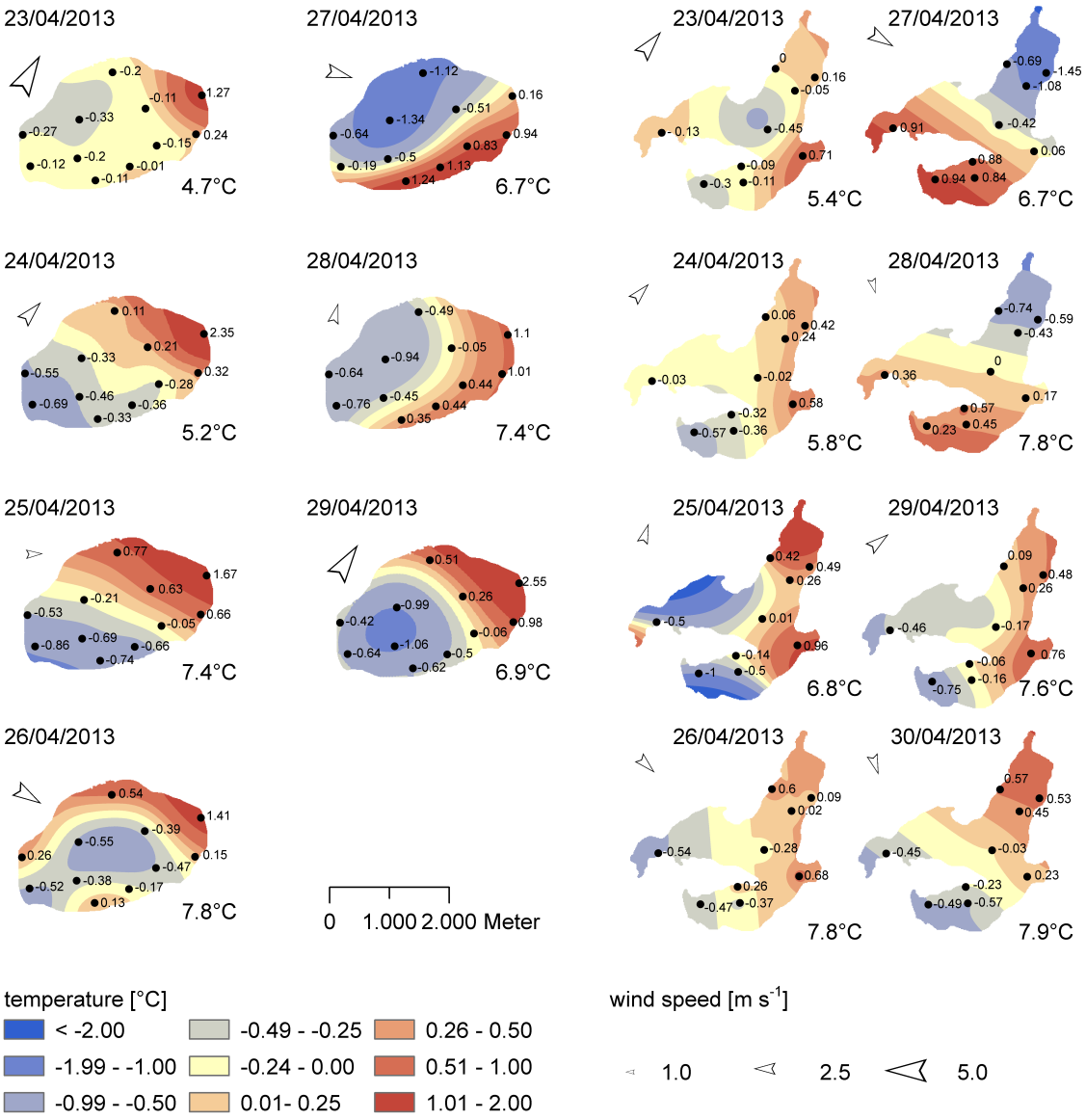

Figure 3.6-4: Daily pattern of the surface temperatures of Lake Arendsee (left columns) and Lake Stechlin (right columns) from 23 to 30 April 2013. The figures are interpolated from the deviations of the spatially averaged temperatures of each day. The daily average temperature is written in the right corner of each single image. Additionally, the average wind direction and wind speed are shown as an arrow in the upper left. Note that the figure shows the local deviations of the daily mean of the entire lake surface.

Lake Arendsee. A constant wind from SW-W on 23 April with velocities of 4 m s^{-1} (± 2 m s^{-1}) was associated with a relatively small lake-wide horizontal temperature gradients of 0.57 °C (neglecting the comparatively high values from logger A03, which was located close to the shoreline at a position with water depth < 1 m, and was presumably affected by local heat sources).

During the following two days the average wind direction remained constant, whereas the average wind speed decreased to 1.9 ± 0.9 m s^{-1}. As a result, the temperature pattern of the 23 April stabilized and the horizontal temperature gradient increased to 1.6 °C.

On 26 April the wind velocity increased again (3.4 ± 2.2 m s^{-1}), and the wind direction rotated counterclockwise from north to south. As a result, the colder area extended over the large part of the lake surface, with warmer waters concentrated along the northern lake shore.

On 27 April the average surface temperature decreased to 1.1 m s^{-1} due to the nighttime drop of the air temperature. The constant wind from NW direction (3.1 ± 1.5 m s^{-1}) lead to a strong surface temperature increase from north-west to south-east. The surface temperature gradient decreased during the following almost windless day.

Constant SW winds (4.7 ± 1.99 m s^{-1}) prevailed over Lake Arendsee during 29 April. This resulted in a similar pattern like on 24 April, but with higher lake-wide temperature differences (3.61 °C).

Lake Stechlin. On 23 and 24 April, the winds over Lake Stechlin followed the same directions as over Lake Arendsee, but with lower wind speeds (3.8 ± 1.4 m s^{-1} and 2.7 ± 0.62 m s^{-1} on 23 and 24 April, respectively). On 23 April no clear pattern associated with possible upwelling of colder waters could be determined in the surface temperatures, with slightly colder deep central part of the lake and warmer littoral areas. In contrast, 381 there was a clear cross-lake temperature gradient on 24 April, with colder surface waters in the upwind southern and western bays and warmer waters in downwind eastern and northern bays. This gradient increased during 25 April, reaching up to 1.96 °C difference across the lake.

The varying wind directions during 26 April (SW-W-N, wind speeds 2.6 ± 1.2 m s^{-1}) reduced the horizontal temperature gradients, however, did not destroy the qualitative pattern with surface temperature increase from southwest to northeast. On 27 April, the constant NW winds with an average wind velocity of 3.2 ± 0.69 m s^{-1} were associated with the opposite lake surface temperature gradient established colder in the northern bay of the lake and warmer areas occurred in the southern and western bay. The temperature range of 2.4 °C at that day is the highest for the entire investigation period. Similarly to Lake Arendsee, the temperature pattern remained through 28 April with a weaker gradient due to the low wind speeds (1.8 ± 0.56 m s^{-1}). The increase of wind speed (2.9 ± 1.76 m s^{-1}) at constant SW wind direction established on 29 April a SW-NE temperature increase persisting also during the 30 April.

Temperature transects

The average vertical temperature difference across the water column of Lake Arendsee was about 2.8 °C (8.1 °C at the surface, 5.3 °C in 12.5 m depth) for all profiles measured on 28 April (Figure 3.6-5), a sign of an appreciable vertical stratification. The vertical stratification was however not evenly distributed over the whole lake. Transect T1 – T6 revealed a stronger vertical stratification in the littoral area and slightly weaker in the pelagial (Figure 3.6-5a), whereas Transect T7 – T12 indicated a tilt of the isotherms from the southern part (T7: 8.7 °C at the surface and 5.4 °C at 12.5 m depth) to the northern part of the lake (T12: 5.8 °C at the surface and 5.2 °C at 12.5 m depth). The surface temperature pattern on 28 April agrees with the findings from CTD transects (Figure 3.6-5c): Higher surface temperatures in the eastern and southern parts of the lake (about 8 °C) and lower temperatures in the northern and western part of the lake (about 6 °C) agree with the slope of the isotherms along the transect and link unambiguously the observed surface temperature pattern to the upwelling of deep colder waters from the stratified lake interior.

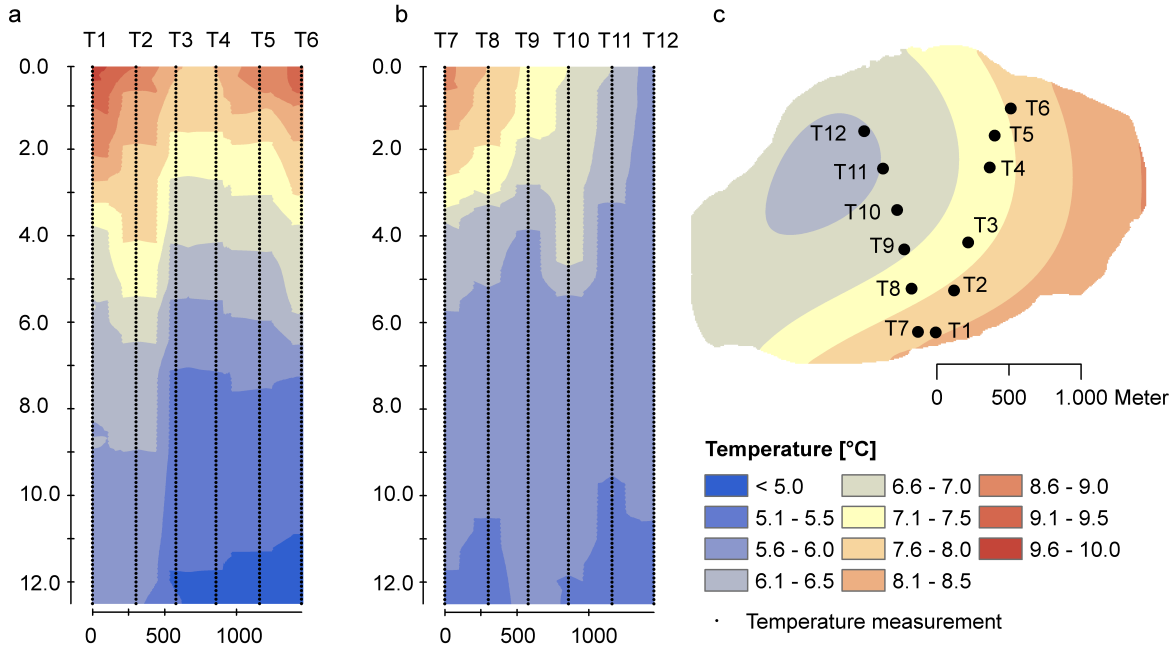

Figure 3.6-5: Upper 12.5 m of CTD-profiles in Lake Arendsee taken on 28 April 2013 between 18:00 and 19:30 h. (a) Transects from the southern to the eastern shore (T1 - T6), (b) from the southern to the northern shore (T7 - T12), and (c) location of transects in the lake and lake surface temperatures calculated based on loggers A01 to A12. The figures (a) and (b) indicate an upwelling of metalimnic water.

Stratification indices and upwelling criteria

The period of the surface temperature observations and airborne measurements covers the early stage of the stratification development (Figure 3.6-6). According to the values of Schmidt Stability *S*, the winter period of inverse stratification (with colder water on top of warmer water) ends around 15 April in Lake Stechlin and lasts until 17 April in Lake Arendsee, followed by 2-3 day long overturn period (full mixing) with zero Schmidt Stability. The Schmidt Stability increases above zero again on 19 April and on 21 April in Lake Stechlin and in Lake Arendsee, respectively. Afterwards *S* increases continuously up to 1000 J m^{-2} in late May. Both the Lake and Wedderburn Numbers demonstrate qualitatively similar development to *S*, and have nearly identical values, with slight divergence between *W* and L_N in Lake Arendsee in May, which can be attributed to a thicker metalimnion (thermocline) in this lake, making application of the two-layered density approximation inherent to the Wedderburn Number less justified. During the study period of 23-30 April (light-gray area in Figure 3.6-6) both numbers continuously grow reaching the threshold value of 1 around 01 May. In Lake Stechlin *W* and L_N remain close to 1 throughout the first decade of May, while in Lake Arendsee stratification develops faster, and the scaling numbers are above 1 from 01 May except several short events, associated apparently with strong wind impulses.

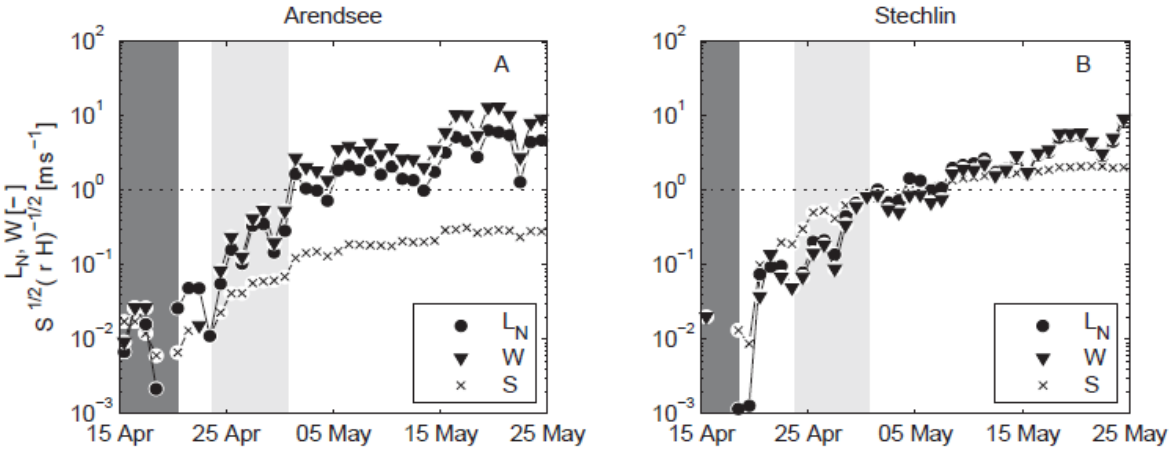

Figure 3.6-6: The Lake number (L_N), the Wedderburn number (W) and the Schmidt Stability (S) in (A) Lake Arendsee and (B) Lake Stechlin. The Schmidt stability is scaled with the mean density ρ_0 and the mean lake depth H, providing a direct estimate of the internal wave speed (see the text for further explanations). Dark gray area with a thick vertical line demarcates the preceding winter stratification and the overturn. The light gray area marks the period of the surface temperature observations. The overturn periods are designated by values $S \leq 0$ seen at the logarithmic plot as 'no value' gaps.

3.6.4 Discussion

The present study demonstrates an overall good agreement of *in-situ* surface temperature measurements and thermal infrared imaging in terms of relative temperature variations over the lake surface. This result justifies validity of the airborne TIR imaging for revealing horizontal surface temperature patterns in small lakes, for which the spatial resolution of satellite imaging is typically insufficient in contrast to large lakes (e.g. Steissberg et al., 2005; Reinart and Reinhold, 2008). The mean positive bias of ~1 °C in absolute values of radiative temperatures against the bulk temperatures measured by the *in-situ* loggers lies within the declared accuracy range of the TIR method, and can be attributed to the differences in accuracy of the spatial resolution (1 m² and 1 mm for the TIR imaging against 500 m² and 10 mm for the temperature loggers), and of the measurement (± 1.5 °C for the TIR imaging against ± 0.002 °C for the temperature loggers). The bias is however persistent throughout the repeated measurements in both lakes that allows suggesting it to result from a 'warm skin', an analogue of the 'cool skin'— an upward negative temperature gradient in a thin viscous layer formed at the ocean surface by molecular processes slowing down the upward heat transport (Soloviev and Lukas, 2013). While appearance of the warm skin was documented also for the ocean (e.g. Murray et al., 2000), it is rather exceptional for the sea surface temperature, because existence of the warm skin suggests the net heat flux directed from the atmosphere to the ocean. The warm skin was reported to appear more frequently in large lakes (Wilson et al., 2013) with typical difference ΔT_S between the radiative 'skin' temperature and the *in-situ* 'bulk' temperature of 0.5 °C. Over small lakes, the air temperatures, and consequently downward heat fluxes are formed predominately by the heat input from the surrounding land, which is significantly warmer in spring than the lake surface due to the lower albedo. Hence, the net downward heat flux and strongly stable atmospheric boundary layer are typical conditions over the small lakes during the initial stage of summer stratification, distinguishing them from large lakes and the ocean. Taking into account typically low wind speeds over small lakes, we can hypothesize that the warm skin with $\Delta T_S \sim 1\ °C$ was the reason of the discrepancy between the radiative and *in-situ* temperatures. The hypothesis cannot be tested in frames of this study, as we do not possess TIR data with sufficient temporal resolution. Still, this indirect indication of generally warmer skin temperatures in small lakes is an important outcome of the present study suggesting that (i) the algorithms for the sea surface temperature estimation from TIR data may require corrections before their application to lake surface temperatures, (ii) the skin correction should be taken into account when modeling processes directly dependent on the skin temperature, such as gas transfer across the air-lake interface.

The agreement between the two independent measurement methods proves the existence of significant horizontal surface temperature gradients (> 1 °C) in dimictic lakes during spring.

Comparison of the observed TIR temperature patterns on 24 and 28 April with the concurrent wind directions indicates colder temperatures at the windward site of the lakes. This suggests upwelling of deeper water is responsible for the horizontal temperature variation at the lake surface. The close relation between wind speed/direction and the development of the colder areas at the windward sides of the lake surface was supported by the *in-situ* data for the entire 8-day study period. The connection between the wind direction and the orientation of the surface temperature gradients is crucial for classifying the observed patterns as results of the upwelling, which otherwise could be attributed to e.g. warm groundwater inflow (Lewandowski et al., 2013) or differential heating/cooling of the lake epilimnion (Forrest et al., 2008).

A further evidence of the wind-driven upwelling development is provided by the temperature depth transects profiles which were taken on 28 April in Lake Arendsee revealing a tilt of the thermocline along the wind direction (Figure 3.6-5). Twelve highly resolved temperature depth profiles were measured along two transects. The profiles link the observed cold surface in the NW part of the lake to the slope of isotherms (Figure 3.6-5a): Isotherms are inclined in the wind direction and indicate upwelling of cold water in the same area where the cold water is found in the surface data (Figure 3.6-5b, c). Comparison of both transects (Figure 3.6-5a, b) suggests that the upwelling brought to the surface the meta- and hypolimnetic water residing otherwise at depths ≥ 7 m. Additionally, the water column in the cold upwelling area (points T11-T12 in Figure 3.6-5b) is homogenized with regard to temperature: the temperature difference across the 12 m deep water column does not exceed 1 °C. This fact demonstrates the efficiency of secondary mixing produced by upwelling, when advective motions locally destroy the vertical stratification and facilitate thereby vertical turbulence. It should be noted, that the cross sections were taken at the end of the upwelling period initiated by northern winds on 26 and 27 April, so that the observed picture was the result of a stronger isotherms inclination accompanied by mixing during the previous day. Also noteworthy are belts of warmer subsurface water along the shallow littoral, outside of the upwelling area (points T1, T6 in Fig. Figure 3.6-5a) as a clear indication of the differential heating between the nearshore areas and the open lake. Hence, a contribution of density currents due to differential heating into horizontal transport within the lake cannot be a priori excluded, while its quantification requires additional observations.

The morphometry of the lake and the length of the wind fetch affect the extension of the upwelling area. The TIR images illustrate, that the cold spot areas in regularly-shaped Lake Arendsee are larger than in the narrow Lake Stechlin. This effect is only evident in the TIR images, while spatial resolution of the *in-situ* loggers is too coarse for identifying a specific upwelling area (Figure 3.6-3): the thermal infrared image indicates that the upwelling area at Lake Stechlin is more restricted to small areas, whereas the interpolation identified a broader area due to a coarser spatial resolution of the measurement technique (Figure 3.6-3). This implies that a higher spatial resolution of surface

temperature measurements is recommended for research questions focusing on the determination of explicit upwelling areas, especially in lakes of irregular shape.

The two dimensionless numbers originally developed as criteria of upwelling appearance - W and L_N - had nearly identical values during our study period, suggesting that both can be used interchangeably, as long as both use the same length scales in the definition of the lake aspect ratio. The result refers partly to the particular choice of the lakes under study: Both Lake Stechlin and Lake Arendsee have relatively steep bathymetry. Hence, both estimations of the Richardson number entering Equation and Equation produce the same values, and discrepancies between W and L_N, discussed e.g. by Coman and Wells (2012) are of minor importance here. In lakes with complex bathymetry a higher divergence between Wedderburn and Lake numbers can be expected, whereas corrections for the effects of sloping bottom and varying basing width along the wind direction might help to improve the scaling (Shintani et al., 2010). The lake morphometry and non-linear response of the stratification to the wind may also affect the threshold value, which is initially set as $W \sim L_N \sim 1$ for simple basin geometry and linear slope of isotherms. Still, the threshold value of $W \sim L_N \leq 1$ can be accepted in most cases, as an order-of-magnitude criterion of upwelling development (Stevens and Lawrence, 1997; Shintani et al., 2010; Coman and Wells, 2012; Simpson et al., 2014). In our observations, $W \sim L_N \leq 1$ throughout the entire period of upwelling existence, supporting the applicability of the simplified scaling to real lakes during the weak stratification in spring.

We have found a several hours up to one day delay between changing wind conditions and establishing a corresponding upwelling-related temperature pattern at the lake surface. The time of initial response of a stratified lake to the wind impulse is known to scale with as the quarter-period of internal basin-scale waves (seiches) $T_i/4$, and the half-period $T_i/2$ is an estimate for establishing nearly steady-state circulation at constant wind (Spigel and Imberger, 1980). The period of the dominant seiche mode is defined as $Ti = 2LC_i^{-1}$, where the seiche wavelength is twice the length of the lake, and C_i is the phase speed (celerity) of the internal wave. The latter can be estimated using the analogy between Ri_W and Ri_S (Equation 3.6-4 and Equation 3.6-6) as $C_i \sim S^{1/2}(\rho H)^{-1/2} \sim 0.1\ m\ s^{-1}$ for the period of observations (Figure 3.6-6). Consequently, $T_i \leq 12$ hrs in both lakes and decreases as stratification increases with time. This relatively quick response of the lakes to the wind forcing explains the evidence that upwelling is not a transient phenomenon, but exists continuously during early formation of density stratification, changing its position and extension over the lake surface following the wind direction and strength. This result is perhaps the most important outcome of the present study demonstrating that there is continuous advection of deeper waters to the lake surface significantly enhancing vertical mixing and water exchange between epi- and hypolimnion. The upwelling mechanism of vertical exchange is apparently more effective than purely vertical

convection during the spring overturn, as it suggests direct transport of deeper waters to the lake surface instead of vertical mixing across the water column. Also, according to our results, the spring upwelling appears to last much longer than the convective overturn period: based on the condition $W \sim L_N \leq 1$ one can estimate the duration of the upwelling existence in Lake Arendsee as about one week, while in Lake Stechlin both criteria remained close to 1 for another 10 days. Compared to relatively short period of complete overturn, these values additionally emphasize the major role of upwelling in the spring circulation and in homogenizing of the lake water column before establishment of the strong summer stratification. Since these conditions can be found for the majority of temperate dimictic lakes, it can be concluded that upwelling needs to be considered as advective transport process during the formation of the summer stratification.

The crucial importance of the 'classical' upwelling for the transport of plankton and substances has been reported in earlier studies on large lakes (e.g. Yaguchi, 1977; Haffner et al., 1984; Webster et al. 1990; Hamblin et al., 2003) and the oceans (e.g. Bruland et al., 2005; Väli et al. 2011; Messié and Chavez, 2015). The spring upwelling, as demonstrated by our study, suggests similar effects on the vertical mass transport in the majority of small temperate lakes. While this period has been found to be short (5-10 days) compared to the seasonal variations, its effects on the lake systems are detectable on longer seasonal-to climatic scale: advection by the spring upwelling provides direct nutrient supply from the nutrient-rich hypolimnion to the upper waters suggesting strong effect on the initial stage of the summer plankton production. Another process affected by the upwelling is the air-lake gas exchange, in particular, the release of the sediment-produced methane into the atmosphere. Methane, produced in anoxic lake sediment, typically accumulates near the lake bottom, especially during winter in lakes seasonally covered by ice (Kirillin et al., 2012). Hence, upwelling could provide a direct pathway of the methane to the lake surface and intensify significantly release of the gas into the atmosphere. Transport by upwelling is essentially three-dimensional and is therefore missed in the conventional one-dimensional models of small lakes, where purely vertical convective transport dominates during the spring overturn, and the wind-produced tilt of the summer thermocline is not able to bring it to the surface, except in lakes of large lateral extent.

3.6.5 Summary and Conclusion

Using a combination of airborne TIR imaging of the lake surface and spatially distributed *in-situ* recording of surface temperatures we obtained first detailed pictures of spatial extent and duration of the cold water upwelling during spring formation of thermal stratification in small temperate lakes. The evidence of permanent upwelling following the spring overturn and lasting for 1-2 weeks suggests its major contribution into the vertical transport of matter across the lake water column. Upwelling

appearances agreed with the criteria, $W \sim L_N \leq 1$ suggesting the effect to take place in all dimictic lakes in spring, when stability necessarily increases from zero to $O(W, L N) = 10^0$. Our findings imply a strong effect of upwelling on the transport of nutrients to the euphotic layer, and dissolved gases to the lake surface, as well as on oxygenation of deeper lake waters. While not the subject of our study, the upwelling should also play a major role in circulation of lakes without stable summer stratification (polymictic lakes), where transient appearances of weak stratification with $W \sim L_N \leq 1$ would inevitably result in development of upwelling at moderate winds.

The key question following from our study is: are lakes mixed completely by purely vertical convection during the overturn, or the observed homogeneity is the result of a more complex circulation, involving advection of deep waters by upwelling during the period of weak stratification? Detailed observations on the vertical distribution of tracers, like oxygen concentration, would help answering the question with a larger degree of certainty. Unfortunately, we did not possess such data from the deep hypolimnion at sufficient accuracy and resolution to answer this question unambiguously. Instead, our work (i) demonstrated that the upwelling mechanism is at least as important as convective mixing during the spring overturn (actually, an order of magnitude more effective, as it follows from the scaling analysis above), (ii) upwelling should inevitably take place at the early stage of stratification in all temperate freshwater lakes (those with surface temperature crossing 4 °C in the annual cycle), and (iii) the period of upwelling lasts typically for a much longer time than the period of complete overturn, the latter being only a couple of days when the near-bottom waters can be entrained into the upper water column by convection. This fact was rarely, if ever, considered by limnologists believing in superpower of spring convection being able to mix completely any water column. This belief contradicts however some basic physics, in particular, the fact that the temperature effect on freshwater density (buoyancy) disappears in the vicinity of the temperature of maximum density ~4 °C. Occasional observations support incomplete mixing by convection during the overturn (see e.g. Section 6 ‘Effects of Salinity’ in Mironov et al. (2002) and the study of Pieters and Lawrence (2009)). While not thoroughly investigated, it can be suggested that the situation when the winter stratification turns into the summer one, without convective mixing of the deep waters is much more common than widely accepted. We suggest that upwelling at weak stratification is the most plausible explanation of the observed homogeneity of lakes in early summer. The major aim of our paper is to spin up the research in this direction, while an ultimate answer on the contribution of the spring upwelling in lake mixing and vertical transport of solutes can be obtained only in a number of further comparative studies.

4. Discussion

4.1 Objectives and limitations of the methods

The presented studies aimed at detecting groundwater flow paths towards and within surface waters. Therefore, various spatial and temporal scales were considered to distinguish the drivers of groundwater flow.

Water levels are easy to measure and are available for most hydro(geo)logical research questions. However, in most cases they were only used to describe the flow direction and flow velocities by determining the gradients and applying Darcy's Law. The study of Lehr et al. (2015, study I) illustrates that the measurements of water levels also contain information about the conductivity of the sediments. This requires a source of a pressure signal and the detection of the signal response by changes in water levels in the area around. In the study's case, the pressure signal originates from a the water level fluctuations of the river and was measured in 15 wells in the adjacent aquifer. It can be assumed that an increase of the well density will also deliver more details about the hydraulic connectivity of the sediments. This is hard to realize due to the high costs of drillings and pressure transducers. However, a regular areal distribution of the groundwater wells would deliver general structures and should be sufficient to distinguish between areas of higher and lower connectivity.

Since the sediment composition is constant the measurements do not need to be long.. But the temporal resolution of the measurements should be chosen so that typical changes of the pressure can easily be detected. For surface waters this should be the fastest possible change in water levels, e.g. an hourly measurement of water levels was adequate for the investigated floodplain at the river Spree.

Nevertheless, the main requirement for this method is a high correlation between the water levels of the surface water and the groundwater. Otherwise, processes others as the fluctuation of surface water such as groundwater recharge, could influence the water level fluctuations within the wells. In that case a subtraction of the spatial mean is not reasonable any longer, since this would impact the results of the principle component analysis.

The main attention of using this approach should be on data collection and processing, especially when different groundwater wells are used. The accuracy of the data loggers must be high enough to capture both spatial and temporal water level differences of the system, e.g. in the case of lowland areas water level changes should be captured with a resolution of about one centimeter.

The main advantage of this approach is the detection of sediment distributions in local flow systems in unconfined aquifers in areas being closely connected to surface water. For instance, this is very useful for groundwater modeling studies. Numerical groundwater models require information on water levels and sediment distribution. So both information would be available in a single measurement.

Furthermore, also field investigations benefit of such information, since it allows direct comparison of areas with different hydraulic connectivity.

Nutrient distribution can also give hints on the distribution of sediments in unconfined aquifers where the water levels are close to the surface (Pöschke et al. 2015 b, study II). Therefore, subsurface flow pattern can be concluded. Assuming that groundwater close to a surface water body belongs to the local flow system, the determination of flow paths and source areas for nutrients is important. Highly resolved vertical nutrient measurements by a Multi-Level Sampler (MLS) allow the distinction of the spatial extension of zones where higher concentration can be assumed. The temporal repetition of samplings allows an estimation of the flow directions. However, this is not possible with a single MLS, since the method allows only general conclusions on the flow behavior. Hence, a verification by different sampling locations is required. Exact measurements of flow directions are difficult in lowland areas due to the generally small gradients. Given this case MLS measurements can deliver a first estimate. However, they never replace an exact flow measurement.

The horizontal investigation by temporary piezometers show that knowledge about the small scale topography already allows the delineation of areas where higher nutrient concentration can be expected. The sediment composition, such as silt or organic layers within the aquifer, can be concluded from the combination of topography and nutrients. However, this method is only limited to a specific zone of the aquifer – namely the area where significant water level fluctuations occur (e.g. floodplain aquifers). Small water level fluctuations imply more constant redox conditions and therefore less significant differences between small scale geomorphological site. Furthermore, it can be assumed, that the extension of the layer of higher concentration is smaller, which makes the sampling more difficult.

Numerical Groundwater modeling is the only possibility to visualize groundwater flow pathways in the subsurface. However, the accuracy depends on the input data, the parameter estimation, the observed scale and on the computational power. Nevertheless, it can give first impressions on the general flow behavior in space and time. This can already improve the elaboration of hypotheses for further investigations in the field and for modeling. Therefore, Haitjema (2015) recommended to start as simple as possible. Simple approaches with general assumptions give an insight on the presence of subsurface flow system in a small groundwater catchment. The presented study (III) followed this approach.

However, it is questionable if a numerical model will be able to reproduce the transient behavior of the groundwater system exactly, which be attributed to the small gradients again. The groundwater level fluctuations at the wells P03 and P37 measure only a few centimeter within a year. Since the data basis consists of monthly manually measured values, the fluctuations are in the range of the measurement

error (± 1 cm). Taking further into account errors and artefacts of the numerical methods, an exact reproduction of the inter-annual variabilities is not realistic. Furthermore, the strong correlation between groundwater levels at P02, P40 and the lake indicates that the changes in lake water level also affect the adjacent groundwater via a pressure signal, similar as observed by Lewandowski et al. (2009) and Lehr et al. (2015, study I). Nevertheless, the available data will not be adequate to prove this assumption, since the temporal resolution of the measurement is too coarse.

Temperature was used as tracer with the aim to detect the groundwater exfiltration areas within the surface water by airborne thermal infrared imagery. The snap-shot produced by TIR may represent the lake's skin surface temperature as a comparison to the *in-situ* measurement illustrations (compare Figure 3.6-3). This was also shown for studies using satellites (e.g. Steissberg et al., 2005, Reinart and Reinold, 2008). In comparison to these studies, the spatial resolution in the present investigation was much higher, which results in a more detailed temperature pattern. An advantage if also smaller areas need to be identified. However, as the spatial resolution of satellites will increase it may be a less cost intensive option in the future. Besides the performance of the method itself, the main challenge is to assign the processes producing the observed temperature pattern. Details will be discussed in Chapter 4.3.

4.2 Subsurface flow paths and flow systems on different scales

Local flow systems are still of major importance concerning the substance input, since upper aquifers are most vulnerable to anthropogenic impacts. Whether an area contributes to surface water eutrophication or not, depends on the hydraulic connectivity to the surface water as well as on the substance load within a specific area. Both are mainly determined by the sediment distribution and characteristics. One method to identify possible sediment heterogeneities delivers Lehr et al. (2015, study I). They were able to identify parts of the aquifer with different connectivity to the surface water on a scale of 10^1 m. The investigation period covered four years and included flood events of several months as well as a restoration measure of the river; nevertheless the general linkage between groundwater and surface water remained the same for the whole period. Hence, spatial heterogeneity of the connectivity is larger than the temporal one. Hence, the subsurface flow nearby surface waters can be seen as temporally constant at least for a given timescale. Furthermore, the study confirms the findings of Schornberg et al. (2010), who showed that heterogeneity of the exchange between groundwater and surface water bases on the sediment distribution of the aquifer and not the sediments in the river. The River Spree represents this case. Even if hydraulic connectivity of the meander has been improved by removing the mud layer, the overall pattern of the connectivity remained.

A similar pattern of higher spatial and lower temporal heterogeneity was also found by Lewandowski and Nützmann (2010) for the nutrient concentrations within the same aquifer and with the same spatial resolution as in the study of Lehr et al. (2015, study I). Since there was no clear evidence on the reason of these findings, Pöschke et al. (2015 b, study II) performed small scale geochemical investigation (10^{-1} – 10^{1} m) on the upper aquifer and found an even larger spatial heterogeneity. Implying that the horizontal flow component is small in comparison to the vertical one, otherwise equilibrium would establish. Further, the results of the Multi-Level Sampler suggest that there is a vertical layering of the groundwater. The upper 1.5 m of the aquifer is impacted by water level fluctuations, which induces different redox conditions throughout the year and therefore variable and high nutrient concentrations in the upper part of the aquifer. Below concentrations are generally low and temporal constant meaning that there is another groundwater origin. It is still unanswered if and how these vertical layers are interacting. Does the interaction take place already on the flow towards the surface water or is it restricted to the area, where the water enters the surface water? Also if the part of the aquifer with the high nutrient concentrations is responsible for the eutrophication of surface waters, is still unknown. However, there are evidences for a lake from Crowe and Schwartz (1981) who discovered, that the water quality of the surface water only changes significantly, when the main part of the aquifer is subjected to a change in concentration. This would not be the case at the aquifer of the River Spree, since the upper 1.5 m of the aquifer represents about 7.5 % of the total aquifer volume.

The numerical modeling of groundwater discharge towards Lake Stechlin was able to illustrate that different vertical flow systems need to be considered when determining the groundwater flow towards a lake in lowland head areas with complex aquifer systems. In general, it can be assumed, that flow systems are more or less constant over a given time, since the temporal variations are small in aquifer systems. Skøien and Blöschl (2003) explain that a landscape tends to remove the temporal variability which is described by a meteorological force and adds spatial variability. The latter one is given by the sediment distribution (Lischeid, 2008). Nevertheless, Winter (1983) discovered a temporal change in the vertical extension of the flow systems due to differences in groundwater recharge. This can also be assumed for the catchment of Lake Stechlin, since there are long term fluctuations of the water levels of P03 and P37 which are not reflected in the lake. Additionally, Holzbecher (2001) describes variable horizontal extension of the groundwater catchment of Lake Stechlin, which also relates to the long term weather conditions. In conclusion, a long term temporal variability of the subsurface catchment of Lake Stechlin can be expected. This must be considered when research questions are addressing transient system behavior, e.g climate change studies.

For the Lowland of North Eastern Germany it could be conclude, that as long as there is no significant change in the water levels of the surface waters, the spatial extension and distribution of the subsurface flow adjacent to surface water will be temporally more or less constant. Therefore, the

detection of the flow paths should focus on the description of the sediment distribution to determine areas with higher transport capacities for mass, substances and energy. Hence, investigations on smaller spatial scales are necessary for these areas. In contrast, the regional flow system can be seen as the lever for the whole hydrogeological system. These areas govern the groundwater discharge over larger scales. Due to the spatial extension of the systems, the reaction on temporal changes is generally slow. Therefore, long term observations are required to capture changes. However, the temporal scales depend on reaction time, which in turn depends on the sediment. Nevertheless, a general characterization of geologic settings is sufficient.

4.3 Thermal impacts of groundwater on surface waters

The studies of Lewandowski et al. (2013, study IV) and Pöschke et al. (2015 a, study V) illustrate that there are at least two different origins for the skin surface temperature pattern of small-to-medium sized lakes in spring: groundwater discharge to the lake and wind induced upwelling of deep water. These studies show that additional information plays an important role in identifying the related process. Lewandowski et al. (2013) used the information about the groundwater discharge pattern, which was found by Meinikmann et al. (2013). Since hydrogeological systems are more or less stable in space and time, it was assumed that the areas where groundwater exfiltrates into lakes are also constant. If further assuming that (1) the lake water temperature is > 4 °C, (2) the air is warmer than the surface water and (3) there is no wind, the groundwater should be detectable as a thin layer floating on the surface water. All these assumptions were met in the mentioned study (IV) and a warm water plume was found by thermal infrared imaging in the area where the highest groundwater discharge occurs (compare Figure 3.5-1). Considering, a plume size of about 1/3 of the lake surface, a plume thickness of 1 cm, a temperature difference between the cold and the warm spot (~ 1°C), and a groundwater temperature of 10 °C, the amount of groundwater can be roughly estimated, which is necessary to increase the surface water temperature with a mixing equation. This results in a volume of about 5000 $m^3\ d^{-1}$, which is in the same magnitude of groundwater exfiltration detected by Meinikmann et al. (2013) (1.3 Mio $m^3\ a^{-1}$).

In contrast, Pöschke et al. (2015 a, study V) used meteorological and lake internal temperature data as additional information. Hence, processes with a higher dynamic and variability than in groundwater systems were considered: meteorological forces and lake internal processes. As a result, the observed temperature pattern could be related to a wind induced deep water upwelling. Furthermore, it was shown by limnophysical parameters (Lake Number, (L_N) Wedderburn Number (W) and Schmidt Stability (S)), that this upwelling events are related to a specific period within a year, during which (1) the lake is slightly stratified and (2) the wind is strong enough to tilt the thermocline.

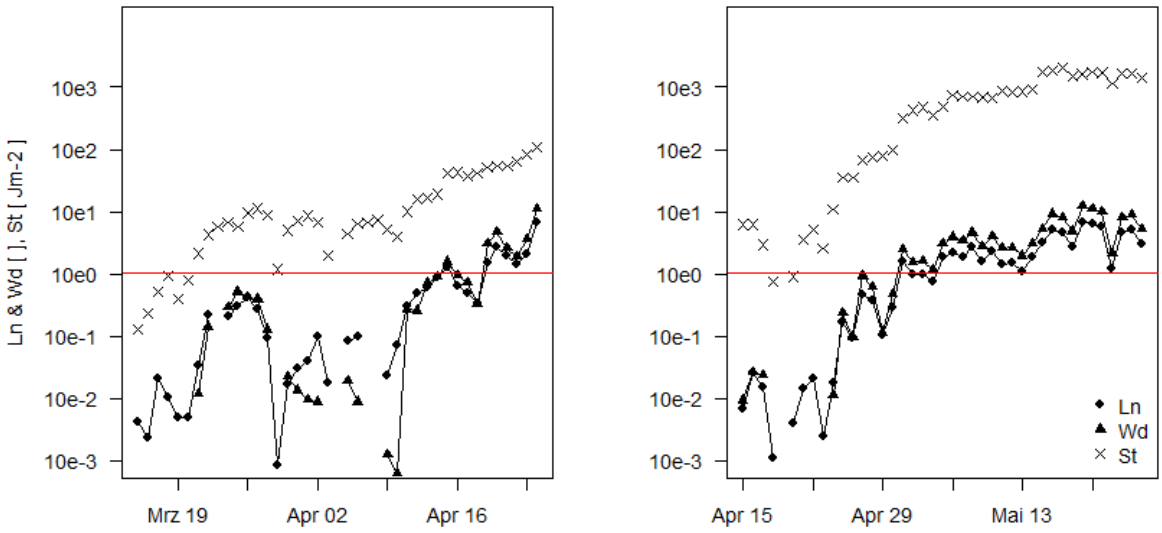

Figure 4.3-1: Time series of the Lake Number (Ln), Wedderburn Number (Wd) and Schmidt Stability (St) of Lake Arendsee in 2012 (left) and 2013 (right). The red line marks the threshold for L and W for upwelling.

A comparison of the limnophysical parameters of the years 2012 (Lewandowski et al., 2013, study IV) and 2013 (Pöschke et al., 2015 a, study V) (Figure 4.3-1) illustrates that also the investigation of 2012 took place during the beginning of the upwelling period identified by Pöschke et al. (2015 a, study V.) (*St* is not zero, L_N and W are smaller than 1). So in general, the conditions of the 22nd March 2012 and the 24th April 2013 are comparable since both events occur at the beginning of the stratification period at Lake Arendsee. However, the main difference between both days is the wind condition. In 2012 there were windless conditions for about 12 hours before the thermal infrared picture was taken (average wind speed 0.8 ms^{-1}) and there was wind from western direction with average wind speeds of 2.6 ms^{-1} 12 hours before the flight in 2013. So the groundwater hypothesis cannot be falsified.

However, there are some hints that weaken the groundwater hypothesis. Imberger and Patterson (1990) stated that upwelling events dominates the temperature distribution within a lake even when there is an overall warming of the lake surface by the solar radiation. The temperature pattern induced by upwelling could last several days (compare Figure 3.6-4). Hence, the observed pattern in 2012 could also be a result of a former upwelling event.

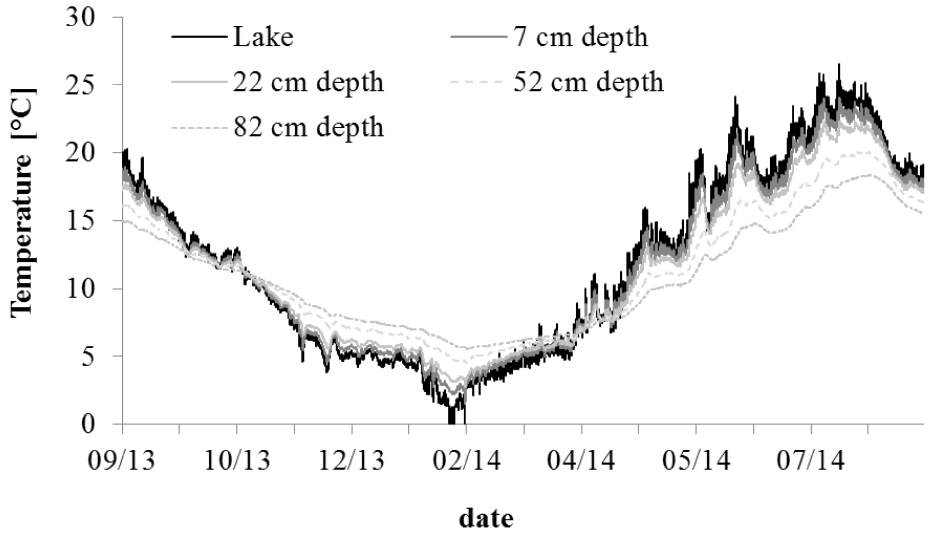

Figure 4.3-2: Temperature time series of different depth in the lake bed sediment of Lake Stechlin. Depth profiles were measured in 2 m distance from the shore.

The study in 2012 assumed that there is a strong groundwater exfiltration. This means that the groundwater entering Lake Arendsee has a temperature of about 10 °C and temperature diffusion only takes place in the water column. However, the smaller the exfiltration rates, the more the surface water impacts the temperature in the sediment. Nützmann et al. (2013) describe this for a lowland river, where the temperature moved opposite to the overall groundwater flow direction. Figure 4.3-2 indicate that this could also be valid for lakes. A temperature depth profile in the lake sediment was measured at Lake Stechlin over a duration of one year. The deepest temperature device was placed 0.82 cm deep in the sediment and shows annual fluctuation of almost 10 °C. Hence, the groundwater that enters the lake already adapted to the lake temperature (average temperature difference between the lake water and 7 cm depth: 0.2 °C ± 0.7 standard deviation). However, this cannot be proven for Lake Arendsee since measurements are missing.

According to the given reasons it has to be mentioned, that the detection of groundwater sources or the thermal impact of groundwater on medium-sized lakes such as Lake Arendsee and Lake Stechlin is biased, due to the dominance of lake internal processes. However, this does not imply that groundwater cannot have an effect on the thermal regime of lakes or that the method of thermal infrared imaging is not applicable in general. The success of the method is assumed to be related to (1) the size and the volume of the lake, (2) the constant and high supply of groundwater discharge, (3) the chemical properties of the groundwater and (4) the weather conditions. According to this, the smaller the lake, the higher the groundwater exfiltration, the lighter the groundwater and during windless conditions it should be possible to detect groundwater exfiltration areas. However, these conditions

seem to be hard to meet in nature. Moreover, the smaller the lake the less probable it is to detect the surface pattern by satellite. Hence, it is required to use higher resolved images which can only be taken via the usage of smaller aircrafts or drones.

A temperature method which is more promising for a broader range of lakes should base on time series which would imply the usage of *in-situ* measurements. Groundwater exfiltration occurs during the whole year in a more or less fixed area. If there is a significant exfiltration, then the groundwater should impact the daily temperature cycle of the surface water by dampening the solar heating. Hence, there should be a significant difference between areas with and without groundwater discharge. This was already pointed out by Beck (2006), who mentioned, that the determination of relative differences is more helpful than absolute temperatures.

5. Summary and Conclusion

The present thesis used two approaches to characterize groundwater flow towards and within surface waters in lowlands: The *hydrogeological approach* was used to contribute to the overall understanding of drivers of groundwater flow on different scales (study I – III). The *limnological/ hydrological approach* was used to establish a remote method to detect groundwater discharge zones in lakes (study IV & V).

Hydrogeological approach. The characterization of subsurface flow in lowlands is difficult since it occurs in unconsolidated sediment which form nested aquifer systems (local, intermediate, and regional). The position of surface water bodies within the landscape cascade (recharge or discharge area) decides about the complexity of groundwater-surface water interactions. Surface waters in recharge areas are dominated by local groundwater flow while surface waters on the lower end of the cascade receive groundwater from all flow systems. The different spatial extent of the flow systems implies that there are different parameters, which dominate the groundwater flow. On the large regional scale the overall geologic and geomorphologic settings as well as the climate conditions are dominant. In contrast, on smaller local scales the sediment distribution, topography, vegetation and short-term water level fluctuations of surface waters are more important. Hence, it is still difficult to identify the subsurface areas which discharge into a surface water body. This makes the estimation of the proportion of groundwater on mass, substance and energy budgets of surface water even more challenging.

Two studies (I & II) belonging to the hydrogeological approach focus only on near-shore subsurface groundwater of a floodplain (local flow). At this scale, the pattern of the sediment composition and chemical compounds in the groundwater is quite important, since sediments which are highly permeable and well connected to the surface water are more relevant for transport of contaminants than sediments which are less permeable. However, near-shore areas are in most cases very heterogeneous due to a sediment distribution originating from fluvial geomorphodynamics. **Hypothesis (1)** assumed that there are linkages between sediment, topography, vegetation and water stage fluctuations of the river in floodplain aquifers. Hence, one parameter can be used to describe the other ones and give insights into the groundwater flow and nutrient distribution on a small scale.

The first small scale hydrogeological study relates water level fluctuations in the aquifer and the surface water body to the hydraulic connectivity of the sediment in the floodplain aquifer (River Spree). This was realized by applying a principle component analysis on a four years long data set of hourly water level measurements. The study could show that the pressure wave induced by surface water fluctuations shows different responses within the aquifer. Good responses can be linked with

high hydraulic connectivity and vice versa. In this way, areas could be identified which are more vulnerable for surface water import into the aquifer.

The second small scale hydrogeological study investigated the nutrient distribution within the local flow system of the same floodplain aquifer. The study hypothesizes that there is a link between the distributions of nutrients and the patterns of sediment, topography and vegetation. Therefore a spatially dense sampling grid of groundwater was combined with a highly resolved digital elevation model and ground penetrating radar. As a result, the study could show that information of small-scale topography could be used to estimate the near-surface groundwater composition in a floodplain aquifer. A difference of 0.5 m in surface elevation results in a different water availabilities for plants, and therefore in different densities of vegetation. As a consequence, different amounts of easily degradable organic matter are available for biological degradation below swales and ridges. Hence, higher amounts of nutrients were found below swales than below ridges.

Both studies illustrate that there are linkages between the different small scale parameters, whereas the detection of these linkages requires data in a sufficient high temporal and spatial resolution. For instance, a spatial data resolution of about 1m is necessary to describe heterogeneities in floodplains. However, findings of the presented studies also imply that only one parameter – water stage fluctuations or topography- is required to get a rough idea of hydraulic connectivity's or nutrient distributions within the aquifer. However, the presented approaches are valuable for general pattern detection, but further investigations are needed to clarify to what extent the detected areas are relevant for nutrient import into surface water. Therefore, the results of both studies should be combined in modeling study, which consider groundwater flow and nutrient transport. The identified hydraulic connectivity (study I) could be used for calibration of hydraulic conductivity. Geochemical transport modelling can clarify to what extent topography dependent nutrient distribution (study II) contributes to nutrient import into the River Spree. However, groundwater flow modeling in floodplains is a big challenge due to the fact that classical groundwater models are not able to reproduce the observed groundwater level fluctuations which are linked to adjacent surface water fluctuations. These fluctuations are not related to water fluxes, rather to pressure wave propagating from the surface water fluctuation towards the groundwater. This is not reflected in the basic equation (Darcy) of groundwater models. Hence, research is need to clarify if and how these pressure waves impacting the groundwater flow in areas close to surface water.

On a large scale, a simple 2D numerical modeling approach tests the **hypothesis (2)** that a regional flow component needs to be considered in the local flow system of the groundwater catchment of Lake Stechlin. The study shows that a part of the groundwater in the originally assigned subsurface catchment leaks into a deeper aquifer. Beside the reduction of the water volume which enters the lake, leakage also increases the length of the groundwater flow path. This is important concerning

groundwater travel times and the time available for chemical reactions. Hence, leakage of groundwater needs to be considered when aligning a subsurface catchment in lowland groundwater recharge areas. However, the study (III) gives a first insight that aquifer leakage needs to be considered for the groundwater flow towards a lake. Further investigations are needed for an exact quantification of the leakage (pumping test), determination of flow paths (tracer tests) or mapping the distribution of the geological layers (geophysics) to improve the validity of the model.

Overall for investigation of groundwater discharge in lowland areas to surface waters it is recommended to start with large scale investigations to estimate the areas contributing to the groundwater discharge and get some first ideas about the sediment distribution. Therefore, groundwater modeling and multi-variate statistics of water levels are adequate tools to limit the areas of interest. Afterwards, small scale investigations are required to characterize the specific areas concerning their flow behavior and substance transport. In most cases, only one of these both spatial scales was used. However, both scales are necessary to understand the nested hydrogeology of lowland areas.

The limnological approach tests **the hypothesis (3)** that groundwater exfiltration areas are detectable as temperature anomaly on the lake surface when warm groundwater is less dense than cold lake water. Therefore, two studies were conducted after spring circulation. Thermal infrared images (TIR) and *in situ* temperature measurements were taken and compared with information of groundwater discharge and lake-internal processes. The studies showed that the detection of groundwater discharge at lake surfaces is very difficult or even impossible, especially if the annual volume of groundwater is much smaller than the total volume of the lake. In the presented cases, lake internal processes induced by wind dominate the temperature pattern of the lake surface.

It could be stated that the usage of integrative measures such as temperature requires a careful elaboration of all processes producing the observed patterns. Therefore, it is recommended to study the heat exchange in lowland areas more closely. To understand the drivers of heat fluxes in a lowland catchment a study should be conducted which measures the following temperatures: groundwater in different depth and distance to the shore of the surface water, depth profiles within the sediment of the surface water at different locations, surface water depth profiles and, the skin of surface water at different locations. Measurements are complete with meteorological data (air temperature, wind speed, wind direction, precipitation, and radiation). The measurements should be done for at least one year to capture temperature changes and the temporal delay of the heat signal within the different water bodies. The data can be used to prove the assumption, that groundwater temperatures are constant throughout the year. Furthermore, it is possible to set up a heat model to quantify the thermal interactions in detail. For instance, the conditions can be elaborated which are necessary to produce a significant impact of groundwater on surface water temperatures.

In summary, the main challenge in all studies was the accuracy of the measurements and the modeling. Lowland areas are generally characterized by low hydraulic gradients which imply e.g. slow flow velocity and slow changes of hydraulic heads. This requires sufficient accurate measurement devices to detect temporal changes on a centimeter or even smaller scale. Furthermore, this implies for transport processes, that the advective component is generally small and diffusion may play a role, as it was shown for temperature. Therefore, innovative measurement methods and modelling approaches are required to detect the groundwater flow towards and within surface waters of low lands. For instance, a promising basis to develop methods to determine the sediment and geological characteristics of aquifers could be time series of water level observation, since there is a close connection between sediment and hydraulic gradients; low permeable sediments tend to have higher gradients and vice versa. Therefore, different weather conditions or surface water level fluctuations, which generate different pressure gradients in the subsurface, could be used as a tracer to detect different sediment distributions. Time series of water level observations are also required to detect the dynamics and interactions of regional and local flow systems, which is very important to estimate the subsurface area contributing to surface water.

References

Alla-aho, P., Rossi, P.M., Kløve, B. 2015. Interaction of esker groundwater with headwater lakes and streams. Journal of Hydrology. 500. 144 – 156.

Amoros, C., Bornette, G. 2002. Connectivity and biocomplexity in waterbodies of riverine floodplains. Freshwater Biology. 47. 761 - 776.

Anderson, M.P., Munter, J.A. 1981. Seasonal Reversals of Groundwater Flow Around Lakes and the Relevance to Stagnation Points and Lake Budgets. Water Resources Research. 17. 1139 – 1150.

Anderson, J. M., Duck, R. W., & McManus, J. 1995. Thermal radiometry — A rapid means of determining surface–water temperature-variations in lakes and reservoirs. Journal of Hydrology.173. 131 - 144.

Anderson, M.P. 2005. Heat as a Groundwater Tracer. Ground Water. 43. 951 – 968.

Anibas, C., Fleckenstein, J.H., Volze, N., Buis, K., Verhoeven, R., Meire, P., Batelaan, O. 2009. Transient or steady-state? Using vertical temperature profiles to quantify groundwater–surface water exchange. Hydrological Processes. 23. 2165 - 2177.

Annan PA. 2006. GPR methods for hydrogeological studies. In Water Science and Technology Library: Hydrogeophysics, Rubin Y, Hubbard SS (ed.). Springer: 185–213.

Barenblatt, G. I. 2003. Scaling. Cambridge University Press

Bear, J. 1988. Dynamics of Fluids and Porous Media. Dover Publications.

Beck, M.W. 2006. Potential for Satellite Remote Sensing of Ground Water. Ground Water. 44. 306 – 318.

Bernhardt, E.S., Sudduth, E.B., Palmer, M.A., Allan, J.D., Meyer, J.L., Alexander, G., Follastad-Shah, J., Hassett, B., Jenkinson, R., Lave, R., Rumps, J., Pagano, L. 2007. Restoring rivers one reach at a time: results from a survey of U.S. river restoration practitioners. Restoration Ecology. 1. 482 - 493.

Bernhardt, J., Kirillin G. 2013. Seasonal pattern of rotation-affected internal seiches in a small temperate lake. Limnology and Oceanography. 58. 1344-1360.

Binley, A., Ullah, S., Heathwaite, A.L., Heppell, C., Byrne, P., Lansdown, K., Trimmer, M., Zhang, H.2013. Revealing the spatial variability of water fluxes at the groundwater-surface water interface. Water Resources Research. 49. 3978 - 3992.

Bjerg, P.L., Christensen, T.H. 1992. Spatial and temporal small-scale variation in groundwater quality of a shallow sandy aquifer. Journal of Hydrology. 131. 133 – 149.

Blair, S.E., Safreed, C.M., Stasny, E.A. 1991. A Monte Carlo approach for determining travel time-related capture zones of wells using convex hulls as confidence regions. Ground Water. 29. 849 – 855.

Blöschl, G. 2011. Scaling and Regionalziation in Hydrology. In: Wilderer, P. (ed.) Treatise on Water Science, vol. 2, Academic Press. 519 – 535.

Bocaniov, S. A., C. Ullmann, K. Rinke, K. G. Lamb, Boehrer, B. 2014. Internal waves and mixing in a stratified reservoir: Insights from three-dimensional modeling. Limnologica. 49. 52 - 67

Boehrer, B., Herzsprung, P., Schultze, M., Millero, F. J. 2010. Calculating density of water in geochemical lake stratification models. Limnology and Oceanography - Methods. 8. 567 - 574.

Böttcher, J., Strebel, O. 1988a. Spatial variability of groundwater solute concentrations at the water table under arable land and coniferous forest. Part 1: Methods of quantifying spatial variability (geostatistics, time series analysis. Fourier transform smoothing. Zeitschrift für Pflanzenernährung und Bodenkunde. 151. 185 - 190.

Böttcher J., Strebel O. 1988b. Spatial variability of groundwater solute concentrations at the water table under arable land and coniferous forest. Part 2: Field data for arable land and statistical analysis. Zeitschrift für Pflanzenernährung und Bodenkunde. 151. 191 - 195.

Böttcher, J., Strebel, O. 1988c. Spatial variability of groundwater solute concentrations at the water table under arable land and coniferous forest. Part 3: Field data for a coniferous forest and statistical analysis. Zeitschrift für Pflanzenernährung und Bodenkunde. 151. 197 - 203.

Boulton, A.J. 2007. Hyporheic rehabilitation in rivers: restoring vertical connectivity. Freshwater Biology. 52. 632–650.

Boulton, A.J., Datry, T., Kasahara, T., Mutz, M., Stanford, J.A. 2010. Ecology and management of the hyporheic zone: stream-groundwater interactions of running waters and their floodplains. Journal of the North American Benthological Society. 29. 26 – 40.

Bridge, J.S. 2003. Rivers and Floodplains: Forms, Processes, and Sedimentary Record. Wiley.

Bruland, K. W., E. L. Rue, J. S. Geoffrey, DiTullio, G. R. 2005. Iron, macronutrientsand diatom blooms in Peru upwelling regime: brown and blue waters of Peru. Marine Chemestry. 93. 81 - 103.

Brunke, M., Gonser, T. 1997. The ecological significance of exchange processes between rivers and groundwater. Freshwater Biology. 37. 1 – 33.

Burt, T.P., Matchett, L.S., Goulding, K.W.T., Webster, C.P., Haycock, N.E. 1999. Denitrification in riparian buffer zones: the role of floodplain hydrology. Journal of Hydrological Processes. 13. 1451 - 1463.

Burt, T.P., Bates, P.D., Stewart, M.D., Claxton, A.J., Anderson, M.G., Price, D.A. 2002. Water table fluctuations within the floodplain of the River Severn,England. Journal of Hydrology. 262. 1 - 20.

Cardiff, M., Barrash, W. 2011. 3-D transient hydraulic tomography in unconfinedaquifers with fast drainage response. Water Resources. Research. 47. W12518.

Charlton, R. 2008. Fundamentals of fluvial geomorphology. Routledge.

Chen, C. T. A., Millero, F. J.. 1986. Precise thermodynamic properties for natural waters covering only limnological range. Limnology and Oceanography. 31. 657 - 662.

Coman, M. A., Wells, M. G. 2012. Temperature variability in the nearshore benthic boundary layer of Lake Opongo is due to wind-driven upwelling events. Canadian Journal of Fisheries and Aquatic Science. 69. 282 - 296.

Cook, J. M., Edmunds,W. M., Robins, N. S. 1991. Groundwater contribution to an acid upland lake (Loch Fleet, Scotland) and the possibilities for amelioration. Journal of Hydrology. 125. 111 -128.

Courtwright, J., Findlay, S.E.G. 2011. Effects of microtopography on hydrology, physicochemistry, and vegetation in a tidal swamp of the Hudson River. Wetlands. 31. 239 - 249.

Cox, M.H., Su, G.W., Constantz, J. 2007. Heat, chloride, and specific conductance asgroundwater tracers near streams. Ground Water . 45. 187 – 195.

Cressie, N. 1991. Statistics for spatial data, 1st ed. Wiley.

Crowe, A.S., Schwartz, F.W. 1981. Simulation of lake-watershed systems: I Description and sensitivity analysis of the model. Journal of Hydrology. 52. 71 – 105.

Danielescu, S., MacQuarrie, K.T.B., Faux, R.N. 2009. The integration of thermal infrared imaging, discharge measurements and numerical simulation to quantify the relative cntributions of freshwater inflows to small estuaries in Atlantic Canada. Hydrological Processes. 23. 2847 – 2859.

Davis, J.L., Annan, P.A. 1989. Ground penetrating radar for high-resolution mapping of soil and rock stratigraphy. Geophyisical Prospecting. 37. 531 - 551.

Davis, S.N., Thompson, G.M., Bentley, H.W., Stiles, G. 1980. Ground-Water tracers – a short review. Ground Water. 18. 14 -22.

Deardorff, J. W. 1970. Convective velocity and temperature scales for the unstable planetary boundary layer and for Rayleigh convection. Journal of the Atmospheric Sciences. 27. 1211 - 1213.

DESTATIS - Statistisches Bundesamt. 2014. Land- und Forstwirtschaft, Fischerei. Bodenfläche nach Art der tatsächlichen Nutzung. Fachserie 3 Reihe 5.1.

Deutscher Wetterdienst. 2014. Climate Data Center ftp://ftp-cdc.dwd.de/pub/CDC/

Diersch, H.-J. G. 2014. FEFLOW Finite Element Modeling of Flow, Mass and Heat Transport in Porous and Fractured Media. Springer.

Dietz, S., Lessmann, D., Boehrer, B. 2012. Contribution of solutes to density stratification in a meromictic lake (Waldsee/Germany). Mine Water and the Environment. 31. 129 - 137.

Dincer, T. 1968. The use of oxygen 18 and deuterium concentrations in the Water Balance of Lakes. Water Resources Research. 4. 1289 – 1306.

Driescher, E. 1999. Development of the landscape in the catchment of the lower River Spree. Berichte des IGB. 9. 25 - 42.

Driescher, E., Gelbrecht, J. 1993. Assessing the diffuse phosphorus input from subsurface to surface waters in the catchment area of the lower River Spree (Germany). Water Science & Technology 28. 337 - 347.

Driescher, E., Gelbrecht, J. 1999. Investigations of groundwater in the floodplain of the lower River Spree. Berichte des IGB. 9. 61 - 102.

Duarte, T. K., Hemond, H. F., Frankel, D., Frankel, S. 2006. Assessment of submarine groundwater discharge by handheld aerial infrared imagery: Case study of Kaloko fishpond and bay, Hawaii. Limnology and Oceanography: Methods. 4. 227 - 236.

Einsele, G., 1975. Eichung von Grundwasser-Ganglinien zur Bestimmung der Grundwasserneubildung und des Grundwasserabflusses. Zeitschrift der deutschen Geologischen Gesellschaft. 126. 293 – 315.

Engelhardt, C., Kirillin G. 2014. Criteria for the onset and breakup of summer lake stratification based on routine temperature measurements, Fundmentals of Applied Limnolology. 183. 183 - 194.

Environmental Protection Agency (EPA). 2007. National Water Quality Inventory. Report to Congress – 2002 Reporting Cycle. United States Environmental Protection Agency, Office of Water.

ESRI (Environmental Systems Resource Institute). 2012. ArcMap 10.1. ESRI, Redlands.

Eriksson, E., Khunakasem, V. 1969. Chloride concentration in groundwater, recharge rate and rate of deposition of chloride in the Israel Coastal Plain. Journal of Hydrology. 7. 178 – 197.

European Commission. 2000. Directive 2000/60/EC of the European Parliament and of the Council establishing a framework for Community action in the field of water policy. European Community. vol. L327, pp. 1–72.

European Environment Agency (EEA). 2005. Source apportionment of nitrogen and phosphorus inputs into the aquatic environment. EEA Report 07/2005.

Falkenmark, M. Allard, B. 1991. Water Quality Genesis and Disturbances of Natural Freshwaters. In: Hutzinger (ed.). The Handbook of Enviromental Chemistry 5, Part A: Water Pollution. Springer. pp. 45 -78.

Feierabend, M., Koschel, R. 2011. Faszination Stechlin. Bebra Verlag.

Ferris, J.G. 1951. Cyclic fluctuations of water level as a basis for determining aquifer transmissibility. U.S. Geological Survey. USGS Unnumbered Series.

Fleckenstein, J. H., Neumann, C., Volze, N., Beer. J. 2009. Spatio-temporal patterns of groundwater lake exchange in an acid mine lake. Grundwasser. 14. 207 – 217.

Fleckenstein, J. H., Krause, S., Hannah, D. M., Boano, F. 2010. Groundwater-surface water interactions: New methods and models to improve understanding of processes and dynamics. Advances in Water Resources. 33. 1291 – 1295.

Forrest, A., B. E. Laval, R. Pieters, Lim, D. S. S. 2008. Convectively driven transport in temperate lakes. Limnology and Oceanography. 53 (5 part 2), 2321-2332.

Frapporti, G., Hoogendoorn, J.H., Vriend, S.P. 1995. Detailed hydrochemical studies as a usefull extension of national groundwater monitoring networks. Ground Water. 33. 817 – 828.

Freeze, R.A., Cherry, J.A. 1979. Groundwater. 5th ed. Prentice Hall.

Frind, E.O., Muhammad, D.S., Molson, J.W. 2002. Delination of three-dimensional well-capture zones for complex mulit-aquifer systems. Ground Water. 60. 586 - 598.

Garcia-Solsona, E., Garcia-Orellana, J., Masque, P., Rodellas, V., Mejias, M., Ballesteros, B., Dominguez, J.A. 2010. Groundwater and nutrient discharge through karstic coastal springs (Castelló, Spain). Biogeosciences. 7. 2625 – 2638.

Gessner, M.O., Hinkelmann, R., Nützmann, G., Jekel, M., Singer, G., Lewandowski, J., Nehls, T., Barjenbruch, M. 2014. Urban Water Interfaces. Journal of Hydrology. 514. 226 – 232.

Gill, A. E. 1982. Atmosphere-ocean dynamics. Academic press.

Ginzel, G., Kaboth, U. 1999. Hydrogeologisches Gutachten NSG Stechlin. unpublished.

Glugla, G., Jankiewicz, P., Rachimow, C., Lojek, K., Richter, H., Fürtig, G., Krahe, P. 2003 BFG Bundestanstalt für Gewässerkunke BAGLUVA – Wasserhaushaltsverfahren zur Berechnung vieljähriger Mittelwerte der tatsächlichen Verdunstung und des Gesamtabflusses – BfG – 1342.

Gorham, E., Boyce, F. M. 1989. Influence of lake surface area and depth upon thermalstratification and the depth of the summer thermocline, Journal of Great Lakes Research. 15. 233 - 245.

Graham, W.D. 2009. An in expensive device for multiple depth sampling of groundwater quality in cohesionless aquifers (cir 943). University of Florida Institute of Food and Agricultural Science: Gainesville. 1- 7. http://edis.ifas.ufl.edu/ae105

Grimm, N.B., Gergel, S.E., McDowell, W.H., Boyer, E.W., Dent, C.L., et al. 2003. Merging aquatic and terrestrial perspectives of nutrient biogeochemistry. Oecologia 137. 485 - 501.

Haffner, G. D., M. L. Yallop, P. D. N. Hebert, Griffiths, M. 1984. Ecological significance of upwelling events in Lake Ontario. Journal of Great Lakes Research. 10. 28 – 37.

Haitjema, H.M. 2015. The cost of modeling. Ground Water. 53. 179.

Hamblin, P. F., H. A. Bootsma, Hecky, R. E. 2003. Modelling nutrient upwelling in Lake Malawi/ Nyasa. Journal of Great Lakes Research. 29. 34 - 47.

Harvey, F. E., Rudolph, D. L., Frape, S. K. 2000. Estimating ground water flux into large lakes: Application in the Hamilton Harbor, western Lake Ontario. Ground Water. 38. 550 - 565.

Hemker, C.J. 1999. Transient well flow in layered aquifer systems: the uniform well-face drawdown solution. Journal of Hydrology. 225. 19 – 44.

Hester, E.T., Gooseff, M.N. 2010. Moving beyond the banks: hyporheic restoration is fundamental to restoring ecological services and functions of streams. Environmental Science and Technology. 44. 1521 - 1525.

Hickin, E.J. 1974. The development of meanders in natural river channels. American Journal of Science. 274. 414 - 442.

Hicks, B. B. 1972. Some evaluations of drag and bulk transfer coefficients over water bodies of different sizes. Boundary Layer Meteorology. 3. 201 – 213.

Hiemstra, P. H., E. J. Pebesma, C .J. W. Twenhofel, Heuvelink, G. M. B. 2008. Real- time automatic interpolation of ambient gamma dose rates from the Dutch Radioactivity Monitoring Network. Computers and Geosciences. 35. 1711 – 1721.

Hill, M.P., Tiedemann, C.R. 2007. Effective groundwater model calibration, with analysis of sensitivities, predictions and uncertainty. Wiley.

Hofmann, H., Knöller, K., Lessmann, D. 2008. Mining lakes as groundwater-dominated hydrological systems: assessment of the water balance of Mining Lake Plessa 117 (Lusatia, Germany) using stable isotopes. Hydrological Processes. 22. 4620 – 4627.

Hölting, B., Coldewey, W.G. 2009. Hydrogeologie. 7th ed. Spektrum

Holzbecher, E. 2001. The dynamics of subsurface water divides – watersheds of Lake Stechlin and neighbouring lakes. Hydrological Processes. 15. 2297 – 2304.

Holzbecher, E., Nützmann, G. 2000. Influence of the subsurface watershed on eutrophication – Lake Stechlin case study: Ecological Engineering. 16. 31 – 38.

Hook, S. J., Prata, F. J., Alley, R. E., Abtahi, A., Richards, R. C., Schladow, S. G., et al. 2003. Retrieval of lake bulk and skin temperatures using Along-Track Scanning Radiometer (ATSR-2) data: A case study using Lake Tahoe, California. Journal of Atmospheric and Oceanic Technology. 20 534 - 548.

Hunt, R.J., Steuer, J.J., Mansor, M.T.C., Bullen, T.D. 2001. Delineating a recharge area for a spring using numerical modeling, Monte Carlo techniques, and geochemical investigation. Ground Water. 39. 702 – 712.

Hupfer, M., Nixdorf, B. 2011. Zustand und Entwicklung von Seen in Berlin und Brandenburg. Materialien der International Arbeitsgruppen IAG Globaler Wandel – Regional Entwicklung. Diskussionspapier 11.

Hupfer, M., Pöthig, R., Brüggemann, R., Geller, W. 2000. Mechanical resuspension of autochthonous calcite (Seekreide) failed to control internal phosphorus cycle in a eutrophic lake. Water Research. 34. 859 - 867.

Hutchinson, G.E. 1957. A treatise on limnology. Volume 1. Geography, physics and chemistry. Wiley.

Hyndman, D., Tronicke, J. 2006. Hydrophyiscal case studies at the local scale: the saturated zone. In Water Science and Technology Library: Hydrogeophysics, Rubin Y, Hubbard SS (ed.). Springer. 391–412.

Imberger, J., Patterson, J.C. 1990. Physical Limnology. Advances in Applied Mechanics. 27. 303 – 475.

Jiang, Z., Mariethoz, G., Taulis, M., Cox, M. 2013. Determination of vertical hydraulic conductivity of aquitards in a multilayer leaky system using water-level signals in adjacent aquifers. Journal of Hydrology. 500. 170 – 182

Johnson, A. G., Glenn, C. R., Burnett,W. C., Peterson, R. N., Lucey, P. G. 2008. Aerial infrared imaging reveals large nutrient-rich groundwater inputs to the ocean. Geophysical Research Letters. 35. L15606.

Jordan, H., Weder, H.-J (eds). 1988. Hydrogeologie. 1st ed. VEB Deutscher Verlag für Grundstoffindustrie.

Kaboth, U., Rechlin, B., Ginzel, G. 2008. Are our lakes endangered by geogene salinisation? Hydrochemical-genetical invesitgations of conditions for alimentation of the lakes in the natural park Stechlin. Brandenburgisch geowissenschaftliche Beiträge. 15. 69 – 79.

Kaiser, K., Heinrich, I., Heine, I., Natkhin, M., Dannowski, R., Lischeid, G., Scheider, T., Henkel, J., Küster, M., Heussner, K.-U., Bens, O., Chmieleski, J. 2015. Multi-decadal lake-level dynamics in north-eastern Germany as derived by a combination of gauging, proxy-data and modelling. Journal of Hydrology. 529. 584 – 599.

Kalbus, E., Reinstorf, F., Schirmer, M.. 2006. Measuring methods for groundwater - surface water interactions: a review. Hydrololgy and Earth System Sciences. 10. 873 – 887.

Kalbus, E., Schmidt, C., Molson, J.W., Reinstorf, F., Schirmer, M. 2009. Influence of aquifer and streambed heterogeneity on the distribution of groundwater discharge. Hydrololgy and Earth System Sciences. 13. 69 - 77.

Kasahara, T., Datry, T., Mutz, M., Boulton, A.J. 2009. Treating causes not symptoms: restoration of surface-groundwater interactions in rivers. Marine and Freshwater Research. 60. 976 - 981.

Käss, W. 2004. Geohydrologische Markierungstechnik. 2nd ed. Schweizerbart.

Kidmose, J., Engesgaard, P., Nilsson, B., Laier, T., Looms, M.C. 2011. Spatial distribution of seepage at a flow-through lake: Lake Hampen, Western Denmark. Vadose Zone. 10. 110 – 124.

Kirillin, G., Engelhardt, C., Golosov, S. 2009. Transient convection in upper lake sediments produced by intemal seiching. Geophysisical Research Letters. 36. L18601.

Kirillin, G., M. Leppäranta, A. Terzhevik, N. Granin, J. Bernhardt, C. Engelhardt, T. Efremova, S. Golosov, N. Palshin, P. Sherstyankin, G. Zdorovennova, Zdorovennov, R. 2012. Physics of seasonally ice-covered lakes: a review. Aquatic Sciences. 74. 659 - 682.

Kirillin, G., W. Philipp, C. Engelhardt, Nützmann, G. 2013a. Net groundwater inflow in an enclosed lake: from synoptic variations to climatic projections, Hydrological Processes 27. 347 - 359.

Kirillin,G., T. Shatwell, Kasprzak, P. 2013b. Consequences of thermal pollution from a nuclear plant on lake temperature and mixing regime. Journal of Hydrology. 496. 47 - 56.

Kishel, H. F., Gerla, P. J. 2002. Characteristics of preferential flow and groundwater discharge to Shingobee Lake, Minnesota, USA. Hydrological Processes. 16. 1921 - 1934.

Kluge, T., Ilmberger, J., von Rohden, C., Aeschbach-Hertig, W. 2007. Tracing and quantifying groundwater inflow into lakes using a simple method for radon-222 analysis. Hydrology and Earth System Sciences. 11. 1621 – 1631.

Kondolf, G.M. 1995. Five elements for effective evaluation of stream restoration. Restoration Ecology. 3. 133 - 136.

Kondolf, G., Micheli, E. 1995. Evaluating stream restoration projects. Environmental Management. 19. 1 - 15.

Kondolf, G.M., Boulton, A.J., O'Daniel, S., Poole, G.C., Rahel, F. J., Stanley, E.H., Wohl, E., Bång, A., Carlstrom, J., Cristoni, C., Huber, H., Koljonen, S., Louhi, P., Nakamura, K. 2006. Process-Based Ecological River Restoration: Visualizing Three-Dimensional Connectivity and Dynamic Vectors to Recover Lost Linkages, Ecology and Society. 11.

Kondolf, G.M., Anderson, S., Lave, R., Pagano, L., Merenlender, A., Bernhardt, E.S. 2007. Two decades of river restoration in California: what can we learn? Restoration Ecology. 15. 516 - 523.

Köppen, W. 1936. Das geographische System der Klimate – Handbuch der Klimatologie. Verlag der Gebrüder Borntraeger.

Krabenhoft, D.P., Bowser, C.J., Kendall, C., Gat, J.R. 1994. Use of O-18 and deuterium to assess the hydrology of groundwater-lake systems. Environmental Chemistry of Lakes and Reservoirs. 237. 67 – 90.

Kratz, T.K., Webster, K., Bowser, C. J., Magnuson, J.J., Bowser, C.J. 1997. The influence of landscape position on lakes in northern Wisconsin. Freshwater Biology. 37. 209 – 217.

Krause, S., Blume, T. 2013. Impact of seasonal variability and monitoring mode on the adequacy of fiber-optic distributed temperature sensing at aquifer-river interfaces. Water Resources Research. 49. 2408 - 2423.

Krause, S., Blume, T., Cassidy, N.J. 2012. Investigating patterns and controls of groundwater up-welling in a lowland river by combining Fibre-optic Distributed Temperature Sensing with observations of vertical hydraulic gradients. Hydrology and Earth System Sciences. 16. 1775 - 1792.

Krause, S., Hannah, D.M., Fleckenstein, J.H., Heppell, C.M., Kaeser, D., Pickup, R., Pinay, G., Robertson, A.L., Wood, P.J. 2011. Inter-disciplinary perspectives on processes in the hyporheic zone. Ecohydrology. 4. 481- 499.

Krause, S., Boano, F., Cuthbert, M.O., Fleckenstein, J. H., Lewandowski, J. 2014. Understanding process dynamics at aquifer-surface water interfaces: An introduction to the special section on new modeling approaches and novel experimental technologies. Water Resources Research. 50. 1847 – 1855.

Krey, L. 1985. Morphology and morphogenesis of the Lake Stechlin area, in: Lake Stechlin: A temperate oligotrophic lake, edited by Casper, S. J., pp. 7-11, Dr. W. Junk Publishers. Dordrecht.

Laskov, C., Herzog, C., Lewandowski, J., Hupfer, M. 2007. Miniaturized photometrical methods for the rapid analysis of phosphate, ammonium, ferrous iron, and sulfate in pore water of freshwater sediments. Limnology and Oceanography – Methods. 4. 63 - 71

Lee, K. 1969. Infrared exploration for shoreline springs: A contribution to the hydrogeology of Mono Basin. (Doctoral dissertation). California: Stanford University.

Lee, D.R. 1977. A device for measuring seepage fluxes in lakes and estuaries. Limnology and Oceanography. 22. 140 – 147.

Lehr, C., Pöschke, F., Lewandowski, J., Lischeid, G. 2015. A novel method to evaluate the effect of a stream restoration on the spatial pattern of hydraulic connection of stream and groundwater. 527. 394 - 401.

Leineweber, R., H.-J. Beug, J. Christiansen, H.-J. Döhle, O. Hartman, M. Hellmund, B. W.Scharf, Schönberg,G. 2009. Zur Entwicklung des Arendsees in der Altmark, Sachsen- Anhalt. NAU. 15. 9 – 11.

Lewandowski, J., Lischeid, G., Nützmann, G. 2009. Drivers of water level fluctuations and hydrological exchange between groundwater and surface water at the lowland River Spree (Germany): field study and statistical analysis. Hydrological Processes. 23. 2117 – 2128.

Lewandowski, J., Nützmann, G. 2010. Nutrient retention and release in a floodplain´s aquifer and in the hyporheic zone of a lowland river. Ecological Engineering. 36. 1156 – 1166.

Lewandowski, J., Nützmann, G. 2011. Geochemical processes in the aquifer of a floodplain before and after re-opening of a meander. In Proceedings of Symposiom H01 held during IUGG 2011 in Melbourne, Australia. IAHS Publ. 345.

Lewandowski, J., Angermann, L., Nützmann, G., Fleckenstein, J.H. 2011. A heat pulse technique for the determination of small-scale flow directions and flow velocities in the streambed of sand-bed streams. Hydrological Processes. 25. 3244 - 3255.

Lewandowski, J., K. Meinikmann, T. Ruhtz, F. Pöschke, Kirillin, G. 2013. Localization of lacustrine groundwater discharge (LGD) by airborne measurement of thermal infrared radiation, Remote Sensing of the Environment. 138. 119–125.

Lischeid, G. 2008. Combining Hydrometric and Hydrochemical data sets for investigating runoff generation processes: tautologies, inconsistencies and possible explanations. Geography Compass. 2. 255 – 280.

Lischeid, G., Natkhin, M., Steidl, J., Dietrich, O. , Dannowski, R., Merz, C. 2010. Assessing coupling between lakes and layered aquifers in a complex Pleistocene landscape based on water level dynamics. Advances in Water Resources. 33 1331 – 1339.

Lischeid, G., Natkhin, M. 2011. The Potential of Land-Use change to Mitigate Water Scarcity in Northeast Germany – a Review. Die Erde. 142. 97 – 113.

Lobeck, A.K. 1939. Geomorphology. McGraw-Hill Book Company. New York.

Longuevergne, L., Florsch, N., and Elsass, P. 2007: Extracting coherent regional information from local measurements with Karhunen-Loève transform: Case study of an alluvial aquifer (Rhine valley, France and Germany), Water Resoures Research vol. 43. WO4430.

LUGV- Landesamt für Umwelt, Gesundheit und Verbraucherschutz Brandenburg. 2009. Umweltdaten Brandenburg 2008/2009.

LUGV - Landesamt für Umwelt, Gesundheit und Verbraucherschutz Brandenburg. 2012. https://luis-bb.brandenburg.de/. Requested: 15.5.2013

Magri, F., Inbar, N., Siebert, C., Rosenthal, E., Guttman, J., Möller, P. 2015. Transient simulations of large-scale hydrogeological processes causing temperature and salinity anomalies in the Tiberias Basin. Journal of Hydrology. 520. 342 – 355.

Malard, F., Tockner, K., Dole-Olivier, M.-J., Ward, J.V. 2002. A landscape perspective of surface–subsurface hydrological exchanges in river corridors. Freshwater Biology. 47. 621 - 640.

Malberg, H. 1997. Meteorologie und Klimatologie – Eine Einführung. 4th ed. Springer.

McBride, M.S., Pfannkuch, H.O. 1975. The distribution of seepage within lakes. Journal Research, U.S. geological survey. 3. 505 – 512.

McDonnell, J.J., Beven, K. 2014. Debates on Water Resources: The future of hydrological sciences: A (common) path forward? A call to action aimed at understanding velocities, celerities and residence time distributions of the head water hydrograph. Water Resources Research.

MacIntyre, S., K. M. Flynn, R. Jellison, Romero, J.R. 1999. Boundary mixing and nutrient fluxes in Mono Lake, California. Limnology and Oceanography. 44. 512 – 529.

MacIntyre, S., Jellison, R. 2001. Nutrient fluxes from upwelling and enhanced turbulence at the top of the pycnocline in Mono Lake, CA. Hydrobiologia. 466. 13 - 29.

Meinikmann, K., Hupfer, M., Lewandowski, J. 2015. Phosphorus in groundwater discharge – A potential source for lake eutrophication. Journal of Hydrology. 524. 214 – 226.

Meinikmann, K., Lewandowski, J., Nützmann, G. 2013. Lacustrine groundwater discharge: Combined determination of volumes and spatial patterns. Journal of Hydrology. 502. 2020 – 211.

Menició, A., Folch, A. and Mas-Pls, J. 2012. Identifying key parameters to differentiate groundwater flow systems using multifactorial analysis. Journal of Hydrology. 472-473. 301-313.

Merz, C., Pekdeger, A. 2011. Anthropogenic Changes in the Landscape Hydrology of the Berlin-Brandenburg Region. Die Erde. 142. 21 – 39.

Messié, M., Chavez, F. P. 2015. Seasonal regulation of primary production in eastern boundary upwelling systems. Progress in Oceanography. 134. 1 – 18.

Mironov, D., A.Terzhevik, G. Kirillin, T. Jonas, 691 J. Malm, Farmer, D. 2002. Radiatively driven convection in ice-covered lakes: Observations, scaling, and a mixed layer model. Journal of Geophysical Research – Oceans. 1978–2012. 107 (C4).

Miyakoshi, A., Uchida, Y., Sakura, Y., Hayashi, T. 2003. Distribution of subsurface temperature in the Kanto Plain, Japan; estimation of regional groundwater flow system and surface warming. Physics and Chemistry of the Earth. 467 – 475.

Monin, A. S., Obukhov, A.M. 1954. Basic laws of turbulent mixing in the surface layer of the atmosphere. Trudy Akademii Nauk SSSR Geophizicheski Institut. 24. 163 - 187.

Mortimer, C.H. 1952. Water Movements in lakes during Summer Stratification: Evidence from the Distribution of Temperature in Windermere. Philos. Trans.R. Soc. Lond., B, Biol. Sci., 236.

Moser, H. Umweltisotope. In: Käss, W. (ed). 2004. Geohydrologische Markierungstechnik. Schweizerbart. 2nd edition. 265 – 287.

Murray, M. J., M. R. Allen, C. J. Merchant, A. R. Harris, Donlon, C. J. 2000. Direct observations of skin-bulk SST variability. Geophysical Research Letters. 27. 1171 - 1174.

Nanson, G.C., Croke, J.C. 1992. A genetic classification of floodplains. Geomorphology. 4. 459 - 486.

Négrel, P., Petelet-Giraud, E., Barbier, J., Gautier, E. 2003. Surface water– groundwater interactions in an alluvial plain: chemical and isotopic systematics. Journal of Hydrology. 277. 248 - 267.

Nützmann, G., Holzbecher, E., Pekdeger, A. 2003. Evaluation of the water balance of Lake Stechlin with the help of chloride data. Advances in Limnology.58. 11 – 23.

Nützmann, G., Lewandowski, J. 2009. Wechselwirkungen zwischen Grundwasser und Oberflächenwasser an einem Tieflandfluss (Spree). Grundwasser 14. 195 - 205.

Nützmann, G., Levers, C., Lewandowski, J. 2013. Coupled groundwater flow and heat transport simulation for estimating transient aquifer-stream exchange at the lowland River Spree (Germany). Hydrological Processes. 28. 4078 – 4090.

Ommen, O. D. A., Kidmose, J., Karan, S., Flindt, M. R., Engesgaard, P., Nilsson, B., et al. 2012. Importance of groundwater and macrophytes for the nutrient balance at oligotrophic Lake Hampen, Denmark. Ecohydrology. 5. 286 - 296.

Ong, J. B., Lane, J. W., Zlotnik, V. A., Halihan, T., White, E. A. 2010. Combined use of frequency-domain electromagnetic and electrical resistivity surveys to delineate near-lake groundwater flow in the semi-arid Nebraska Sand Hills, USA. Hydrogeology Journal. 18. 1539 - 1545.

van Overmeeren, R.A. 1997. Radar facies of unconsolidated sediments in the Netherlands: A radar stratigraphy interpretation method for hydrology. Journal of Applied Geophysics 40. 1 - 18.

Ozmidov, R. V. 1990. Diffusion of contaminants in the ocean. English translation. Kluwer.

Padisák, J., Reynolds, C. S. 2003. Shallow lakes: the absolute, the relative, the functional and the pragmatic. Hydrobiologia. 506. 1 - 11.

Padman, L. 1991 . Near-surface mixing in a freshwater lake. Australian Journal of Marine & Freshwater Research. 42. 655 - 673.

Page, R.M., Lischeid, G., Epting, J., Huggenberger, P. 2012. Principal component analysis of time series for identifying indicator variables for riverine groundwater extraction management. Journal of Hydrology. 432–433, 137 – 144.

Pander, J., Geist, J. 2013. Ecological indicators for stream restoration success. Ecological Indicators 30. 106 - 118.

Pawlowicz, R. 2008. Calculating the conductivity of natural waters. Limnology and Oceanography – Methods. 6. 489 - 501.

Pawlowicz, R., R. Beardsley, S. Lentz, E. Dever, Anis, A. 2001. Software simplifies air - sea data estimates. EOS. 82. 2.

Peeters, F., Kipfer, R. 2009. Currents in Stratfied Water Bodies 1: Density driven flow. In: Likens, G.E. (ed.). Lake Ecosystem Ecology. Elsevier. pp. 124 – 133.

Peterson, R.N., Burnett, W.C., Glenn, C.R., Johnson, A.G. 2009. Quantification of point-source groundwater discharges to the ocean from the shoreline of the Big Island, Hawaii. Limnology and Oceanography. 54. 890 – 904.

Pebesma, E. J. 2004. Multivariable geostatistics in S: the gstat package, Computer and Geosciences. 30. 683 – 691.

Pfannkuch, H. O., Winter, T. C. 1984. Effect of anisotropy and groundwater system geometry on seepage through lakebeds. 1. Analog and dimensional analysis. Journal of Hydrology. 75. 213 - 237.

Pieters, R., Lawrence, G. A. 2009. Effect of salt exclusion from lake ice on seasonal circulation. Limnology and Oceanography. 54. 401 – 412.

Pinay, G., Decamps, H., Arles, C., Lacassin-Seres, M. 1989. Topographic influence on carbon and nitrogen dynamics in riverine woods. Archiv für Hydrobiologie. 114. 401 - 414.

Plattner, S., D. M. Masin, G. A. Leshkevich, D. J. Schwab, Rutherford, E. S. 2006. Classifying and Forecasting of Coastal Upwellings in Lake Michigan Using Satellite Derived Temperature Images and Buoy Data. Journal of Great Lakes Research. 32. 63– 76.

Pöschke, F., Lewandowski, J., Engelhardt, C., Preuß, K., Oczipka, M., Ruhtz, T., Kirillin, G. 2015 a. Upwelling of deep water during thermal stratification onset - A major mechanism of vertical transport in small temperate lakes in spring? Water Resources Research. 51. 9612 – 9627.

Pöschke, F., Lewandowski, J., Nützmann, G. 2015 b. Impacts of alluvial structures on small-scale nutrient heterogeneities in near-surface groundwater. Ecohydrology. 8. 682 – 694.

Pringle, C.M. 2001. Hydrologic connectivity and the management of biological reserves: a global perspective. Ecological Applications. 11. 981 - 998.

R Core Team. 2014. R: A language and environment for statistical computing. R Foundation for Statistical Computing. Vienna. Austria.

Read, J. S., D. P. Hamilton, I. D. Jones, K. Muraoka, L. A. Winslow, R. Kroiss, C. H. Wu, Gaiser, E. 2011. Derivation of lake mixing and stratification indices from high resolution lake buoy data. Environmental Modelling and Software. 26. 1325 – 1336.

Reddy, K.R., Kadlec, R.H., Flaig, E., Gale, P.M. 1999. Phosphorus Retention in Streams and Wetlands: A Review. Critical Reviews in Environmental Science and Technology. 29. 83 – 146.

Reinart, A., Reinold, M. 2008. Mapping surface temperature in large lakes with MODIS data. Remote Sensing of the Environment. 112. 603 – 611.

Richter, D. 1997. Das Langzeitverhalten von Niederschlag und Verdunstung und dessen Auswirkungen auf den Wasserhaushalt des Stechlinseegebietes. Berichte des Deutschen Wetterdienstes.

Rivett, M.O., Buss, S.R., Morgan, P., Smith, J.W.N., Bemment, C.D. 2008. Nitrate attenuation in groundwater: A review of biogeochemical controlling processes. Water Research. 42. 4215 – 4232.

Robertson, D. M., Imberger, J. 1994. Lake Number, a Quantitative Indicator of Mixing Used to Estimate Changes in Dissolved Oxygen, Hydrobiologia. 79. 159 – 176.

Rosenberry, D.O. and LaBaugh, J.W. 2008. Field techniques for estimating water fluxes between surface water and ground water: U.S. Geological Survey Techniques and Methods 4–D2.

Rosenberry, D.O., Lewandowski, J., Meinikmann, K., Nützmann, G. 2015. Groundwater – the disregarded component in lake water and nutrient budgets: Effects of groundwater on lake hydrology. Hydrological Processes. DOI: 10.1002/hyp.10403.

Rundquist, D.,Murray, G., Queen, L. 1985. Airborne thermalmapping of a “flow-through” lake in the Nebraska Sandhills. Water Resources Bulletin. 21. 989– - 994.

Samek, R. 2000. Hydrogeochemische Untersuchungen zur Genese des Grundwassers im Einzugsgebiet des Stechlinsees. diploma thesis. Free University of Berlin.

Schindler, D.W. 2006. Recent advances in the understanding and management of eutrophication. Limnology and Ocenanography. 51. 356 – 363.

Schindler, U., Müller, L., Eulenstein, F., Dannowski, R. 2008. A Long-Term Hydrogeological Soil Study on the Effects of Soil and Land Use on Deep Seepage Dynamics in Northeast Germany. Archives of Agronomy and Soil Sciences. 54. 451 – 463.

Schirmer, M., Luster, J., Linde, N., Perona, P., Mitchell, E.A.D., Barry, D.A., Cirpka, O.A., Schneider, P., Vogt, T., Durisch-Kaiser, E. 2013. River restoration: morphological, hydrological, biogeochemical and ecological changes and challenges. Hydrology and Earth System Sciences. 10. 10913 - 10941.

Schladow, S. G., Pálmarsson, S. Ó. , Steissberg, T.E. , Hook, S. J. , Prata, F. E. 2004. An extraordinary upwelling event in a deep stratified lake. Geophysical Research Letter. 31. L15504.

Schmidt, C., Bayer-Raich, M., Schirmer, M. 2006. Characterization of spatial heterogeneity of groundwater-stream water interaction using multiple depth streambed temperature measurements at the reach scale. Hydrology and Earth System Sciences. 10. 849 – 859.

Schmidt, W. 1928. Über Temperatur und Stabilitätsverhältnisse von Seen. Geograf. Annaler. 10. 145 – 177.

Schornberg, C., Schmidt, C., Kalbus, E., Fleckenstein. J.H. 2010. Simulating the effects of geological heterogeneity and transient boundary conditions on streambed temperatures – Implications for temperature-based water flux calculations. Advances in Water Resources. 33. 25. 234 – 245.

Schott, J. R. 1979. Temperature—Measurement of cooling water discharged from power-plants. Photogrammetric Engineering and Remote Sensing. 45. 753 - 761.

Schot, P.P, Pieber, S.M. 2012. Spatial and temporal variations in shallow wetland groundwater quality. Journal of Hydrology. 422 – 423. 43 – 52.

Schuetz, T., Weiler, M. 2011. Quantification of localized groundwater inflow into streams using ground-based infrared thermography. Geophysical Research Letters. 38. L03401.

Schüring, J., Schliecker, M., Hencke, J. 2000. Redox front in aquifer systems and parameters controlling their dimension. In Redox: fundamentals, processes, and application, Schüring, J., Fischer, W.R. Duijnisveld WHM (eds). Springer. 135 - 151.

Schwoerbel,J., Brenelberger, 2005. Einführung in die Limnologie. 9th ed. Spektrum. München.

Selker, J., van de Giesen, N., Westhoff, M., Luxemburg, W., Parlange, M.B. 2006a. Fiber optics opens window on stream dynamics. Geophysical Research Letters. 33. L24401.

Selker, J.S., Thévenaz, L., Huwald, H., Mallet, A., Luxemburg, W., van de Giesen, N., Stejskal, M., Zeman, J., Westhoff, M., Parlange, M.B. 2006b. Distributed fiberoptic temperature sensing for hydrologic systems. Water Resources Research. 42. W12202.

Seibert, J., Bishop, K., Rodhe, A., McDonnell, J.J. 2003. Groundwater dynamics along a hillslope: A test of the steady state hypothesis. Water Resources Research. 39. 1014.

Shaban, A., Khawlie, M., Abdallah, C., Faour, G. 2005. Geologic controls of submarine groundwater discharge: Application of remote sensing to north Lebanon. Environmental Geology. 47. 512 - 522.

Shaw, R. D., & Prepas, E. E. 1990. Groundwater lake interactions. 2. Nearshore seepage patterns and the contribution of ground-water to lakes in Central Alberta. Journal of Hydrology. 119. 121 - 136.

Siegel, S., Castellan, N.J. 1988. Non parametric statistics for behavioral science. McGraw-Hill Humanities/Social Sciences/Languages. NewYork.

Shintani, T., A. de la Fuente, Y. Nino, Imberger, J. 2010. Generalizations of the Wedderburn number: Parameterizing upwelling in stratified lakes. Limnology and Oceanography. 55. 1377 - 1389.

Simpson, J. H., Lucas, N. S., Powell, B., Maberly, S. C. 2014. Dissipation and mixing during the onset of stratification in a temperate lake, Windermere. Limnology and Oceanography. 60. 29 – 41.

SkØien, J.O., Blöschl., G. 2003. Characteristic space scales and timescales in hydrology. Water Resources Research. 39. SWC 11.

Soloviev, A., Lukas, R. 2013. The near-surface layer of the ocean: structure, dynamics and applications. Springer Science and Business Media.

Solzbacher, M. 2013. Zeitlich-räumliche Variabilität der Grundwasserneubildung im Einzugsgebiet Großer Stechlinsee. Vergleich von Methoden auf unterschiedlichen Raum- und Zeitskalen. diploma thesis. Albert-Ludwigs-Universität Freiburg i-Br.

Sophocleous, M. 2002. Interactions between groundwater and surface water: the state of the science. Hydrogeology. 10. 52 - 67.

Sophocleous, M., Koussis, A., Martin, J.L., Perkins, S.P. 1995. Evaluation of simplified stream-aquifer depletion models for water rights administration. Ground Water. 33. 579 - 588.

Spalding, R.F., Exner, M.E. 1980. Areal, Vertical and Temporal Differences in Groundwater Chemistry: I. Inorganic Constituents. Journal of Environmental Qualities. 9. 466 - 479.

Spigel, R. H., Imberger, J. 1980. The classification of mixed-layer dynamics in lakes of small to medium size, Journal of Physical Oceanography. 10. 1104 –1121.

Steissberg, T.E., Hook, S.J., Schladow, S.G. 2005. Characterizing partial upwelling and surface circulation at Lake Tahoe, California-Nevada, USA with thermal infrared images. Remote Sensing. 99. 2 – 15.

Stevens, C., Imberger, J. 1996. The initial response of a stratified lake to a surface shear stress. Journal of Fluid Mechanics. 312. 39–66.

Stevens, C. L., Lawrence, G. A. 1997. Estimation of wind-forced internal seiche amplitudes in lakes and reservoirs, with data from British Columbia, Canada. Aquatic Sciences. 59. 115 – 134.

Stonestrom, D.A., Constantz, J. (eds). 2003. Heat as a Tool for Studying the Movement of Groundwater Near Streams (cir. 1260). U.S. Geological Survey. Reston. Virginia. http://pubs.water.usgs.gov/circ1260/

Takatert, N., Sánchez-Pérez, J.M., Trémolieres, M. 1999. Spatial and temporal variations of nutrient concentration in the groundwater of a floodplain: Effect of hydrology, vegetation and substrate. Hydrological Processes. 13. 1511 - 1526.

Thompson, R. O. R. Y., Imberger, J. 1980. Response to a numerical model of a stratified lake to wind stress, in: Proceedings 2nd Symposium Stratified Flows. Trondheim June 1980. 1. 562 – 570.

Tiemeyer, B., Frings, J., Kahle, P., Köhne, S., Lennartz, B. 2007. A comprehensive study of nutrient losses, soil properties and groundwater concentrations in a degraded peatland used as an intensive meadow – Implications for re-wetting. Journal of Hydrology. 345. 80 - 101.

Todd, D.K. 1980. Groundwater Hydrology. 2nd edition. Wiley.

Torgersen, C.E., Faux, R.N., McIntosh, B.A., Poage, N.J., Norton, D.J. 2001. Airborne thermal remote sensing for water temperature assessment in rivers and streams. Remote Sensing of the Environment. 76. 386 – 398.

Tóth, J. 1963. A theoretical analysis of groundwater flow in small drainage basins. Journal of Geophysical Research. 68. 4795 – 4812.

Troitskaya, E., Blinov, V., Ivanov, V., Zhdanov, A., Gnatovsky, R., Sutyrina, E., Shimaraev, M. 2014. Cyclonic circulation and upwelling in Lake Baikal, Aquatic Sciences. 76 1015 – 1621.

Uusi-Kämppäa, J., Turtola, E., Hertikainen, H., Yärant, T. 1997. The ineractions of buffer zones and phosphorus runoff. In Buffer Zones: Their Processes and Potential in Water Protection, Haycock NE, Burt, T.P., Goulding, K., Pinay, G. (eds). Haycock Associated Limited. Hertfordshire. 43 - 53.

Vanek, V. 1987. The interactions between lake and groundwater and their ecological significance. Stygologia. 3. 1 - 23.

Van Geer, F.C. 1987. Detection of natural and artificial causes of groundwater fluctuations. The influence of climate change and climatic variability on the hydrologic regime and water resources. Proceedings of the Vancouver Symposium. IAHS Publ. no. 168.

Väli, G., Zhurbas, V., Lannemets, J., Elken, J. 2011. Simulation of nutrient transport from different depth during an upwelling event in the Gulf of Finland. Oceanology. 53. 431 – 448.

Wassen, M.J., Peeters, W.H.M., Venterink, H.O. 2002. Patterns in vegetation, hydrology, and nutrient availability in an undisturbed river floodplain in Poland. Plant Ecology. 165. 27- 43.

Webster, I.T. 1990. Effect of wind on the distribution of phytoplankton cells in lakes. Limnology and Oceanography. 35. 989 – 1001.

Webster, K., Kratz, T.E., Bowser, C.J., Magnusin, J.J. 1996. The influence of landscape position on lake chemical response to drought in northern Wisconsin. Limnology and Oceanography. 41. 977 – 984.

Whiting, J. M. 1975. Determination of groundwater inflow to prairie lakes using remote sensing. Paper 61 presented at the Symposium on Machine Processing of Remotely Sensed Data. The laboratory for applications of remote sensing. West Lafayette, Indiana: Purdue University (http://docs.lib.purdue.edu/lars_symp/61).

Wilson, R. C., Hook, S. J., Schneider, P., Schladow, S. G. 2013. Skin and bulk temperature difference at Lake Tahoe: A case study on lake skin effect. Journal of Geophysical Research. Athmospheres. 118. 332 – 346.

Winter, T.C. 1983. The Interaction of Lakes with Variably Saturated Porous Media. Water Resources Research, 19, 1203 – 1218.

Winter, T.C. 1995. Recent advances in understanding the interaction of groundwater and surface water. Reviews of Geophysics. 33. 985 – 994.

Winter, T.C.1999. Relation of streams, lakes and wetlands to groundwater flow systems. Hydrogeology Journal. 7. 28 – 45.

Winter, T.C. 2005. The Hydrology of Lakes. In: O´Sullivan, P.E., Reynolds, C.S. (eds.): The Lake Handbook – Volume 1 – Limnology and Limnetic Ecology. Blackwell. 61 – 79.

Winter, T.C., Harvey, J.W., Franke, O.L, Alley, W.M. 1998. Groundwater and Surface Water a single Resource. US Geological Survey Circular 1139.

Winter, T.C., Rosenberry, D.O., LaBaugh, J.W. 2003. Where does the Ground Water in Small Watersheds Come From? Ground Water – Watersheds Issue. 41. 989 – 1000.

Woessner, W.W. 2000. Stream and fluvial plain groundwater interactions: Rescaling hydrogeological thought. Ground Water. 38. 423 – 429.

Woolsey, S., Capelli, F., Gonser, T., Hoehn, E., Hostmann, M., Junker, B., Paetzold, A., Roulier, C., Schweizer, S., Tiegs, S.D., Tockner, K., Weber, C., Peter, A. 2007. A strategy to assess river restoration success. Freshwater Biology. 52. 752 - 769.

Wondzell, S.M. 2015. Groundwater – surface water interactions: perspectives on the development of the science over the last 20 years. Freshwater Science. 34. 368 – 376.

Wüest, A., Lorke, A. 2003. Small-scale hydrodynamics in lakes. Annual Review of Fluid Mechanics. 35. 373 - 412.

Yaguchi, E. M. 1977. Nutrients and Productivity as indicators of thermal effluent- upwelling interactions in Lake Michigan. Journal of Great Lakes Research. 3 57 – 64.

Yeh, T.-C.J., Liu, S. 2000. Hydraulic tomography: development of a new aquifer test method. Water Resources Research. 36. 2095 - 2105.

Yeh, T.-C.J., Xiang, J., Suribhatla, R.M., Hsu, K.-C., Lee, C.-H., Wen, J.-C. 2009. River stage tomography: a new approach for characterizing groundwater basins. Water Resources Research. 45. W05409.

Zhu, J., Yeh, T.-C.J. 2005. Characterization of aquifer heterogeneity using transient hydraulic tomography. Water Resources Research. 41. W07028.

Zilitinkevich, S. S., Kreiman, K. D., Terzhevik, A. Y. 1992. The thermal bar. Journal of Fluid Mechanics. 236. 27 - 42.